

# UC Berkeley

## Research Reports

### Title

Fault Detection And Tolerant Control For Lateral Guidance Of Vehicles In Automated Highways

### Permalink

<https://escholarship.org/uc/item/40r4082f>

### Author

Patwardhan, Satyajit Neelkanth

### Publication Date

1994

**This paper has been mechanically scanned. Some errors may have been inadvertently introduced.**

CALIFORNIA PATH PROGRAM  
INSTITUTE OF TRANSPORTATION STUDIES  
UNIVERSITY OF CALIFORNIA, BERKELEY

# **Fault Detection and Tolerant Control for Lateral Guidance of Vehicles in Automated Highways**

**Satyajit Neelkanth Patwardhan**

**California PATH Research Report  
UCB-ITS-PRR-94-17**

This work was performed as part of the California PATH Program of the University of California, in cooperation with the State of California Business, Transportation, and Housing Agency, Department of Transportation; and the United States Department of Transportation, Federal Highway Administration.

The contents of this report reflect the views of the authors who are responsible for the facts and the accuracy of the data presented herein. The contents do not necessarily reflect the official views or policies of the State of California. This report does not constitute a standard, specification, or regulation.

August 1994

ISSN 1055-1425

Fault Detection and Tolerant Control for Lateral Guidance of Vehicles  
in Automated Highways

by

Satyajit Neelkanth Patwardhan

B.E. (University of Poona, India) 1987

M.Tech. (Indian Institute of Technology, Bombay) 1989

A dissertation submitted in partial satisfaction of the  
requirements for the degree of

Doctor of Philosophy

in

Engineering-Mechanical Engineering

in the

GRADUATE DIVISION

of the

UNIVERSITY of CALIFORNIA at BERKELEY

Committee in charge:

Professor Masayoshi Tomizuka, Chair

Professor Karl Hedrick

Professor Pravin Varaiya

The dissertation of Satyajit Neelkanth Patwardhan is  
approved:

<u>Masanishi Amizuka</u>	<u>4/28/94</u>
Chair	Date
<u>J.K. Hedrick</u>	<u>4/28/94</u>
	Date
<u>Ramin Vazirani</u>	<u>20 April '94</u>
	Date

University of California at Berkeley

Fault Detection and Tolerant Control for Lateral Guidance of Vehicles  
in Automated Highways

©1994

by

Satyajit Neelkanth Patwardhan

Abstract

**Fault Detection and Tolerant Control for Lateral Guidance of Vehicles  
in Automated Highways**

by

Satyajit Neelkanth Patwardhan

Doctor of Philosophy in Engineering-Mechanical Engineering  
University of California at Berkeley  
Professor Masayoshi Tomizuka, Chair

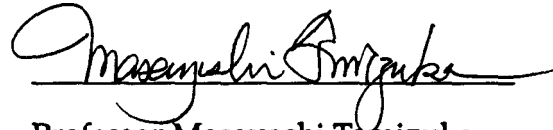
In this dissertation, the problem of fault tolerant control of automobiles is addressed. The ultimate goal is to improve safety and reliability of the cars while operating under the automated highway scenario. The three main problems handled in the dissertation are tire burst, sensor fault detection and slip angle control. The tire burst and sensor faults are important failure modes for automated highways, whereas the slip angle control problem is important during severe maneuvers for enhancing the vehicle safety.

For the tire burst problem, a model was developed to predict the behavior of the car when a tire burst occurs. Based on the model, a controller was designed to keep the car running within the lane boundaries. Two methods for the tire burst detection, one based on the tire pressure and the other based on the roll rate error, were evaluated. The tire burst model was finally verified by the tire burst experiments performed on a full size car.

For the sensor fault detection, a model based fault detection scheme was developed. The sensor faults were detected by comparing the sensor outputs with the corresponding estimates predicted by the mathematical model. The algorithm was successfully used to detect sensor faults in an experimental laboratory car. In addition to the sensor fault detection, a likelihood ratio test was proposed to improve the performance of direction sensitive filters.

Finally, the idea of slip angle control to improve cornering performance of ve-

hicles was developed. Since there is no direct way of measuring the slip angle, estimation schemes were developed for slip angle estimation. A slip angle controller structure was designed to maintain the slip angles below the tire characteristics saturation point. The slip angle controller achieved performance improvements by generating larger accelerations while cornering.



**Professor Masayoshi Tomizuka**  
Chairman, Thesis Committee



### **Dedication**

To my parents, Neelkanth and Suneeta Patwardhan, to my brother Prasad, without whose encouragement, I would have never pursued my higher education, and to my wife Vaishali.

# Contents

<b>List of Figures</b>	<b>vi</b>
<b>List of Tables</b>	<b>ix</b>
<b>1 Introduction</b>	<b>1</b>
1.1 Objectives	1
1.2 Previous Work	4
1.3 Contributions of This Dissertation	6
1.4 Organization of the Dissertation	8
<b>2 Tire Blow-Out</b>	<b>9</b>
2.1 Background	10
2.2 Modelling	10
2.2.1 Car modelling	10
2.2.2 Tire burst modelling	21
2.2.3 Simulations	34
2.3 Burst Controller Design	37
2.3.1 Designing a controller with modified performance index	41
2.3.2 Four wheel steering	43
2.3.3 Both tire burst	44
2.3.4 Better actuator	45
2.3.5 Feed-forward controller	45
2.3.6 Torque reduction	54
2.3.7 Controller simulations	55
2.4 Tire Burst Detection	57
2.5 Experiments	59
2.5.1 Experimental setup	59
2.5.2 Experimental results	66
2.6 Conclusions	68

<b>3</b>	<b>Sensor Fault Detection</b>	<b>69</b>
3.1	Introduction	69
3.2	System Description and Modelling	71
3.2.1	Simplified model	71
3.3	Robust Fault Detector	73
3.3.1	Application to lateral control problem	76
3.4	Simulations	76
3.5	Experiments	82
3.6	Conclusions.	85
<b>4</b>	<b>Enhancing Performance of Direction Sensitive Filters</b>	<b>86</b>
4.1	Introduction	86
4.2	Detection Filter	87
4.3	Adding Additional Failures	89
4.4	Regression	90
4.5	Ratio Test ( <i>known failure time</i> )	90
4.6	Ratio Test ( <i>unknown failure time</i> )	<b>93</b>
4.7	Some Properties	94
4.8	Simulations	96
4.9	Conclusions.	97
<b>5</b>	<b>Slip Angle Control</b>	<b>102</b>
5.1	Introduction	102
5.2	Definitions	103
5.3	Slip Angle Estimation	104
5.3.1	Method #1	104
5.3.2	Method #2	107
5.3.3	Method #3	108
5.4	Slip Angle Controller	109
5.5	Conclusions.	112
5.6	Future Research	113
<b>6</b>	<b>Conclusions and Future Research</b>	<b>114</b>
6.1	Conclusions.	114
6.2	Future Research	116
	<b>Bibliography</b>	<b>117</b>
<b>A</b>	<b>Direction cosines of a rotating frame</b>	<b>124</b>
<b>B</b>	<b>Tire Force Generation</b>	<b>126</b>
<b>C</b>	<b>Simplified Model</b>	<b>129</b>

# List of Figures

1.1	A fault tolerant control system . . . . .	2
2.1	Car model - Axis definition . . . . .	11
2.2	Effect of tire burst on vehicle dynamics . . . . .	22
2.3	Tire burst, radius change . . . . .	24
2.4	Time of deflation vs. area of opening . . . . .	26
2.5	Geometry of flat tire . . . . .	26
2.6	Suspension force rearrangement . . . . .	27
2.7	Suspension force rearrangement . . . . .	28
2.8	Rotation of burst tire. . . . .	30
2.9	Roll resistance coefficient Vs. pressure . . . . .	31
2.10	Moments about king pin . . . . .	32
2.11	Effect of pressure on tire-road interaction force . . . . .	34
2.12	Tire burst - zero steering command . . . . .	35
2.13	Tire burst - zero steering command . . . . .	35
2.14	Tire burst - fixed <b>nonzero</b> steering command . . . . .	36
2.15	Tire burst - fixed <b>nonzero</b> steering command . . . . .	37
2.16	Tire burst conditions . . . . .	38
2.17	Tire burst effects . . . . .	38
2.18	FSLQ burst controller structure . . . . .	42
2.19	4WS burst controller performance . . . . .	43
2.20	Force imbalance after a tire burst . . . . .	44
2.21	Both tires burst. . . . .	45
2.22	Definition of system output . . . . .	48
2.23	Feed-forward controller, structure . . . . .	49
2.24	Feed-forward controller, performance . . . . .	50
2.25	Feed-forward terms: actual & approximate . . . . .	51
2.26	Simplified feed-forward controller, structure . . . . .	51
2.27	Simplified feed-forward controller, performance . . . . .	52
2.28	Simplified feed-forward controller, performance . . . . .	53
2.29	Simplified feed-forward controller, performance . . . . .	53

2.30	Tire force generation . . . . .	55
2.31	Performance improvement after engine torque reduction . . . . .	56
2.32	Performance of combined controller . . . . .	56
2.33	Tire burst detection . . . . .	58
2.34	Experiment site . . . . .	60
2.35	Tire burst, experimental arrangement . . . . .	61
2.36	Tire burst, experimental arrangement . . . . .	62
2.37	Tire burst, experimental arrangement . . . . .	62
2.38	Tire burst, experimental arrangement . . . . .	63
2.39	Tire burst, experimental arrangement . . . . .	64
2.40	Tire burst, experimental arrangement . . . . .	64
2.41	Tire burst, experimental arrangement . . . . .	65
2.42	Tire burst, experimental arrangement . . . . .	65
2.43	Tire burst, experimental results . . . . .	66
2.44	Tire burst, experimental results . . . . .	67
2.45	Tire burst, experimental results . . . . .	67
3.1	Sensor fault detection . . . . .	70
3.2	Robust observer . . . . .	74
3.3	Frequency response of uncertainties . . . . .	77
3.4	Lateral position fault indicator . . . . .	78
3.5	Lateral acceleration fault indicator . . . . .	78
3.6	Yaw rate fault indicator . . . . .	79
3.7	Cornering stiffness variation . . . . .	79
3.8	Lateral position fault indicator: icy roadway . . . . .	80
3.9	Lateral acceleration fault indicator: icy roadway . . . . .	80
3.10	Yaw rate fault indicator: icy roadway . . . . .	81
3.11	Cornering stiffness: icy roadway . . . . .	81
3.12	Schematic of experimental vehicle . . . . .	82
3.13	Lateral position fault indicator: experiment . . . . .	84
3.14	Lateral acceleration fault indicator: experiment . . . . .	84
3.15	Yaw rate fault indicator: experiment . . . . .	85
4.1	Bank of filters. . . . .	89
4.2	Regression . . . . .	98
4.3	Known failure time . . . . .	98
4.4	Known failure time . . . . .	99
4.5	Known failure time . . . . .	99
4.6	Unknown failure time . . . . .	100
4.7	Unknown failure time, estimate of $\theta$ . . . . .	100
5.1	Typical tire-road interaction characteristics . . . . .	103
5.2	Slip angle definition . . . . .	104

5.3 Vehicle kinematics . . . . .	105
5.4 Vehicle top view, free body diagram . . . . .	106
5.5 $\alpha$ -control structure . . . . .	110
5.6 Slip angle controller performance: trajectory . . . . .	111
5.7 Slip angle controller performance: steering command . . . . .	112
B.1 Longitudinal tire force characteristics . . . . .	128
B.2 Lateral tire force characteristics . . . . .	128
C.1 Schematic of simplified vehicle . . . . .	130

# List of Tables

2.1 List of variables . . . . .	12
2.2 $G(k, \rho), k = 1$ . . . . .	52
3.1 Parameters of simplified model . . . . .	72
3.2 Specifications of experimental car. . . . .	83
4.1 Fault detection decision table . . . . .	97

## Acknowledgment

Firstly, I would like to express my sincere gratitude to Prof. Tomizuka who provided me with encouragement, support and valuable guidance throughout my PhD career.

The work in this dissertation was sponsored by Partners for Advanced Transit and Highways (PATH), California Department of Transportation. We are grateful for their support. We are also grateful to Nippon Denso Co., Ltd. for the experimental vehicle provided by them. Specifically, I would also like to thank Mr. Wei-Bin Zhang from PATH, for valuable discussions and fruitful comments. I am also grateful to Mr. Peter Develin of PATH, who guided me while designing and building the tire burst experimental setup. I would also like to thank him for his valuable efforts during the tire burst experiments. My office-mates, Carlos Osorio, David Love, Tom Hessburg, Wonshik Chee and my former room-mates Addis Tesfaye, and Viiay Joshi also helped me in performing the experiments. I would like to thank them for their sincere help.

I would like to thank my friends at Berkeley Some of them I knew before and some of them I met at Berkeley, who have helped me in many aspects of my life. To name a few, I would like to mention Addis Tesfaye, Dattaprabodh Godbole, Vishwajeet Girase and Vinay Joshi.

I would like to express my special thanks to my parents and and my brother, who encouraged me and supported me to pursue my graduate study

Last but not the least, I would like to thank my wife Vaishali, whose persistent encouragement has helped me finishing the thesis.



# Chapter 1

## Introduction

### 1.1 Objectives

In any complex computer controlled system, it is important that the system should have fault handling/tolerancing capability. If a system is not complex, then a separate fault handling algorithm may not be justified and safety and reliability designed into the sub components of the system could be enough, but with the increase in the complexity of the modern control systems, one has to pay special attention to the behavior of the system under faulty conditions. The fault handling capability is important to achieve higher reliability and safety levels with reduction in hazard. In addition, it can improve the mean time between failures by timely detection of problems that could potentially result in down time of the system. A fault tolerant controller can provide graceful degradation of performance along with sustained operation at the degraded performance level to avoid catastrophic consequences.

A reliable system refers to the system in which the probability of a failure is very low. On the other hand, a safe system is designed such that even under a faulty condition, the consequences are not hazardous. Most of the systems are required to be reliable as well as safe for operation. Higher reliability of each sub system is crucial for higher reliability of the overall system. One can improve reliability of the subsystems by incorporating redundancy For example, one can

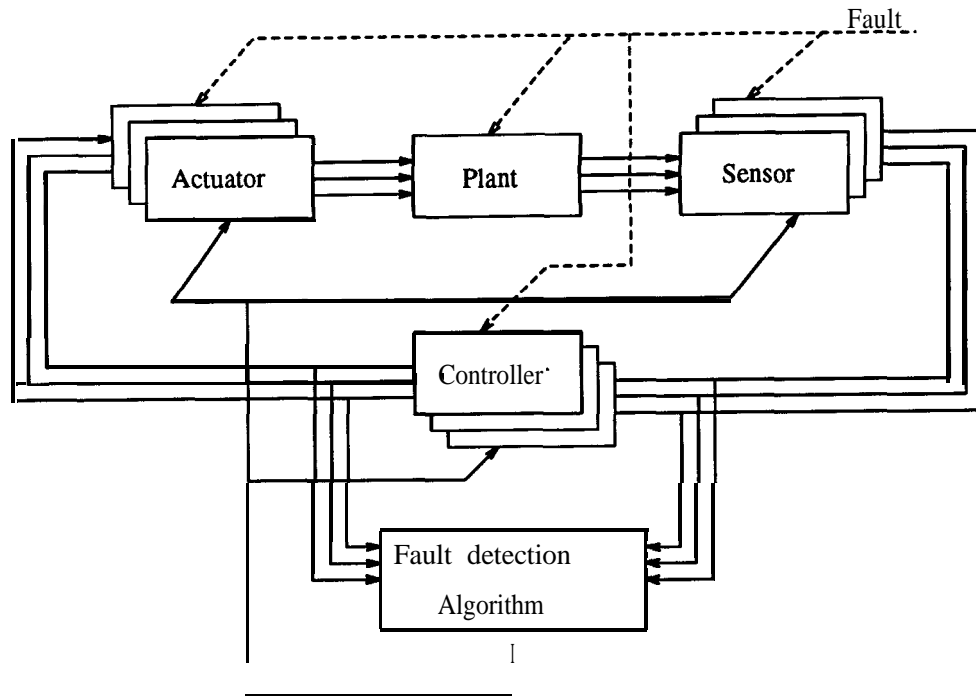


Figure 1.1: A fault tolerant control system

have redundant sensors to measure the crucial quantities, and switch within the set of sensors when one or more of them fail. Similar concepts are applied while using redundant actuators and computers. In such systems, it is important to have a mechanism of detecting a fault and to isolate it. These mechanisms are termed as *fault detection and identification* (FDI) algorithms [1]. Depending on the outcome of the FDI algorithms, the system can be reconfigured and faulty components can be taken out of operation. The faulty components will be replaced by the redundant components, and the system can continue to operate reliably (See Fig. 1.1). In order to improve the safety of the system, each of the system components and their interactions should be designed in such a way that even under the failure, the system continues to operate in a degraded mode of operation without producing hazardous consequences. On a lower level, fail safe operation can be built into the system by proper design. For example, when the hydraulic power assist of an automobile steering system fails, the torsion bar in the steering column still keeps the steering wheel connected to the tires of the car and the catastrophic effects like

loss of steering are avoided. Obviously, the automobile will continue to operate at a degraded performance level. In a more complex system, in addition to the safe operation of individual components, it is important to consider the interaction between the different components so that the fault does not propagate in the whole system. This calls for the FDI algorithms to monitor the system operation and to either halt the system before the fault propagates farther into the system or to reconfigure the system for continued operation. Sometimes the fault monitors may just give warning to the human operator involved so that the necessary steps to reduce the hazard can be taken.

As discussed above, the fault handler should take certain actions based on the outcomes of the FDI algorithms. These actions are categorized as *the fault tolerant control* actions and may involve switching from the nominal controller to emergency controller and reconfigurations of sensors, actuators or other hardware [2]. There are several approaches while designing the emergency controllers. It is possible to design the nominal controller (the controller in operation during no-fail mode) in such a way that it is robust to the faulty conditions. This generally means compromising the nominal performance. Also it is difficult to design controllers that are robust for the wide range of parameter variations or uncertainties that are typical in a faulty conditions. An alternative is to completely redesign the controller for the failure mode operation.

The IVHS<sup>1</sup> program of *Partners for Advanced Transit and Highways* (PATH) in California aims at computerized navigation of automobiles on roadways [4]. The system is complex enough to qualify for application of the fault detection and tolerancing concepts [5]. The cars will travel in the form of platoons of multiple vehicles under automated lateral guidance. Since the reliability of the overall roadway system will be product of reliabilities of its individual components, in order to maintain a satisfactory level of reliability for the overall automated roadway system, it is imperative that individual car, along with its control system should have a high level of reliability. Fault in a single car could have severe effects on the overall

---

<sup>1</sup>IVHS stands for *Intelligent Vehicle Highway System*

flow on the highways [5]. With the decrease in human control, high dependability of car controllers, sensors, roadside computers, inter-car communication links and the car itself, become the crucial factors for safe operation of the whole PATH-IVHS system.

The research presented in this thesis is focused on *Fault Tolerant Control Systems* and aims at achieving higher safety levels through sensor validation and fault tolerant controller design that can handle faulty conditions effectively and maintain safe operation of the system. The fault tolerancing problems associated with automated highway system will be addressed. Specifically, tire burst problem and sensor fault detection problem will be discussed at length in this dissertation. This will be followed by the slip angle control problem [53], which improves the cornering performance of vehicle during severe maneuvers. The slip angle control problem is important from safety viewpoint because it aims at improving the safety of the vehicles during emergency maneuvers such as tire burst.

## 1.2 Previous Work

The fault detection problem can be handled either by hardware redundancy or by analytical redundancy[1]. As mentioned earlier, hardware redundancy is quite straightforward and utilizes redundant sensors. On the other hand analytical redundancy requires the mathematical model of the system under observation. Various approaches to FDI using analytical redundancy have been reported in the last two decades. The number of different approaches however can be traced back to a few basic concepts. Among them are the detection filters [16][17], the innovation test using a single Kalman filter[21], the parity space approach [23], the parameter estimation technique [24] and expert system application [20]. The fault detection filter (also called BJ filter or direction sensitive filter) is a full-order state estimator with a special choice of the gain matrix. This approach was first proposed by Beard and Jones [16]. The gain matrix of the fault detection filters are designed such that the output error due to a particular fault is constrained to a

single direction or plane in the output error space independent of the mode (size or time history) of the failure. The most simple configuration used for sensor fault detection is a single estimator (observer or Kalman filter), where a single full or reduced-order estimator is driven by only one sensor output, and the full output is reconstructed. The comparison of the actual output  $\mathbf{y}$  with the estimated output  $\hat{\mathbf{y}}$ , using a threshold logic allows in principle, a unique detection and isolation of a single faulty sensor. The parity space approach consists of checking the consistency between the mathematical model of the plant and the actual observations. A fault is detected once the inconsistency exceeds the predetermined error bounds. The parameter estimation method is an alternative approach to the above described methods based on the state estimation. It makes use of the fact that faults of a dynamic system are reflected in the physical parameters as for example, friction, mass, viscosity etc. The idea of the parameter identification approach is to detect the faults via estimation of the parameters of the mathematical model of the plant. Decision on a fault can be made by exploiting the relationships between faults and changes in the physical parameters. This approach is useful for detection of incipient faults. The knowledge based methods (expert systems) complement the existing analytical and algorithmical methods of fault detection. While the algorithmic methods use the quantitative analytical model, the expert system approach makes use of qualitative models based on the available knowledge of the system. The combination of both strategies allows the evaluation of all available information and knowledge of the system for fault detection. Such additional knowledge may be for example, the operational environment, used or worn out tools etc.

There have been several successful applications of model based fault detection schemes to automobile problems [25][26][27]. Several fault detection schemes are also based on spectral signature of the faults [28][29]. Spectral analysis can also be used to detect sensor faults. Faults like disconnection, short circuit usually change the frequency content of the noise in the sensor output,

Specific applications of the fault tolerant control schemes in this dissertation are on the lateral guidance of vehicles for automated highway systems.

Vehicle lateral dynamics have been studied by several researches in the past. Segel [6] developed a three degree of freedom vehicle models which includes the yaw, lateral and roll motions. This model was modified to the bicycle model or the half car model [7][8] by neglecting the roll motion. In addition, vehicle model with more degrees of freedom were also developed [9][10][30]. In one of the recent vehicle models, Peng [30] used a six degrees of freedom model to represent the vehicle. In the previous modelling efforts, the tire burst effects were not modelled.

Several researches have studied the lane following problem for vehicles [8][11][12][13][14][15]. More recently Peng and Tomizuka [30] developed lane following the controllers using the steering wheel as the control input. They utilized the FSLQ (Frequency Shaped Linear Quadratic) design methodology for designing the control law. The controller was essentially designed to operate in the absence of tire blow-out.

Tire forces can be modelled by analytical relations or empirical relations. Doniselli and Mastinu [32] have developed analytical models for tire forces. On the other hand Bakker et al [33][34] proposes an empirical relation that fits the experimental data. There has been significant effort towards controlling the tire forces in longitudinal direction [35]-[46]. All the applications of longitudinal tire force control were limited to braking force control [35]-[40]. The brake is used as a control input in order to maintain the tire slip ratio at optimum point, so that maximum braking force can be generated. Recently, some efforts were made to control the tractive force generated by the tires [54]. The issue of directional stability while braking was studied by Taheri [46].

### **1.3 Contributions of This Dissertation**

As mentioned earlier, the three specific problems addressed in this dissertation are the tire burst problem, the sensor fault detection and the slip angle control. The tire burst and sensor fault detection problems serve as excellent examples for application of fault detection and tolerancing schemes. Slip angle control is

important during severe maneuvers for enhancing the vehicle safety.

Tire burst: The first specific problem handled in this dissertation is the tire burst problem. Tire blow-out is a hazardous situation from the viewpoint of controlling the car. Under a sudden blow-out, the car could become uncontrollable and has a danger of exceeding the lane boundaries. In the IVHS environment, this is an extremely hazardous situation. The tire blow out could occur because of nails or other such pieces on the road. Also it could occur during severe cornering maneuvers [56]. In the past, the car modeling efforts have always excluded the tire blow out problem. This was primarily because the need for automatic control of the car under the tire blow out was felt only recently because of the IVHS concepts. For describing the tire blow out one can not use any of the low order models described in [6],[7],[8]. Because of the complexity of the effects of the tire blow out, one has to develop a higher order model for its description. In this dissertation, a model that can describe the tire blow out effectively, will be developed. The model is used for designing a compensator for tire blow out. The tire blow out controller design is considerably different from any of the previous lateral controller designs. The proposed tire blow out controller that would take over after the tire burst has two parts, a feedback part and a feedforward part. Following the tire burst modeling and controller design, tire burst detection scheme will be developed. Two methods, one based on analytical redundancy approach and one based on tire pressure measurement will be presented. Finally, the tire blow-out experiments to validate the tire burst model were performed

Sensor fault detection: Although there has been research in the area of sensor fault detection, it was primarily focused in the field of aerospace applications [58]. In the absence of IVHS concepts the need for advanced fault detection algorithms was not felt in the field of automobiles. This thesis addresses the sensor fault detection problem for automobiles in the IVHS scenario. Sensor fault detection algorithm based on generalized observer scheme [22] is developed to detect the faults in lateral position, lateral acceleration and yaw rate sensors. Following the sensor fault detection the fault detection problem by using the direction sensitive *filters* will be addressed. When a failure occurs, the output error of the detection

filter will tend to grow in a direction characteristics to that failure. Thus there will be a multiple number of directions in the output error space to which, one will have to match the residue growth direction. To do this efficiently, a probability ratio test is developed to process the output error generated by the detection filters.

Slip angle control: The final problem addressed in the dissertation is the slip angle control or the a-control. Several of the previous research efforts in controlling the tire force were focused towards traction control or brake control. These controllers aim at controlling the tire slip ratio in order to maximize the longitudinal tire force. The anti-lock break systems available on most of today's cars are examples of slip ratio controllers. In this dissertation, the slip angle, a quantity analogous to slip ratio will be controlled in order to improve the response of the vehicle to the cornering commands. The final aim being to design a system similar to ABS (Anti-lock Brake System) for steering commands in order to improve the cornering performance of the vehicle.

## **1.4 Organization of the Dissertation**

The outline of this dissertation is as follows. In chapter 2, tire blow out problem will be detailed. The chapter will consist of four main sections that will address burst modelling, controller design, tire burst detection and model verification by experiments. This will be followed by the sensor fault detection algorithm in chapter 3. A sensor fault detection algorithm will be designed using a simplified model of the car and tested in simulations and experiments. In chapter 4, the model based fault detection problem will be considered. A method to improve the performance of fault detection filters will be proposed in this chapter. Detailed description of the a-control will be given in chapter 5. Finally, conclusions will be drawn in chapter 6.



## Chapter 2

### Tire Blow-Out

This chapter concentrates on one specific failure scenario, viz. tire burst. One of the prime important factors in the road safety is that the vehicles in a platoon keep within their respective lanes, and do not go into the adjacent lanes. Under the tire burst scenario, there is a tendency of the vehicle to go in either left or right direction, depending on which side tire has blown out. It will be demonstrated that the disturbances that come into action because of the tire blow out are so severe that one needs to have a special controller to take care of the lateral deviations. This calls for a tire blow out monitor and a tire burst controller, so that the monitor **will** detect the tire blow out and in case of a blow out, it will switch to the tire burst controller. This type of controller/monitor structure will preserve the nice ride quality during normal operation, and also provide enhanced safety against the tire burst failure.

Organization of this chapter is as follows. In section 2.1, problem definition and background will be stated. Section 2.2 will discuss tire burst modelling. Section 2.3 will deal with the tire burst controller design and simulation study. This will be followed by the tire blow-out detection schemes in section 2.4. Finally, section 2.5 will discuss the experimental verification of the model under tire burst.

## **2.1 Background**

Tire blow out is one of the important failure scenarios in lateral control of vehicles in IVHS. Tire burst affects the road-tire interaction as well as the geometry of the vehicle to certain extent. In addition it has effect on the operating condition of the vehicle. All these changes affect lateral as well as longitudinal dynamics of the vehicle. In lateral control of the automobile, tire burst has a effect of throwing the car off course. If special consideration is not given to controller design, the tire blow out could be a potentially hazardous scenario.

A car can be modelled by a set of second order differential equations that arise from Newton's third law of motion and Euler's equations. These equations need to be modified under the tire blow out scenario. As a first task, the tire blow out and its effects on the car behavior will be modelled. This model will be used to analyze the behavior of the car in terms of lateral displacements. Based on the study of car behavior, a need for emergency controller will be demonstrated. Subsequently, a controller and tire blow-out detection algorithms will be designed to handle the tire blow out.

## **2.2 Modelling**

Tire burst modelling can be best understood by starting from the relevant facts about car modelling. Section 2.2.1 will discuss the relevant details of car modelling, followed by the tire burst model in section 2.2.2.

### **2.2.1 Car modelling**

A car is a three dimensional body with external forces acting on it because of the road-tire interaction, wind and gravity. Thus the car has twelve state variables. Three positions along the three axis, three angular positions about the three axis, and the corresponding six velocities make up the twelve states. In addition, the tire angular velocities of each of the four wheels add to the state space of the model,

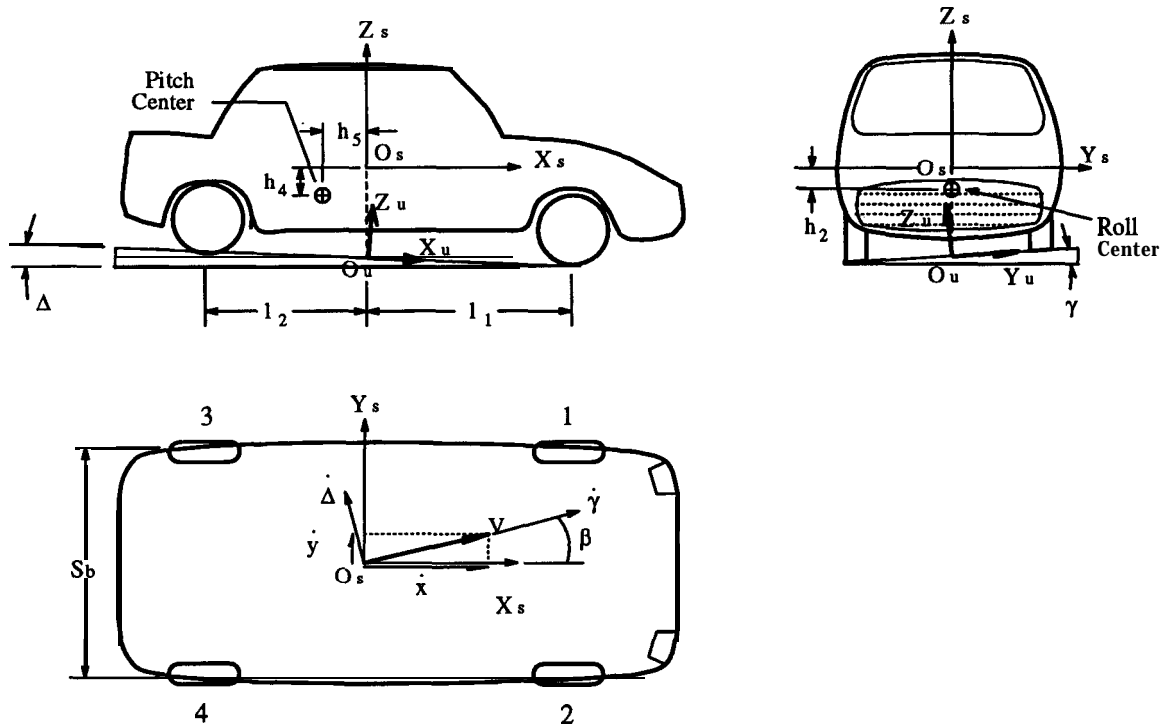


Figure 2.1: Car model - Axis definition

making a sixteen state model for the whole car. The equations governing the linear motion of the car can be derived from Newton's third law of motion applied in the direction of three axis. Equations for rotational motion can be derived from Euler's equations for the three dimensional body. Thus, the equations of motion come by following two steps:

- 1) deriving the linear/angular accelerations and velocities of the car ( linear accelerations and velocities refer to the center of gravity (CG) of the car ) in terms of the state variables.
- 2) deriving the forces acting on the car.

Quantities derived in the above two steps then go into the Newton's and Euler's equations of motion.

Figure 2.1 shows the definition of axis and the concerned variables required for deriving the car's equations of motion. Definition of the variables used in the car modelling is given in table 2.1.

Table 2.1: List of variables

Symbol	Description
$x$	displacement along $X_s$ axis
$y$	displacement along $Y_s$ axis
$z$	displacement along $Z_s$ axis
$\phi$	rotation about $X_s$ axis (roll angle)
$\theta$	rotation about $Y_s$ axis (pitch angle)
$\epsilon$	rotation about $Z_s$ axis (yaw angle)
$\epsilon_d$	desired yaw angle
$y_r$	lateral displacement of vehicle CG from road center
$\beta$	vehicle slip angle (effective)
$\gamma$	road superelevation angle in the vertical plane perpendicular to V. +ve direction of $\gamma$ : when road is sloping down towards right of the car.
$A$	road gradient angle in the vertical plane containing V. +ve direction of $A$ : when vehicle is on down going slope.
$\delta_i$	steering angle of $i^{th}$ tire
$m$	mass of the vehicle
$I_x$	moment of inertia of the sprung mass about X axis
$I_y$	moment of inertia of the sprung mass about Y axis
$I_z$	moment of inertia of the sprung mass about Z axis
$l_1$	distance of CG from front axle
$l_2$	distance of CG from rear axle
$h_2$	vertical distance of CG from roll center
$h_4$	vertical distance of CG from pitch center
$h_5$	longitudinal distance of CG from pitch center
$s_b$	track of the axles
$O_s$	CG of the sprung mass
$O_u$	projection point of unperturbed 0, on the road surface
$O_s X_s Y_s Z_s$	coordinate frame attached to the car body and along the principle axis of the car.
$O_u X_u Y_u Z_u$	coordinate frame fixed on the unsprung mass

In Fig. 2.1, point 0, is coinciding with the CG of car.  $X_s, Y_s,$  and  $Z_s$  axis are fixed to the car. Axis  $X_s$  is in the longitudinal plane of symmetry such that if it is parallel to the ground then, the car is standing on a horizontal pavement. Axis  $Z_s$  is perpendicular to  $X_s$  and is contained in the longitudinal plane of symmetry. Finally,  $Y_s$  is perpendicular to both, the  $X_s$  and  $Z_s$  axis. These axis will be assumed to be principal axis of the car so that  $I_{xy} = I_{yz} = I_{zx} = 0$ . Call  $O_s X_s Y_s Z_s$  as  $S$  frame.

The next useful co-ordinate frame is the  $U$  frame,  $O_u X_u Y_u Z_u$ , defined as follows: Point 0, is the projection of 0, on the road surface. Translate the  $S$  frame so that 0, and 0, coincide. Rotate  $S$  about  $Y_s$  by angle  $-\theta$ , so that  $X_s$  meets road surface. Call the frame that is obtained as intermediate frame (IF). Rotate IF about new  $X_s$  (that is also same as  $X_u$ ) by angle  $-\phi$  so that  $Y_s$  of IF meets ground. Call this frame as the  $U$  (see Fig. 2.1).

Both of these frames are moving frames. These frames are defined because it is convenient to calculate kinematics of the vehicle in terms of  $S$  frame, and it is convenient to calculate the forces and moments acting on the car in  $U$  frame. Now, for the sake of completeness, define a frame OXYZ which is fixes to the ground, an inertial frame. Since the kinematic and force calculations will be done in two different frames,  $S$  and  $U$ , it will be required to frequently convert vectors described in one frame to their corresponding descriptions in other frame. For this, one needs the direction cosines of  $S$  frame in terms of  $U$  frame.

#### Finding the direction cosines of $S$ in terms of $U$ :

Appendix A describes a way of finding direction cosines of a frame rotating with respect to other. Equation (A.2) can be applied to frames  $S$  and  $U$  with  $S$  rotated with respect to  $U$  by amounts  $\phi$  and  $\theta$  about  $X_s$  and  $Y_s$  axis respectively. For modelling a car in Fig. 2.1,  $D_r, \delta_x, \delta_y$  and  $\delta_z$  in Eq. (A.2) are respectively,

$$D_r = \begin{bmatrix} 1 & 0 & 0 \\ 0 & 1 & 0 \\ 0 & 0 & 1 \end{bmatrix} \quad \delta_x = \phi, \delta_y = \theta \quad \text{and} \quad \delta_z = 0 .$$

Applying Eq. (A.2) one gets the direction cosines of  $S$  as,

$$D_s = \begin{bmatrix} 1 & 0 & -\theta \\ 0 & 1 & -\phi \\ -\theta & \phi & 1 \end{bmatrix}$$

Thus, if  $\mathbf{V}_s$  and  $\mathbf{V}_u$  are descriptions of a vector in  $S$  and  $U$  frames respectively, then

$$\mathbf{V}_s = \begin{bmatrix} 1 & 0 & -\theta \\ 0 & 1 & -\phi \\ -\theta & \phi & 1 \end{bmatrix}^{-1} \mathbf{V}_u \quad (2.1)$$

Notice that  $U$  frame is obtained by rotation of  $S$  frame, or in other words,  $S$  is obtained by rotation of  $U$  frame about  $X_u$  and  $Y_u$  axis. Thus angular velocity of frame  $S$  with respect to  $U$  will be

$$\omega_{s/u} = \begin{bmatrix} \dot{\phi} \\ \dot{\theta} \\ 0 \end{bmatrix}_s \quad (2.2)$$

where the subscript  $S$  on right hand side indicates that the angular velocity vector is described in the frame  $S$ . In order to find the angular velocity of frame  $S$  with respect to the inertial frame OXYZ, one needs to find out the angular velocity  $\omega_u$  of  $U$  with respect to OXYZ and then add it to  $\omega_{s/u}$ . In the following, we will find the components of  $\omega_u$  in terms of  $U$  frame.

- 1 Road superelevation: Vector  $\dot{\gamma}$  of road tilting rate is pointing in the direction of vehicle velocity, which is at an angle  $\beta$  to the  $X_u$  axis. Thus, components of  $\omega_u$  due to road superelevation will be:

$$\begin{bmatrix} \dot{\gamma} \cos \beta & \dot{\gamma} \sin \beta & 0 \end{bmatrix}_U^T \approx \begin{bmatrix} \dot{\gamma} & \dot{\gamma} \beta & 0 \end{bmatrix}_U^T$$

Here again, the subscript  $U$  indicates that the quantity is expressed in terms of the  $U$  frame.

- 2 Road gradient: Vector  $\dot{\Delta}$  is in the direction perpendicular to vehicle velocity (see Fig. 2.1). Thus an addition to  $\omega_u$  due to road gradient will be:

$$\begin{bmatrix} -\dot{\Delta} \sin \beta & +\dot{\Delta} \cos \beta & 0 \end{bmatrix}_U^T \approx \begin{bmatrix} -\dot{\Delta} \beta & +\dot{\Delta} & 0 \end{bmatrix}_U^T$$

3 Car Yaw Rate: Define the angular velocity of rotation of  $X_u$  axis when seen in the top view of the car to be  $\dot{\epsilon}$ . This gives the additional contribution to  $w_u$ ,

$$\begin{bmatrix} -\Delta\dot{\epsilon} & \gamma\dot{\epsilon} & \dot{\epsilon} \end{bmatrix}_U^T$$

Summing the three quantities in (1), (2), and (3) gives

$$\omega_u = \begin{bmatrix} \dot{\gamma} - \dot{\Delta}\beta - \Delta\dot{\epsilon} & \dot{\gamma}\beta + \dot{\Delta} + \gamma\dot{\epsilon} & \dot{\epsilon} \end{bmatrix}_U^T \quad (2.3)$$

Finally, the angular velocity of the  $S$  frame, as described in the  $S$  frame, becomes:

$$\begin{aligned} \omega_s &= \begin{bmatrix} \dot{\phi} & \dot{\theta} & 0 \end{bmatrix}^T + D_s^{-1} \begin{bmatrix} \dot{\gamma} - \dot{\Delta}\beta - \Delta\dot{\epsilon} & \dot{\gamma}\beta + \dot{\Delta} + \gamma\dot{\epsilon} & \dot{\epsilon} \end{bmatrix}^T \\ &= \begin{bmatrix} \dot{\phi} + (\theta - \Delta)\dot{\epsilon} + \dot{\gamma} - \beta\dot{\Delta} \\ \dot{\theta} + (\phi + \gamma)\dot{\epsilon} + \dot{\Delta} + \beta\dot{\gamma} \\ \dot{\epsilon} + (\Delta\theta + \phi\gamma)\dot{\epsilon} - (\theta + \phi\beta)\dot{\gamma} - (\phi - \theta\beta)\dot{\Delta} \end{bmatrix}_S \end{aligned} \quad (2.4)$$

Let the the velocity  $V$  of 0, be  $\begin{bmatrix} \dot{x} & \dot{y} & \dot{z} \end{bmatrix}^T$ : i.e.  $V = \dot{x}\hat{i}_s + \dot{y}\hat{j}_s + \dot{z}\hat{k}_s$ , where,  $\hat{i}_s, \hat{j}_s$  and  $\hat{k}_s$  represent unit vectors in the directions of  $X_s, Y_s$ , and  $Z_s$  respectively.

Differentiating the velocity  $V$  with respect to time gives

$$\begin{aligned} \dot{V} &= \ddot{x}\hat{i}_s + \ddot{y}\hat{j}_s + \ddot{z}\hat{k}_s + \dot{x}\omega_s \times \hat{i}_s + \dot{y}\omega_s \times \hat{j}_s + \dot{z}\omega_s \times \hat{k}_s \\ &= \begin{bmatrix} \ddot{x} - \dot{y}\dot{\epsilon} + \theta\dot{\gamma}\dot{y} - \theta\beta\dot{\Delta}\dot{y} - \Delta\theta\dot{y}\dot{\epsilon} + \phi\beta\dot{\gamma}\dot{y} + \phi\dot{\Delta}\dot{y} + \phi\gamma\dot{\epsilon}\dot{y} \\ \quad + \dot{\theta}\dot{z} + \beta\dot{\gamma}\dot{z} + \dot{\Delta}\dot{z} + \gamma\dot{\epsilon}\dot{z} + \phi\dot{\epsilon}\dot{z} \\ \ddot{y} + \dot{\epsilon}\dot{x} - \theta\dot{\gamma}\dot{x} + \theta\beta\dot{\Delta}\dot{x} + \Delta\theta\dot{\epsilon}\dot{x} - \phi\beta\dot{\gamma}\dot{x} - \phi\dot{\Delta}\dot{x} - \phi\gamma\dot{\epsilon}\dot{x} \\ \quad - \dot{\phi}\dot{z} - \dot{\gamma}\dot{z} + \beta\dot{\Delta}\dot{z} + \Delta\dot{\epsilon}\dot{z} - \theta\dot{\epsilon}\dot{z} \\ \ddot{z} - \dot{\theta}\dot{x} - \beta\dot{\gamma}\dot{x} - \dot{\Delta}\dot{x} - \gamma\dot{\epsilon}\dot{x} - \phi\dot{\epsilon}\dot{x} + \dot{\phi}\dot{y} + \dot{\gamma}\dot{y} \\ \quad - \beta\dot{\Delta}\dot{y} - \Delta\dot{\epsilon}\dot{y} + \theta\dot{\epsilon}\dot{y} \end{bmatrix}_S \end{aligned} \quad (2.5)$$

Let  $\omega_s = [\omega_{sx} \ \omega_{sy} \ \omega_{sz}]^T$ . Differentiating each of  $w_x$ ,  $w_y$  and  $w_z$  gives,

$$\begin{bmatrix} \dot{\omega}_{sx} \\ \dot{\omega}_{sy} \\ \dot{\omega}_{sz} \end{bmatrix} = \begin{bmatrix} \ddot{\phi} + \ddot{\epsilon}(\theta - \Delta) + \dot{\epsilon}(\dot{\theta} - \dot{\Delta}) + \ddot{\gamma} - \dot{\Delta}\dot{\beta} - \beta\ddot{\Delta} \\ \ddot{\theta} + \ddot{\epsilon}(\phi + \gamma) + \dot{\epsilon}(\dot{\phi} + \dot{\gamma}) + \ddot{\Delta} + \dot{\gamma}\dot{\beta} + \beta\ddot{\gamma} \\ \ddot{\epsilon} - \ddot{\epsilon}(-\Delta\theta + \phi\gamma) - \dot{\epsilon}(-\dot{\Delta}\theta - \Delta\dot{\theta} + \dot{\phi}\gamma + \phi\dot{\gamma}) \\ -\ddot{\gamma}(\theta + \phi\beta) - \dot{\gamma}(\dot{\theta} + \dot{\phi}\beta + \phi\dot{\beta}) - \dot{\Delta}(\phi - \theta\beta) \\ -\dot{\Delta}(\dot{\phi} - \dot{\theta}\beta - \theta\dot{\beta}) \end{bmatrix} \quad (2.6)$$

This completes the calculations of the vehicle kinematics. Now, consider the forces acting on the car.

- 1 Air drag: Air drag that acts on the vehicle has the direction opposite to the vehicle velocity and is proportional to it. This gives the wind force  $\mathbf{F}_w$  to be

$$\mathbf{F}_w = \begin{bmatrix} F_{wx} \\ F_{wy} \\ F_{wz} \end{bmatrix}_S = \begin{bmatrix} -K_{wx}\dot{x} \\ -K_{wy}\dot{y} \\ -K_{wz}\dot{z} \end{bmatrix}_S \approx \begin{bmatrix} -K_{wx}\dot{x} \\ -K_{wy}\dot{y} \\ 0 \end{bmatrix}_S \quad (2.7)$$

where,  $K_{wx}$ ,  $K_{wy}$  and  $K_{wz}$  are the air drag coefficients in the respective directions.

- 2 Gravity: Gravitational force acts vertically through the CG of the car. This gives the gravitational force  $\mathbf{F}_G$ , expressed in  $S$  and  $U$  frames as

$$\begin{aligned} \mathbf{F}_G &= \begin{bmatrix} F_{gx} \\ F_{gy} \\ F_{gz} \end{bmatrix}_U \approx \begin{bmatrix} mg\Delta \\ -mg\gamma \\ -mg \end{bmatrix}_U \\ \mathbf{F}_G &= \begin{bmatrix} mg(\Delta + \theta) \\ -mg(\gamma + \phi) \\ -mg(1 - \Delta\theta - \gamma\phi) \end{bmatrix}_S \approx \begin{bmatrix} mg(\Delta + \theta) \\ -mg(\gamma + \phi) \\ -mg \end{bmatrix}_S \end{aligned} \quad (2.8)$$

The  $\approx$  sign is used to emphasize the small angle approximations.



3 Suspension force: The suspension of the vehicle is assumed to consist of a spring and a shock absorber at each of the wheels. The spring and the damper forces are determined by the deflections and rates of deflections of the suspension struts. These deflections can be calculated from the basic geometry of the vehicle as follows. Letting  $e_i, i = 1, \dots, 4$  to represent the deflections of the suspension struts,

$$\begin{aligned} e_1 &= z_0 - z + h_5\theta + l_1\theta - \frac{s_{b1}}{2}\phi \\ e_2 &= z_0 - \delta + h_5\theta + l_1\theta + \frac{s_{b1}}{2}\phi \\ e_3 &= z_0 - z + h_5\theta - l_2\theta - \frac{s_{b1}}{2}\phi \\ e_4 &= z_0 - z + h_5\theta - l_2\theta + \frac{s_{b1}}{2}\phi \end{aligned} \quad (2.9)$$

where  $z_0$  is the original height of the CG from ground and all other quantities are defined in Table 2.1. The spring force is assumed to be governed by :

$$P_{Fi} = C_{1i}(e_i + C_{2i}e_i^5) \quad i = 1, \dots, 4 \quad (2.10)$$

where  $C_{1i}$  and  $C_{2i}$  are spring constants. The damping force is modelled as:

$$\begin{aligned} P_{Di} &= D_i\dot{e}_i & |\dot{e}_i| < \bar{w} \quad i = 1, \dots, 4 \\ &= D_i\bar{w} + \bar{D}_i(\dot{e}_i - \bar{w}) & \dot{e}_i \geq \bar{w} \\ &= -D_i\bar{w} + \bar{D}_i(\dot{e}_i + \bar{w}) & \dot{e}_i \leq -\bar{w} \end{aligned} \quad (2.11)$$

Finally, the vertical force acting on each of the tires becomes:

$$\begin{aligned} F_{Pi} &= \frac{mgl_2}{2(l_1 + l_2)} + F_{Di} + F_{Fi} \quad i = 1, 2 \\ F_{Pi} &= \frac{mgl_1}{2(l_1 + l_2)} + F_{Di} + F_{Fi} \quad i = 3, 4 \end{aligned} \quad (2.12)$$

Thus, the suspension force  $\mathbf{F}_{Pi}$  acting at the  $i^{\text{th}}$  strut becomes:

$$\mathbf{F}_{Pi} = \begin{bmatrix} 0 \\ 0 \\ F_{Pi} \end{bmatrix}_{IU} = \begin{bmatrix} -\theta \mathbf{1}_i \\ \phi F_{Pi} \\ F_{Pi} \end{bmatrix}_s \quad (2.13)$$

4 Tire force: Tire and road interaction generates force that depends on the factors like slip angle, slip ratio, road condition, normal force acting on each of the tires.

Slip angle ( $\alpha$ ) is the angle between the plane of a tire and the linear velocity vector of the coincident point of the car. Let  $\zeta_i$  be the angle that velocity vector of  $i^{\text{th}}$  wheel makes with the  $X_s$  axis. Then the slip angle  $\alpha_i$  of the  $i^{\text{th}}$  wheel can be defined as follows:

$$\alpha_i = \delta_i - \zeta_i \quad (2.14)$$

where,

$$\begin{aligned} \tan(\zeta_1) &= \frac{\dot{y} + l_1\dot{\epsilon}}{\dot{x} - \frac{s_{b1}\dot{\epsilon}}{2}} & \tan(\zeta_2) &= \frac{\dot{y} + l_1\dot{\epsilon}}{\dot{x} + \frac{s_{b1}\dot{\epsilon}}{2}} \\ \tan(\zeta_3) &= \frac{\dot{y} - l_2\dot{\epsilon}}{\dot{x} - \frac{s_{b2}\dot{\epsilon}}{2}} & \tan(\zeta_4) &= \frac{\dot{y} - l_2\dot{\epsilon}}{\dot{x} + \frac{s_{b2}\dot{\epsilon}}{2}} \end{aligned} \quad (2.15)$$

The tire slip ratio  $\lambda_i$  for  $i^{\text{th}}$  tire is defined as

$$\begin{aligned} \lambda_i &= \frac{r_i\omega_i - V_i \cos(\alpha_i)}{V_i \cos(\alpha_i)} & \text{for braking} \\ \lambda_i &= \frac{r_i\omega_i - V_i \cos(\alpha_i)}{r_i\omega_i} & \text{for traction} \end{aligned} \quad (2.16)$$

Here,  $V_i$  is the translational speed of the  $i^{\text{th}}$  tire, computed from

$$\begin{aligned} V_1 &= \sqrt{(\dot{y} + l_1\dot{\epsilon})^2 + (\dot{x} - \frac{s_{b1}\dot{\epsilon}}{2})^2} \\ V_2 &= \sqrt{(\dot{y} + l_1\dot{\epsilon})^2 + (\dot{x} + \frac{s_{b1}\dot{\epsilon}}{2})^2} \\ V_3 &= \sqrt{(\dot{y} - l_2\dot{\epsilon})^2 + (\dot{x} - \frac{s_{b2}\dot{\epsilon}}{2})^2} \\ v_4 &= \sqrt{(\dot{y} - l_2\dot{\epsilon})^2 + (\dot{x} + \frac{s_{b2}\dot{\epsilon}}{2})^2} \end{aligned} \quad (2.17)$$

$r_i$  is the effective radius of the  $i^{\text{th}}$  tire, and  $\omega_i$  is the angular velocity of the  $i^{\text{th}}$  tire.  $r_i$  is computed by

$$r_i = r_{out} - \frac{F_{Pi}}{K_{zi}} \quad (2.18)$$

where  $r_{out}$  is the outer radius of the tire and  $K_{zi}$  is the stiffness of the tire in vertical direction.

Let's define a road condition factor  $r_c$ . The road condition factor  $r_{ci}$  of the  $i^{th}$  tire is a scaling factor for corresponding tire force. This factor is used to account for the various factors such as temperature, tire slip speed, camber angle, and road pavement material.  $r_{ci}$  takes values between zero and one depending on all the above factors. Appendix B describes the empirical functions  $F_{ta}(\alpha, \lambda, F_P, r_c)$  and  $F_{tb}(\alpha, \lambda, F_P, r_c)$  to calculate the tire forces.  $F_{ta}$  is the tire force generated in the plane of the tire and  $F_{tb}$  is the tire force in the direction perpendicular to the plane of the tire. Finally the tire force generated at the  $i^{th}$  tire in lateral and longitudinal directions become:

longitudinal tire force

$$F_{txi} = F_{tai} \cos(\delta_i) - F_{tbi} \sin(\delta_i) \quad (2.19)$$

lateral tire force

$$F_{tyi} = F_{tai} \sin(\delta_i) + F_{tbi} \cos(\delta_i) \quad (2.20)$$

where,  $F_{tai} = F_{ta}(\alpha_i, \lambda_i, F_{Pi}, r_{ci})$ , and  $F_{tbi} = F_{tb}(\alpha_i, \lambda_i, F_{Pi}, r_{ci})$ . Equations (2.19) and (2.20) give the  $i^{th}$  tire force  $\mathbf{F}_{Ti}$  to be:

$$\mathbf{F}_{Ti} = \begin{bmatrix} F_{txi} \\ F_{tyi} \\ 0 \end{bmatrix}_U = \begin{bmatrix} F_{txi} \\ F_{tyi} \\ \theta F_{txi} - \phi F_{tyi} \end{bmatrix}_S \quad (2.21)$$

Combining Eqs. (2.7), (2.8), (2.13) and (2.21), force acting on the vehicle  $\mathbf{F}$  becomes:

$$\begin{aligned} \mathbf{I} \dot{\mathbf{v}} &= \mathbf{F}_w + \mathbf{F}_G + \sum_{i=1}^4 \mathbf{F}_{Pi} + \sum_{i=1}^4 \mathbf{F}_{Ti} \\ \mathbf{F} &= \begin{bmatrix} -K_{wx}\dot{x} + mg(\Delta + \theta) - \sum_{i=1}^4 \theta F_{Pi} + \sum_{i=1}^4 F_{txi} \\ -K_{wy}\dot{y} - mg(\gamma + \phi) + \sum_{i=1}^4 \phi F_{Pi} + \sum_{i=1}^4 F_{tyi} \\ -K_{wz}\dot{z} - mg(1 - \Delta\theta - \gamma\phi) + \sum_{i=1}^4 F_{Pi} + \sum_{i=1}^4 (\theta F_{txi} - \phi F_{tyi}) \end{bmatrix}_S \end{aligned} \quad (2.22)$$

The moments acting on the car will be first computed in the  $U$  frame and then converted into the  $S$  frame. The moments in the  $U$  frame are

$$M_{xu} = \left(\frac{s_{b1}}{2} + h_2\phi\right)F_{P1} + \left(\frac{s_{b2}}{2} + h_2\phi\right)F_{P3} - \left(\frac{s_{b1}}{2} - h_2\phi\right)F_{P2}$$

$$- \left( \frac{s_{b2}}{2} - h_2\phi \right) F_{P4} + (z - h_5\theta) \sum_{i=1}^4 F_{tyi} \quad (2.23)$$

$$\begin{aligned} M_{yu} &= (l_2 + h_4\theta)(F_{P3} + F_{P4}) - (l_1 - h_4\theta)(F_{P1} + F_{P2}) \\ &- (z - h_5\theta) \sum_{i=1}^4 F_{txi} \end{aligned} \quad (2.24)$$

$$\begin{aligned} M_{zu} &= (l_1 - h_4\theta)(F_{ty1} + F_{ty2}) - (l_2 + h_4\theta)(F_{ty3} + F_{ty4}) \\ &- \left( \frac{s_{b1}}{2} + h_2\phi \right) F_{tx1} - \left( \frac{s_{b2}}{2} + h_2\phi \right) F_{tx3} + \left( \frac{s_{b1}}{2} - h_2\phi \right) F_{tx2} \\ &+ \left( \frac{s_{b2}}{2} - h_2\phi \right) F_{tx4} \end{aligned} \quad (2.25)$$

These moments when converted into  $S$  frame give

$$\begin{bmatrix} M_{xs} \\ M_{ys} \\ M_{zs} \end{bmatrix}_S = \begin{bmatrix} M_{xu} - \theta M_{zu} \\ M_{yu} + \phi M_{zu} \\ M_{zu} + \theta M_{xu} - \phi M_{yu} \end{bmatrix} \quad (2.26)$$

The equations governing the dynamics of the vehicle can be written from Newton's law and the Euler's equations as

$$\mathbf{F} = m\dot{\mathbf{V}} \quad (2.27)$$

$$M_{xs} = I_x \dot{\omega}_{sx} - (I_y - I_z) \omega_{sy} \omega_{sz} \quad (2.28)$$

$$M_{ys} = I_y \dot{\omega}_{sy} - (I_z - I_x) \omega_{sz} \omega_{sx} \quad (2.29)$$

$$M_{zs} = I_z \dot{\omega}_{sz} - (I_x - I_y) \omega_{sx} \omega_{sy} \quad (2.30)$$

Combining Eqs. (2.27)-(2.30) with Eqs. (2.4)-(2.6) and Eqs.(2.22)-(2.26) gives the final equations of vehicle dynamics as

$$\begin{aligned} m[\ddot{x} - \dot{y}\dot{\epsilon} + \theta\dot{\gamma}\dot{y} - \theta\beta\dot{\Delta}\dot{y} - \Delta\theta\dot{y}\dot{\epsilon} + \phi\beta\dot{\gamma}\dot{y} + \phi\dot{\Delta}\dot{y} + \phi\gamma\dot{\epsilon}\dot{y} \\ + \dot{\theta}\dot{z} + \beta\dot{\gamma}\dot{z} + \dot{\Delta}\dot{z} + \gamma\dot{\epsilon}\dot{z} + \phi\dot{\epsilon}\dot{z}] = \\ -K_{wx}\dot{x} + mg(\Delta + \theta) - \sum_{i=1}^4 \theta F_{Pi} + \sum_{i=1}^4 F_{txi} \end{aligned} \quad (2.31)$$

$$\begin{aligned} m[\ddot{y} + \dot{\epsilon}\dot{x} - \theta\dot{\gamma}\dot{x} + \theta\beta\dot{\Delta}\dot{x} + \Delta\theta\dot{\epsilon}\dot{x} - \phi\beta\dot{\gamma}\dot{x} - \phi\dot{\Delta}\dot{x} - \phi\gamma\dot{\epsilon}\dot{x} \\ - \dot{\phi}\dot{z} - \dot{\gamma}\dot{z} + \beta\dot{\Delta}\dot{z} + \Delta\dot{\epsilon}\dot{z} - \theta\dot{\epsilon}\dot{z}] = \\ -K_{wy}\dot{y} - mg(\gamma + \phi) + \sum_{i=1}^4 \phi F_{Pi} + \sum_{i=1}^4 F_{tyi} \end{aligned} \quad (2.32)$$

$$\begin{aligned}
& m[\ddot{z} - \dot{\theta}\dot{x} - \beta\dot{\gamma}\dot{x} - \dot{\Delta}\dot{x} - \gamma\dot{\epsilon}\dot{x} - \phi\dot{\epsilon}\dot{x} \\
& + \dot{\phi}\dot{y} + \dot{\gamma}\dot{y} - \beta\dot{\Delta}\dot{y} - \Delta\dot{\epsilon}\dot{y} + \theta\dot{\epsilon}\dot{y}] = \\
& -K_{\omega z}\dot{z} - mg(1 - \Delta\theta - \gamma\phi) + \sum_{i=1}^4 F_{Pi} + \sum_{i=1}^4 (\theta F_{txi} - \phi F_{tyi}) \tag{2.33}
\end{aligned}$$

$$\begin{aligned}
I_x[\ddot{\phi} + \ddot{\epsilon}(\theta - A) + \dot{\epsilon}(\dot{\theta} - A) + \ddot{\gamma} - \dot{\Delta}\dot{\beta} - \beta\ddot{\Delta}] - (I_y - I_x)(\dot{\theta} + \dot{\Delta})\dot{\epsilon} = \\
M_{xu} - \theta M_{zu} \tag{2.34}
\end{aligned}$$

$$\begin{aligned}
I_y[\ddot{\theta} + \ddot{\epsilon}(\phi + \gamma) + \dot{\epsilon}(\dot{\phi} + \dot{\gamma}) + \ddot{\Delta} + \dot{\gamma}\dot{\beta} + \beta\ddot{\gamma}] - (I_z - I_x)(\dot{\phi} + \dot{\gamma})\dot{\epsilon} = \\
M_{yu} + \phi M_{zu} \tag{2.35}
\end{aligned}$$

$$\begin{aligned}
I_z[\ddot{\epsilon} - \ddot{\epsilon}(-\Delta\theta + \phi\gamma) - \dot{\epsilon}(-\dot{\Delta}\theta - \Delta\dot{\theta} + \dot{\phi}\dot{\gamma} + \phi\dot{\gamma}) - \ddot{\gamma}(\theta + \phi\beta) \\
- \dot{\gamma}(\dot{\theta} + \dot{\phi}\beta + \phi\dot{\beta}) - \ddot{\Delta}(\phi - \theta\beta) - \dot{\Delta}(\dot{\phi} - \dot{\theta}\beta - \theta\dot{\beta})] \\
- (I_z - I_y)(\dot{\phi} + \dot{\gamma})(\dot{\theta} + \dot{\Delta}) = \\
M_{zu} + \theta M_{xu} - \phi M_{yu} \tag{2.36}
\end{aligned}$$

Let the moment of inertia of the front and rear axles, and the associated rotating parts be  $I_f$  and  $I_r$ . For the driving wheels, the moment of inertia consist of the moment of inertia of rotating parts of the drive train and the engine, calculated at wheel speed. Then, the dynamics of the wheels of the car can be described by

$$T_{ei} - r_i \cdot F_{tai} = I_i \dot{\omega}_i \tag{2.37}$$

where  $I_i = I_f$  for  $i = 1, 2$  and  $I_i = I_r$ , for  $i = 3, 4$  and  $T_{ei}$  represents the engine torque acting on the  $i^{\text{th}}$  wheel.

Equations (2.31) to (2.37) represent the dynamic equations of the vehicle and the wheels.

### 2.2.2 Tire burst modelling

A tire burst that severely affects the vehicle behavior may be caused by rupturing of the tire suddenly because of the nails or any such items that the tire may encounter. This could also happen in case of severe maneuvers when the bead detachment occurs because of the severe lateral forces.

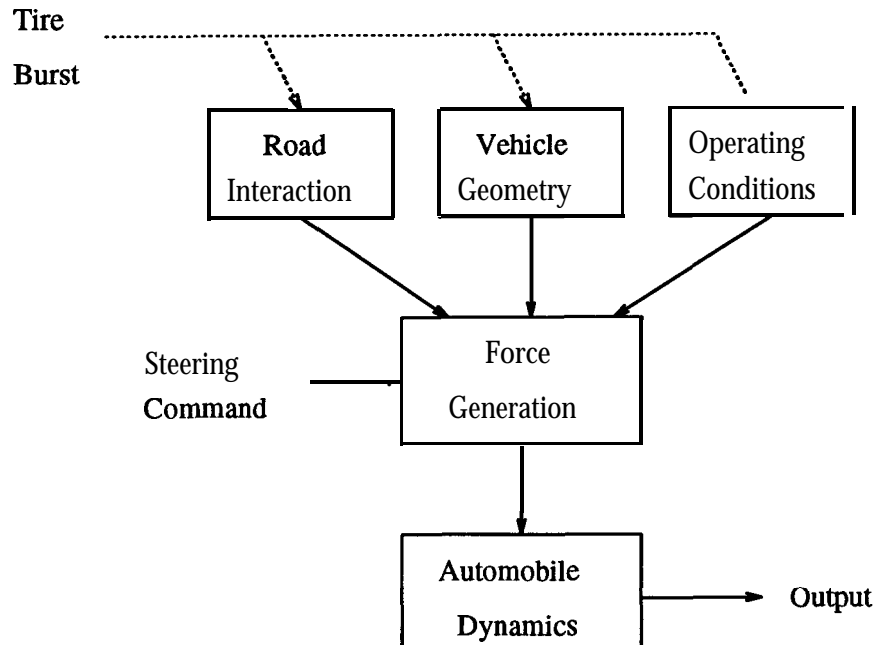


Figure 2.2: Effect of tire burst on vehicle dynamics

At very first there is a opening in the walls of the tire. The air then escapes through the opening. As time progresses, the pressure of the air inside the tire goes on decreasing until it reaches atmospheric pressure. Tire stiffness in vertical direction depends directly on pressure in the tire. In turn, as the pressure in the tire goes on decreasing, the tire flattens out under the load of the vehicle. Several of the tire burst effects are consequences of the geometry changes that happen because of tire flattening out. Other effects of the tire burst come from the **tire-road** characteristics changes, changes in the tire itself, and changes in operating conditions of the vehicle (see Fig. 2.2). All of these effects start affecting the car dynamics from the instance of tire wall rupture and progressively increases in intensity until all the air in the tire has escaped. In the following, each of the effects of tire burst are discussed in detail.

1 Tire radius change: Equation (2.18) governs the effective tire radius under no

burst condition. It is repeated here for convenience.

$$r_i = r_{out} - \frac{F_{Pi}}{K_{tyre_i}}$$

Let  $\tau$  be the instance of tire burst and  $T$  be the time required for complete flattening of the tire. From time  $t = \tau$  to time  $t = \tau + T$ , **the tire stiffness goes** on decreasing from initial value to zero. In addition, when the wheel rim touches ground, the stiffness of the tire goes to a very high value. Specifically, if  $j^{\text{th}}$  tire has blown out, then the wheel vertical deflection characteristics of that tire become

$$\begin{aligned} K_{tyre_j} &= K_{zj} & t, \tau \\ K_{tyre_j} &= K_{zj} - K_{zj} \frac{t - \tau}{T} & \tau \leq t \leq \tau + T \\ K_{tyre_j} &= 0 & t > \tau + T \end{aligned} \quad (2.38)$$

and

$$\begin{aligned} r_j &= r_{out} - \frac{F_{Pj}}{K_{tyre_j}} & F_{Pj} < (r_{out} - r_{in})K_{tyre_j} \\ r_j &= r_{in} & F_{Pj} \geq (r_{out} - r_{in})K_{tyre_j} \end{aligned}$$

Because of the change in the the effective radius, the slip ratio at the contact point C changes (Fig 2.3).

2 Time required for deflation: The time required for complete deflation of the tire can be estimated from the following calculations.

Let

- $v_i$  = volume of air inside the tire before burst
- $v_f$  = volume of air inside the tire after burst
- $p, v$  = integration variables for pressure and volume of air in the tire
- $p^*$  = gauge tire pressure before burst
- $p_a$  = atmospheric pressure
- $\rho_a$  = air density at  $p_a$
- $T$  = time required for deflation
- $A$  = area of the opening in the tire
- $C_q$  = flow coefficient of the opening
- $u_a$  = velocity of air at the opening
- $m_t$  = mass flow rate at the opening

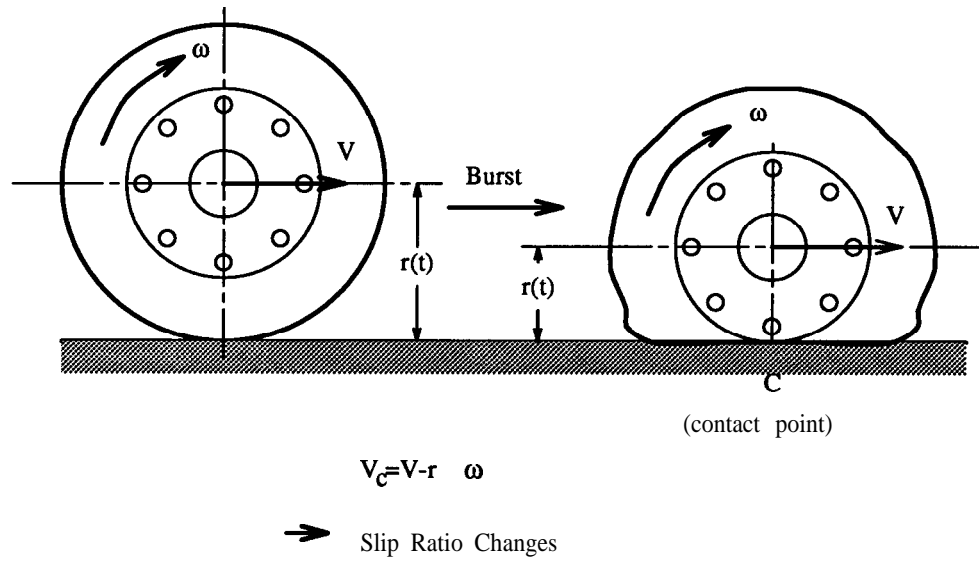


Figure 2.3: Tire burst, radius change

It is assumed that air inside the tire expands adiabatically, and the pressure inside the tire falls linearly from  $p^* + p_a$  to  $p_a$  in time  $T$ .

Consider a unit mass of air with pressure  $p_t$  and volume  $v_t$  inside the tire before it approaches the opening. When this mass of air goes to the opening, it expands to the pressure  $p_a$  with volume  $\frac{1}{\rho_a}$ . Under the adiabatic assumption,  $p v^{1.4} = \text{constant}$  during the expansion: i.e.

$$p_t v_t^{1.4} = p_a \frac{1}{\rho_a^{1.4}} \Rightarrow v_t = \left( \frac{p_a}{p_t} \right)^{0.71} \frac{1}{\rho_a}$$

Work done by the air during this expansion is

$$W = \int_{v_t}^{\frac{1}{\rho_a}} p \, dv$$

Note that,  $p v^{1.4} = \text{const}$  implies  $p \, dv = -0.71 v \, dp$ . Thus,

$$W = -0.71 \int_{p_t}^{p_a} v \, dp = 0.71 \int_{p_a}^{p_t} \left( \frac{p_a}{p} \right)^{0.71} \frac{1}{\rho_a} \, dp = 2.45 \frac{p_a}{\rho_a} \left[ \left( \frac{p_t}{p_a} \right)^{0.29} - 1 \right]$$

This work will appear in the form of kinetic energy of the unit mass of air.

Then the velocity of the unit mass at the opening becomes

$$\frac{1}{2} u_a^2 = 2.45 \frac{p_a}{\rho_a} \left[ \left( \frac{p_t}{p_a} \right)^{0.29} - 1 \right] \Rightarrow u_a = \sqrt{4.9 \frac{p_a}{\rho_a} \left[ \left( \frac{p_t}{p_a} \right)^{0.29} - 1 \right]}$$



This gives the mass flow rate of air to be  $\dot{m}_t = A\rho_a C_q u_a$ . Total mass of air escaped in time  $T$  is

$$\begin{aligned}
 \int_0^T \dot{m}_t dt &= \text{initial mass} - \text{final mass} \\
 &\Rightarrow A\rho_a C_q \int_0^T \sqrt{4.9 \frac{p_a}{\rho_a} \left[ \left( \frac{p_t}{p_a} \right)^{0.29} - 1 \right]} dt \\
 &= v_i \rho_a \left( \frac{p^* + p_a}{p_a} \right)^{0.71} - v_f \rho_a \\
 &\Rightarrow \frac{2.21 A C_q}{\sqrt{\rho_a}} \int_0^T \sqrt{\left[ \left( \frac{p_t}{p_a} \right)^{0.29} - 1 \right]} dt \\
 &= v_i \frac{(p^* + p_a)^{0.71}}{p_a^{1.21}} - v_f \frac{1}{p_a^{0.5}} \tag{2.39}
 \end{aligned}$$

Equation (2.39) can be solved for  $A$  if  $T$  is specified. Plot of  $T$  vs.  $A$  is shown in Fig. 2.4 for the following values of other variables ( $r_o = 0.3044m$ ,  $r_i = 0.1825m$ , and  $w = 0.15m$  are outer radius, inner radius and width of the tire respectively, see Fig. 2.5):

$$\begin{aligned}
 v_i &= \pi(r_{out}^2 - r_{in}^2)w = 0.0280m^3 \\
 v_f &= (\pi(r_{out}^2 - r_{in}^2) - \sin^{-1}\left(\frac{2\sqrt{r_{out}^2 - r_{in}^2}}{2r_{out}}\right)r_{out}^2 \\
 &\quad + r_{in}\sqrt{r_{out}^2 - r_{in}^2})w = 0.0217m^3 \\
 \rho_a &= 1.2kg/m^3 \\
 p_a &= 1.014 \times 10^5 N/m^2 \\
 p^* &= 300 \times 10^3 N/m^2 \\
 C_q &= 0.7
 \end{aligned}$$

Figure 2.4 helps to determine what is a reasonable guess for the deflation time of the tire. For example, if one asserts that a hole of about an inch diameter is a typical opening in case of a burst, the time of deflation can be read off the Fig. 2.4 to be about 0.8sec.

- 3 Suspension force rearrangement: The static components of forces in each of the four suspension changes under the effect of tire burst. The reason

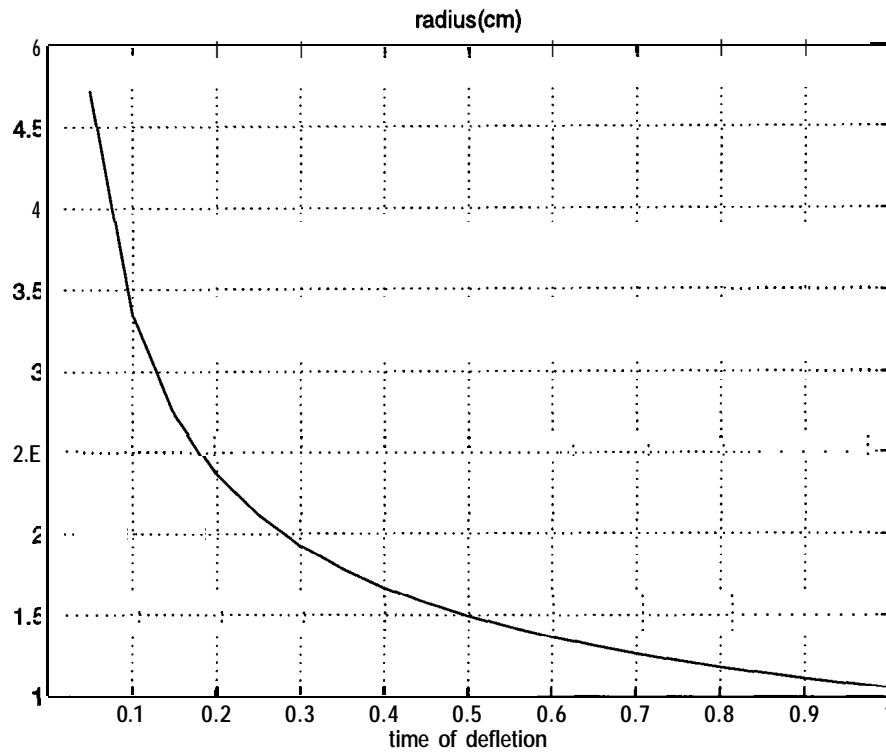


Figure 2.4: Time of deflation vs. area of opening

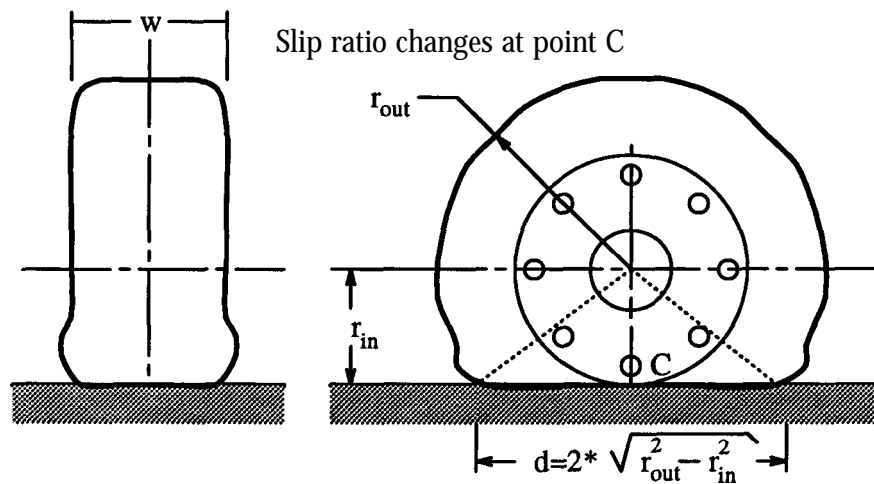


Figure 2.5: Geometry of flat tire

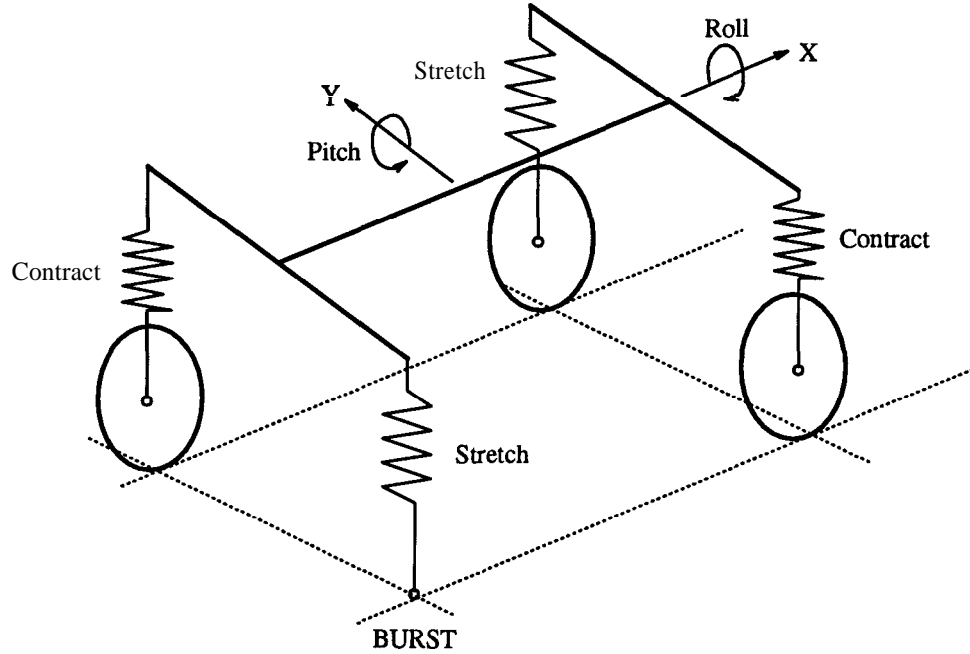


Figure 2.6: Suspension force rearrangement

for this to happen is that after the tire burst, suspension at the tire that has blown and the one at diagonally opposite point get stretched. Remaining two suspensions get compressed (see Fig. 2.6). Suspension force rearrangement can be computed by considering the geometry in Fig. 2.7. Summation of vertical forces gives

$$F_{P1} + F_{P2} + F_{P3} + F_{P4} = mg$$

Also, taking moments about EB, CD, ED, and BC give

$$F_{P1} + F_{P2} = \frac{l_2}{l_1 + l_2} mg$$

$$F_{P3} + F_{P4} = \frac{l_1}{l_1 + l_2} mg$$

$$F_{P1} + F_{P3} = F_{P2} + F_{P4}$$

Solving these equations,

$$F_{P1} = \frac{1}{2} \left( \frac{mgl_2}{l_1 + l_2} - f \right) \quad F_{P2} = \frac{1}{2} \left( \frac{mgl_2}{l_1 + l_2} + f \right)$$

$$F_{P3} = \frac{1}{2} \left( \frac{mgl_1}{l_1 + l_2} + f \right) \quad F_{P4} = \frac{1}{2} \left( \frac{mgl_1}{l_1 + l_2} - f \right) \quad (2.40)$$

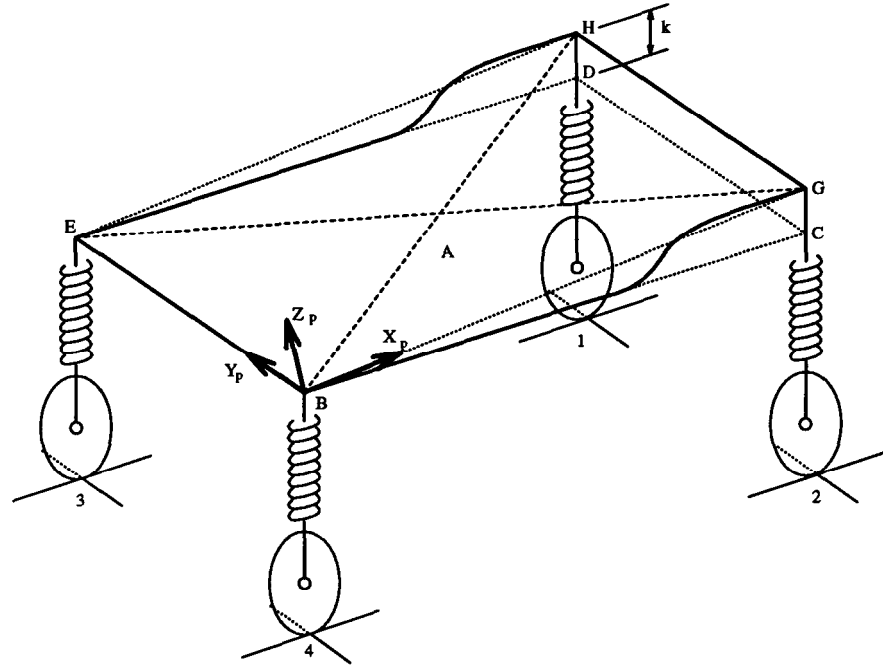


Figure 2.7: Suspension force rearrangement

where,  $f$  is a free parameter to be determined as follows. Let the  $h_i(\cdot)$  be the equation governing the spring force in  $i^{\text{th}}$  suspension. i.e. if  $z_p$  is the length of  $i^{\text{th}}$  suspension with force,  $F_{P_i}$  then  $F_{P_i} = h_i(z_p)$ . Also let the front suspensions be  $k$  meters longer than the rear suspensions. By equating the positions of point A derived from (i) pair EC and from (ii) pair BD in Fig. 2.7, one gets

$$\begin{aligned} r_1 + r_4 + h_1^{-1}(F_{P1}) + h_4^{-1}(F_{P4}) - k = \\ r_2 + r_3 + h_2^{-1}(F_{P2}) + h_3^{-1}(F_{P3}) - k \end{aligned} \quad (2.41)$$

Solution of Eq. (2.40) and Eq. (2.41) gives each of the suspension forces. These equations need to be solved whenever the tire radius changes in case of a tire blow out.

- 4 Rotation because of tire burst: Consider the plane EBGH of Fig. 2.7. Fix a co-ordinate frame on this plane with  $X_p$  axis along EB,  $Y_p$  along BG, and  $Z_p$  being normal to the plane. Let the direction cosines of  $X_p Y_p Z_p$  before burst

and in static condition be:

$$\begin{bmatrix} \mathbf{n} & 0 \\ 0 & \mathbf{1} \\ -l & 0 \end{bmatrix}$$

with  $n = \cos(\angle GBC)$  and  $l = -\sin(\angle GBC)$ . Let  $[\Delta l_1 \ \Delta m_1 \ \Delta n_1]^T$ ,  $[\Delta l_2 \ \Delta m_2 \ \Delta n_2]^T$ , and  $[\Delta l_3 \ \Delta m_3 \ \Delta n_3]^T$  be changes in direction cosines of frame  $X_p Y_p Z_p$ . Then, using Eq. (A.2), one can write

$$\begin{bmatrix} \Delta l_1 & \Delta l_2 & \Delta l_3 \\ \Delta m_1 & \Delta m_2 & \Delta m_3 \\ \Delta n_1 & \Delta n_2 & \Delta n_3 \end{bmatrix} = \begin{bmatrix} n & 0 & l \\ 0 & 1 & 0 \\ -l & 0 & n \end{bmatrix} \begin{bmatrix} 0 & -\delta_{z_o} & \delta_{y_o} \\ \delta_{z_o} & 0 & -\delta_{x_o} \\ -\delta_{y_o} & \delta_{x_o} & 0 \end{bmatrix} \quad (2.42)$$

where  $\delta_{x_o}$ ,  $\delta_{y_o}$ , and  $\delta_{z_o}$  are rotations in  $X_p Y_p Z_p$  frame. Let the vehicle rotate by  $\delta_x$  and  $\delta_y$  about  $X_s$  and  $Y_s$  because of the tire burst. This means that the vehicle rotates by

$$\begin{bmatrix} \delta_{x_o} \\ \delta_{y_o} \\ \delta_{z_o} \end{bmatrix} = \begin{bmatrix} n & 0 & -l \\ 0 & 1 & 0 \\ l & 0 & n \end{bmatrix} \begin{bmatrix} \delta_x \\ \delta_y \\ 0 \end{bmatrix} = \begin{bmatrix} n\delta_x \\ \delta_y \\ l\delta_x \end{bmatrix} \quad (2.43)$$

Combining Eq. (2.42) and (2.43);

$$\begin{bmatrix} \Delta l_1 & \Delta l_2 & \Delta l_3 \\ \Delta m_1 & \Delta m_2 & \Delta m_3 \\ \Delta n_1 & \Delta n_2 & \Delta n_3 \end{bmatrix} = \begin{bmatrix} -l\delta_y & 0 & n\delta_y \\ l\delta_x & 0 & -n\delta_x \\ -n\delta_y & \delta_x & -l\delta_y \end{bmatrix}$$

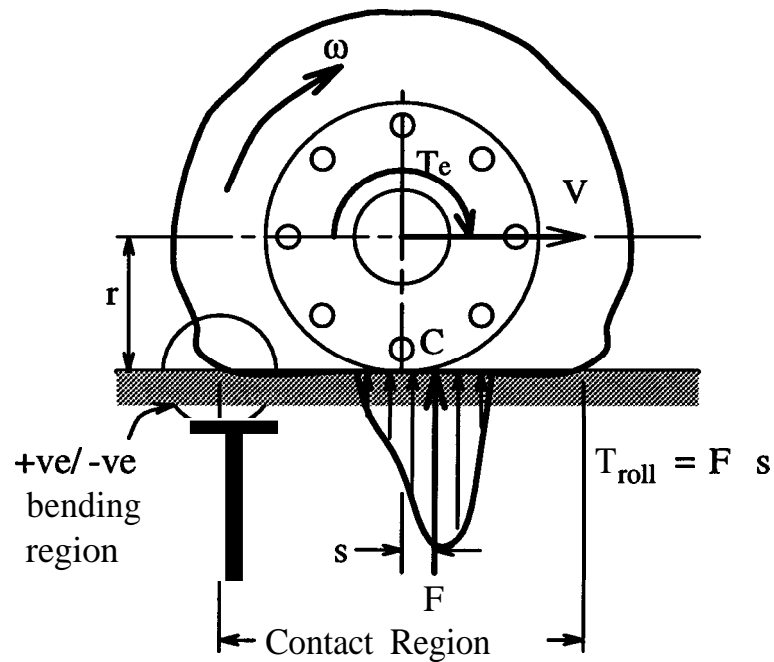
which implies

$$\delta_y = \frac{\Delta l_3}{n} \quad \text{and} \quad \delta_x = \frac{-\Delta m_3}{n}$$

After the tire blow-out, the rotation angles  $\phi$  and  $\theta$  of vehicle rotation about  $X_s$  and  $Y_s$  axis will become

$$\phi_{new} = \phi_{old} + \delta_x \quad \theta_{new} = \theta_{old} + \delta_y \quad (2.44)$$

where  $\phi_{old}$  and  $\theta_{old}$  are the rotation angles before burst, and  $\phi_{new}$  and  $\theta_{new}$  are their new values respectively.



$$T_e = \text{Engine Torque} \quad \omega = \text{Wheel speed}$$

$$T_{\text{roll}} = \text{Roll resistance}$$

Figure 2.8: Rotation of burst tire.

5 Increase in roll resistance: When the tire bursts, the shape of the tire near the contact point is dramatically different from its shape at any other place. When this tire rotates, there is positive and negative bending of tire material as it passes to and departs from the contact region (see Fig.2.8). This leads to dissipation of energy and the tire material heats up. This energy is supplied by the increase in the roll resistance that the tire offers for the rotation. As shown in Fig.2.8, when the burst tire rolls, the normal reaction offered by the ground shifts in the direction of velocity. This normal force then has a moment arm about the rotation axis of the tire. The torque so produced ( $T_{\text{roll}}$ ) is the roll resistance torque [47]. If  $r$  and  $F_P$  are the effective tire radius and tire normal force respectively, then roll resistance coefficient  $f_{\text{roll}}$  is defined as

$$f_{\text{roll}} = \frac{T_{\text{roll}}}{r F_P} \quad (2.45)$$

An empirical relation giving roll resistance coefficient, as a function of the tire

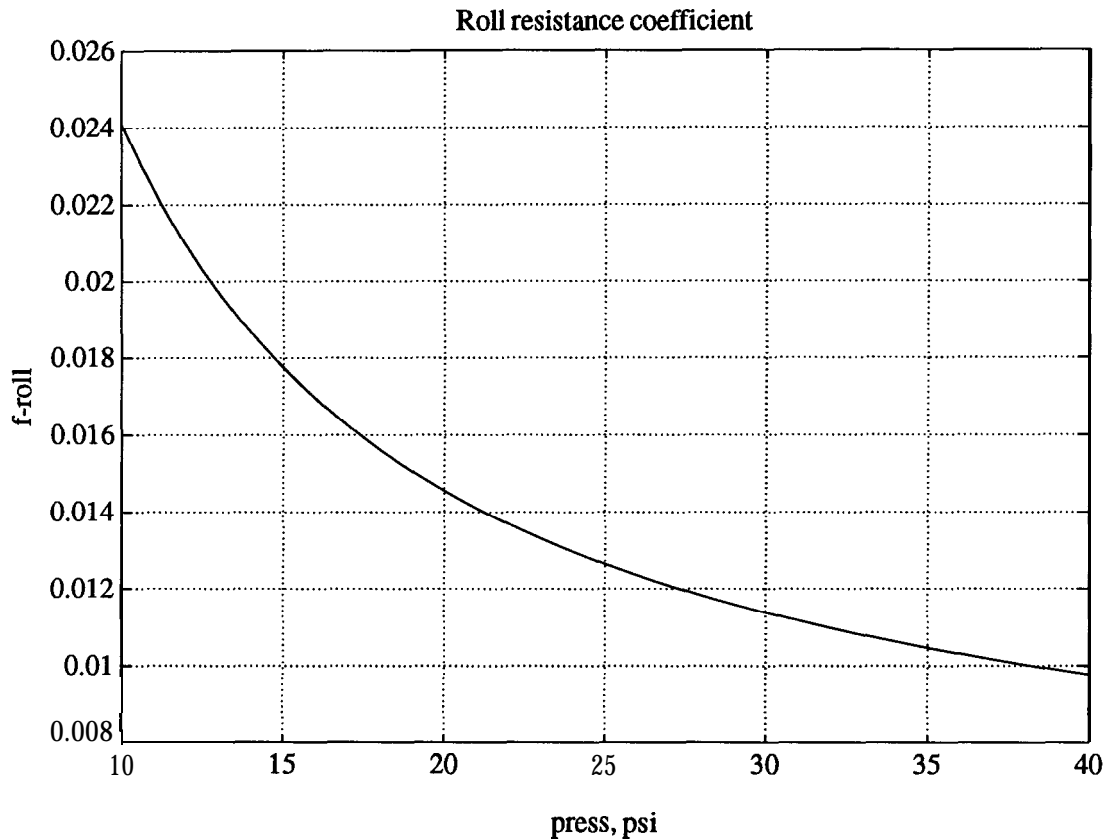


Figure 2.9: Roll resistance coefficient Vs. pressure

pressure is [47]

$$f_{roll} = 0.005 + \frac{.15}{p} + \left( \frac{0.67}{p} \right) \left( \frac{V}{100} \right) \quad (2.46)$$

where  $p$  is the tire pressure in psi, and  $V$  is the velocity of vehicle in mph. Fig. 2.9 shows the plot of the roll resistance coefficient when plotted as a function of tire pressure. Equation (2.46) is not valid for extremely low tire pressure. Since the roll resistance depends on shape of the tire, one can use the tire pressure for which the tire shape is as in the Fig. 2.8. This pressure can be computed by  $p = \frac{F_p}{A_c}$ , where  $A_c$  is the area of contact region.

Equation (2.37) governs the dynamics of rotation of the wheels. When  $j^{\text{th}}$  tire

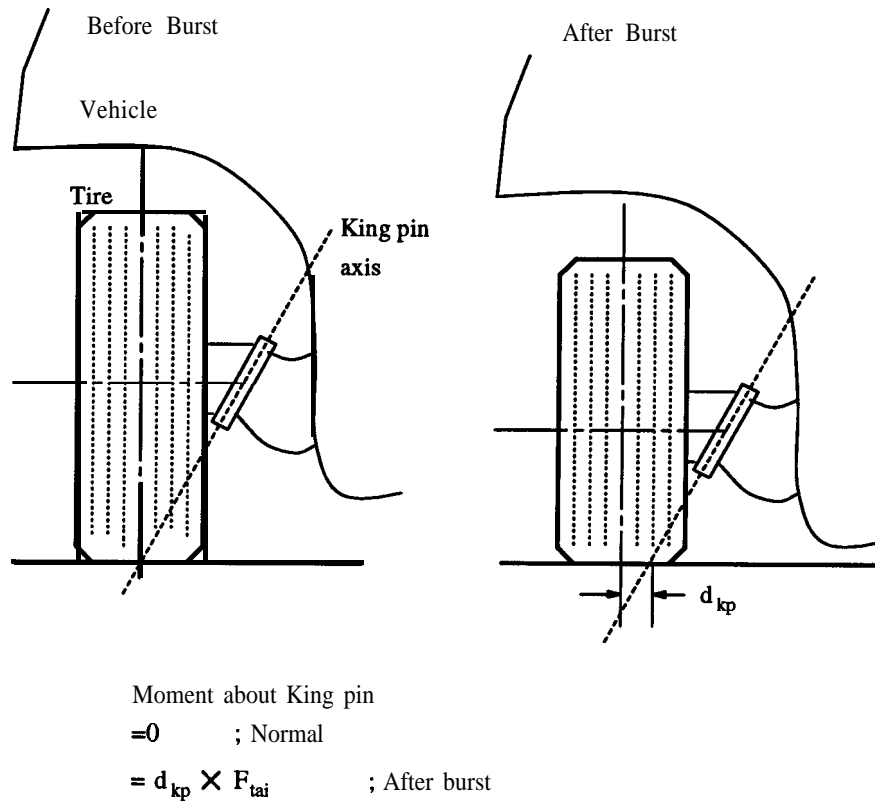


Figure 2.10: Moments about king pin

bursts, the corresponding wheel dynamics becomes

$$T_{ei} - T_{roll} - r_i \cdot F_{tai} = I_i \dot{\omega}_i \quad i = j \quad (2.47)$$

- 6 Increased moment about king pin The steering wheels (front wheels) of a car are pivoted about what is called king pin. When the wheels are steered, they rotate about the king pm. This king pm axis is having an inclination with respect to the vertical. The inclination is very small and is intentionally kept so that the wheels come back to zero steering angle position when the steering wheel is released. The geometry of the king pm is such that the axis of the king pm passes through the point where tires touch ground (see Fig 2.10). This means that the forces generated at the tire have no moment about the king pin. The moment arm of the tire forces about the king pin is called the scrub radius. The scrub radius is termed outboard scrub radius if king pin axis



and wheel centerline intersect above ground, and is called inboard when the two axis intersect below ground. The inboard/outboard scrub radii produce self steering effect [60]. When tire burst occurs, this geometry of the king pin and tires is changed. The king pin axis will no longer pass through the point where tire forces are generated. This will create an inboard scrub radius. As a consequence, (depending on the stiffness of the steering system), tire forces will tend to deflect the steering system. Equation (2.48) gives the deflection of the wheels because of this effect. The steering command and the actual steering angle produced will no longer agree with each other. They are related by

$$\begin{aligned}\delta_i &= \delta_{i_c} + \frac{F_{tai} \times d_{kp}}{K_{st}} & i = 1 \\ \delta_i &= \delta_{i_c} - \frac{F_{tai} \times d_{kp}}{K_{st}} & i = 2\end{aligned}\quad (2.48)$$

where  $K_{st}$  is the steering system stiffness,  $d_{kp}$  is the inboard scrub radius and  $\delta_{i_c}$  is the steering angle command.

7 Reduction in cornering stiffness: Cornering stiffness is the slope of the tire lateral force characteristics at slip angle  $\alpha = 0$ . Force generation capability of a tire is dependent on the tire pressure. Kappler and Godthelp [59] have studied the effect of tire pressure variation on vehicle handling. Their results give subjective description of the overall vehicle behavior operating with reduced tire pressure. Experimental results presented by Limpert [47] (Fig. 2.11) show the effect of tire pressure variation on lateral force generation capability. It is observed that under the tire burst condition, the tire generate less force than it would have generated without burst. To account for this, a scaling down factor  $R_b (< 1)$  will be applied to the tire force after the tire burst. When the  $j^{\text{th}}$  tire bursts, the tire forces  $F_{tai}$  and  $F_{tbi}$  become

$$F_{tai} = R_{bi} \times F_{ta}(\alpha_i, \lambda_i, F_{Pi}, r_{ci}) \quad (2.49)$$

$$F_{tbi} = R_{bi} \times F_{tb}(\alpha_i, \lambda_i, F_{Pi}, r_{ci}) \quad (2.50)$$

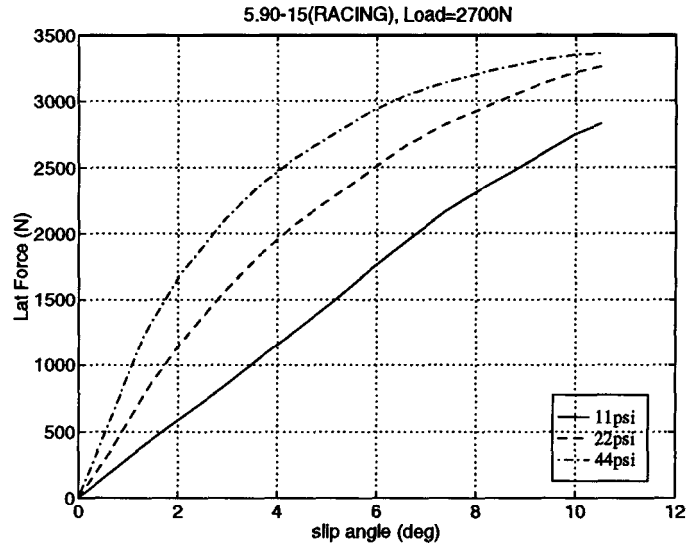


Figure 2.11: Effect of pressure on tire-road interaction force

where

$$R_{bi} = 1 \quad \text{for } i \neq j \quad (2.51)$$

$$R_{bj} = 1 \quad \text{for } t < \tau \quad (2.52)$$

$$R_{bj} = 1 - \frac{t - \tau}{T} (1 - R_b) \quad \text{for } \tau \leq t < \tau + T \quad (2.53)$$

$$R_{bj} = R_b \quad \text{for } t \geq \tau + T \quad (2.54)$$

### 2.2.3 Simulations

Simulations were conducted to see the effect of tire burst on the behavior of the car. The first set of simulations were conducted when different tires blow out at time  $t = 10\text{sec}$  when the car is going on a straight road at different speeds i.e. these simulations show the open loop behavior of the car when the steering command was kept zero. Figure 2.12 shows the vehicle motion when the front left tire blows out at different speeds, and Fig. 2.13 shows the vehicle motion when different tires blow out at  $25\text{mi/hr}$ . These figures show the lateral displacement of the vehicle from the center line of the roadway. As expected, the car deviates in the direction of the tire burst. i.e. the car deviates towards left if the left tire bursts. The severity

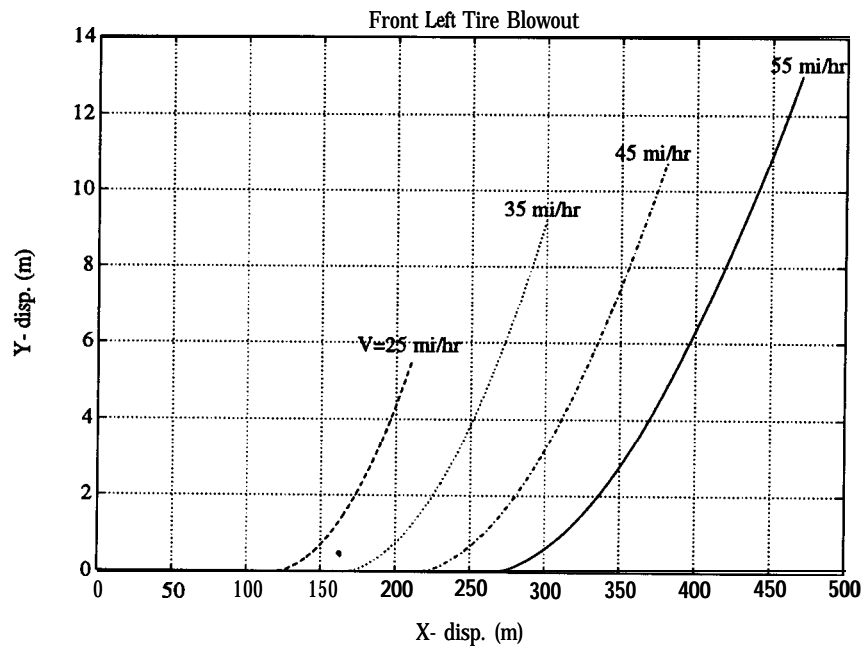


Figure 2.12: Tie burst - zero steering command

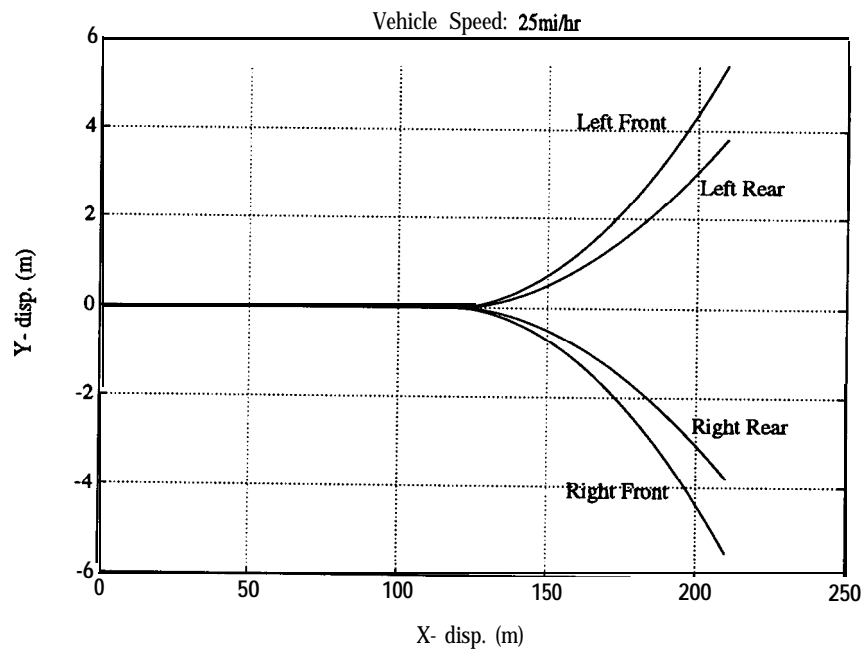


Figure 2.13: Tire burst - zero steering command

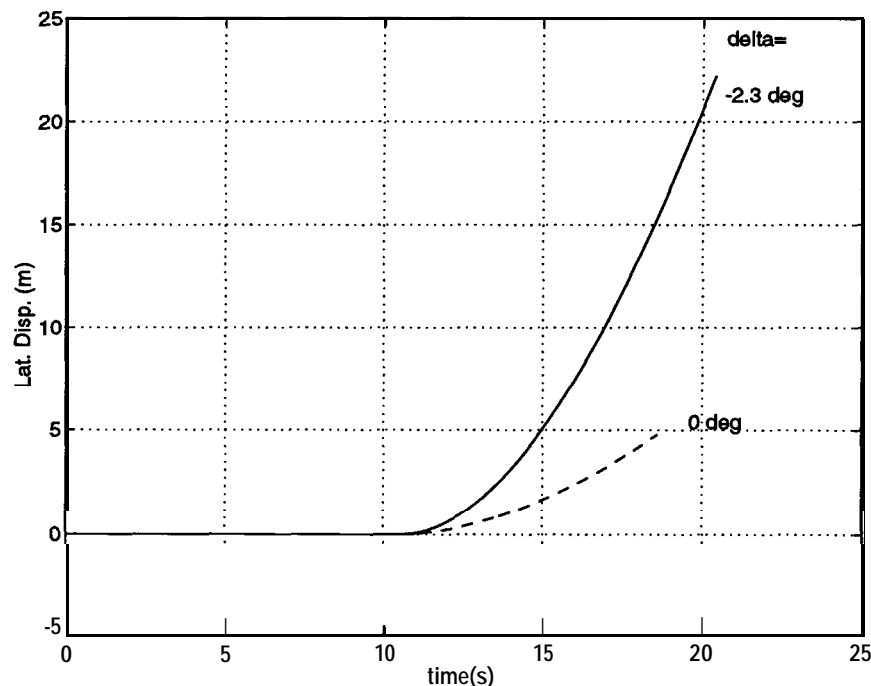


Figure 2.14: Tire burst - fixed nonzero steering command

of the burst effect on lateral deviation increases with the speed of the vehicle. In addition, one can see that the lateral deviations of the car are more if the front tire bursts. The reason for this is that these are the steering as well as driving tires of the car (front wheel drive car).

In the subsequent simulations (Fig. 2.14 and 2.15), the effect of a tire burst on the vehicle when traveling on a curve is investigated. The overall behavior of the car is **similar** to the behavior when traveling on straight road. When the outer front (outer side is with reference to the curve) tire bursts, the lateral deviations are more than the case of an inside tire burst. This is because of the fact that the centrifugal force acting on the car tends to increase the lateral deviations when outer side tire bursts. Exactly opposite phenomena happens when the inner side tire bursts. The behavior of the car when rear tires burst can be explained as follows. When a rear tire blows out, the rear tire tend to slide outward under the centrifugal force. This changes the yaw angle, and the car points towards inner side of the curve. This leads to the negative displacements in case of the inner tire

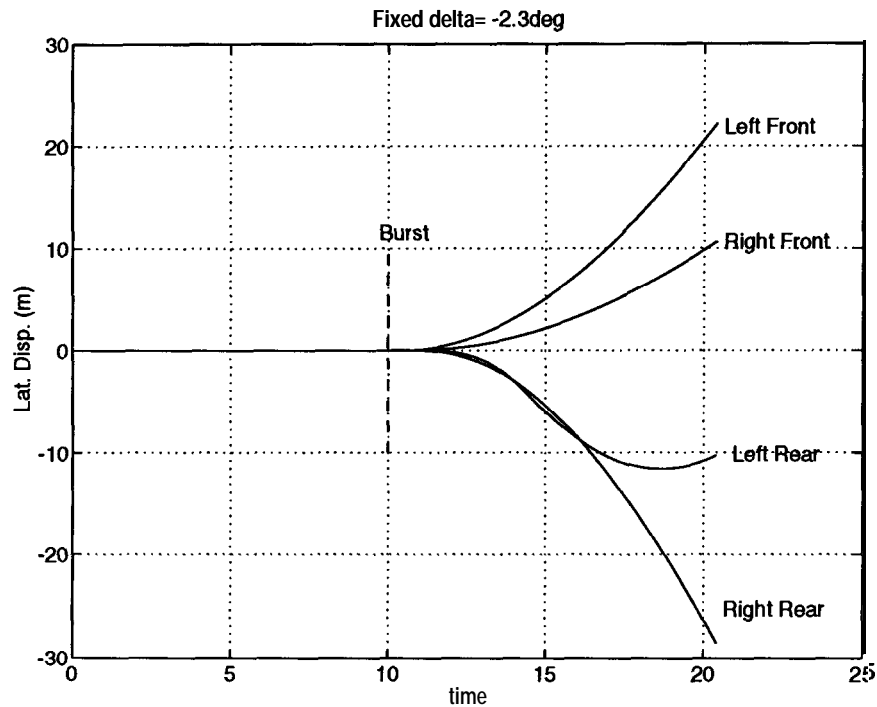


Figure 2.15: Tie burst - fixed **nonzero** steering command

bursts. This effect dominates in the initial period when the outer rear tire bursts. Then the out-throwing effect of the outer tire blow-out takes over and the plot of lateral displacement turns outward.

## 2.3 Burst Controller Design

The effect of tire burst that one is concerned with from the viewpoint of safety is the increase in lateral deviation of the vehicle. Figures 2.16 and 2.17 show the results of simulations that were performed for the vehicle going on a curve of 75 meters radius with the steering actuator time-constant of  $0.15s$  and a rate limit of  $7.5^\circ/s$ . Outer front tire burst effects are shown in the figure. These simulations were performed with the FSLQ controller [30] connected in close loop with the car. FSLQ stands for the Frequency *Shaped Linear Quadratic* controller. As the name suggests, this controller is a modified version of *the Linear Quadratic* controller

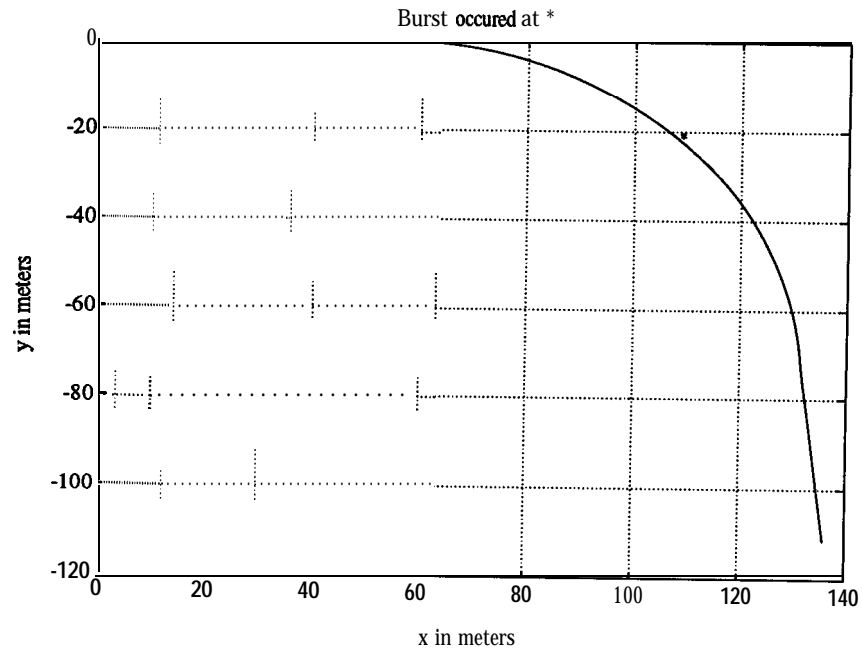


Figure 2.16: Tire burst conditions

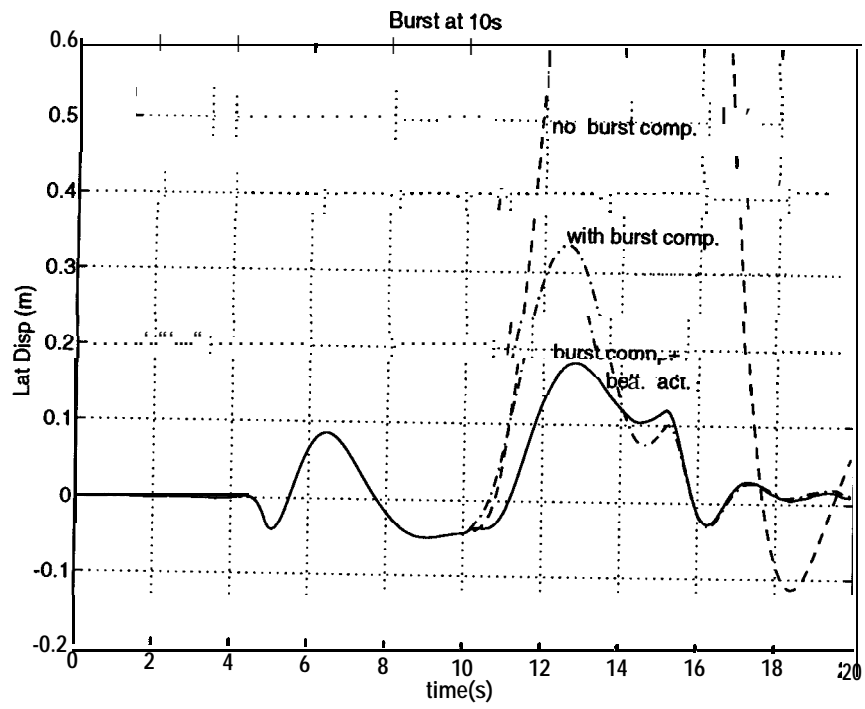


Figure 2.17: Tire burst effects

in which the performance index is frequency shaped, so that the performance of the system in certain frequency ranges is ignored, and in other parts of the frequency range, it is given extra importance. This controller is described in detail in [49]. Only relevant features of the controller will be described here. This type of controller was investigated primarily because the controller was demonstrated to work satisfactorily for the automobile lateral control problem. In designing this controller, a performance index is first selected. The performance index is of the form:

$$J = \frac{1}{2\pi} \int_{-\infty}^{\infty} [\mathbf{x}^*(j\omega)\mathbf{Q}(j\omega)\mathbf{x}(j\omega) + \mathbf{u}^*(j\omega)\mathbf{R}(j\omega)\mathbf{u}(j\omega)] d\omega \quad (2.55)$$

where  $*$  denotes the complex conjugate,  $\mathbf{x}$  is the  $n \times 1$  state vector,  $\mathbf{u}$  is the  $m \times 1$  vector of inputs,  $\mathbf{Q}(j\omega)$  and  $\mathbf{R}(j\omega)$  are proper Hermitian weighting matrices of appropriate dimensions. Let the dynamic system to be controlled have the realization  $(A, B, C, D)$ . Equation (2.55) can be transformed into time domain by Parseval's theorem:

$$J = \int_0^{\infty} [\mathbf{x}^T(t)\mathbf{Q}\mathbf{x}(t) + \mathbf{u}^T(t)\mathbf{R}\mathbf{u}(t)] dt \quad (2.56)$$

This LQ problem can be subsequently solved for getting the solution of the FSLQ problem. Here,  $\mathbf{Q}(j\omega)$  is positive semidefinite ( $\text{rank}(\mathbf{Q}) = p_Q < n$ ), and  $\mathbf{R}(j\omega)$  is positive definite. Furthermore, they must be in the form so that they can be decomposed into their spectral factors as

$$\begin{aligned} \mathbf{Q}(j\omega) &= G_{\mathbf{x}}^*(j\omega)G_{\mathbf{x}}(j\omega) \\ \mathbf{R}(j\omega) &= G_{\mathbf{u}}^*(j\omega)G_{\mathbf{u}}(j\omega) \end{aligned}$$

where  $G_{\mathbf{x}} \in C^{p_Q \times n}$  and  $G_{\mathbf{u}} \in C^{m \times m}$ ,  $G_{\mathbf{x}}$  is proper, and  $G_{\mathbf{u}}$  is proper but not strictly proper. We define the filtered states  $\mathbf{x}_1$  and filtered inputs  $\mathbf{u}_1$  by

$$\begin{aligned} \mathbf{x}_1 &= G_{\mathbf{x}}\mathbf{x} \\ \mathbf{u}_1 &= G_{\mathbf{u}}\mathbf{u} \end{aligned}$$

Let  $(A_1, B_1, C_1, D_1)$  and  $(A_2, B_2, C_2, D_2)$  be minimal realizations of  $G_{\mathbf{x}}$  and  $G_{\mathbf{u}}$  respectively, and the states of the filters  $G_{\mathbf{x}}$  and  $G_{\mathbf{u}}$  be denoted by  $\mathbf{z}_1$  and  $\mathbf{z}_2$  respectively

The FSLQ problem then becomes.

$$\begin{aligned}
J &= \frac{1}{2\pi} \int_{-\infty}^{\infty} [\mathbf{x}^*(j\omega)\mathbf{Q}(j\omega)\mathbf{x}(j\omega) + \mathbf{u}^*(j\omega)\mathbf{R}(j\omega)\mathbf{u}(j\omega)] d\omega \\
&= \frac{1}{2\pi} \int_{-\infty}^{\infty} [\mathbf{x}_1^*(j\omega)\mathbf{x}_1(j\omega) + \mathbf{u}_1^*(j\omega)\mathbf{u}_1(j\omega)] d\omega \\
&= \int_0^{\infty} [\mathbf{x}_1^*(j\omega)\mathbf{x}_1(j\omega) + \mathbf{u}_1^*(j\omega)\mathbf{u}_1(j\omega)] dt \\
&= \int_0^{\infty} \left[ \begin{array}{cccc} \mathbf{x}^T & \mathbf{z}_1^T & \mathbf{z}_2^T & \mathbf{u}^T \end{array} \left| \begin{array}{cccc} D_1^T D_1 & D_1^T C_1 & 0 & 0 \\ C_1^T D_1 & C_1^T C_1 & 0 & 0 \\ 0 & 0 & C_2^T C_2 & C_2^T D_2 \\ 0 & 0 & D_2^T C_2 & D_2^T D_2 \end{array} \right| \begin{array}{c} X \\ \mathbf{z}_1 \\ \mathbf{z}_2 \\ \mathbf{u} \end{array} \right] dt \\
&= \int_0^{\infty} \left[ \begin{array}{cc} \mathbf{x}_e^T & \mathbf{u}^T \end{array} \right] \begin{bmatrix} Q_e & N_e \\ N_e^T & R_e \end{bmatrix} \begin{bmatrix} \mathbf{x}_e \\ \mathbf{u} \end{bmatrix} dt \quad (2.57)
\end{aligned}$$

which is in the standard LQ form with the augmented state vector  $\mathbf{x}_e = \left[ \begin{array}{ccc} \mathbf{x}^T & \mathbf{z}_1^T & \mathbf{z}_2^T \end{array} \right]^T$ . The state and output equations in terms of  $\mathbf{x}_e$  are

$$\begin{aligned}
\dot{\mathbf{x}}_e(t) &= \mathbf{A} \begin{bmatrix} 0 & \mathbf{1} \\ B_1 & A_1 & 0 \\ 0 & 0 & A_2 \end{bmatrix} \mathbf{x}_e(t) + \begin{bmatrix} B \\ 0 \\ B_2 \end{bmatrix} \mathbf{u}(t) \equiv \mathbf{A}_e \mathbf{x}_e(t) + \mathbf{B}_e \mathbf{u}(t) \\
\mathbf{y}(t) &= \left[ \begin{array}{ccc} c & 0 & 0 \end{array} \right] \mathbf{x}_e(t) \quad (2.58)
\end{aligned}$$

where  $\mathbf{y}(t)$  is the output vector. The solution of the FSLQ problem will come from solving the infinite horizon LQ problem described by Eqs. (2.57) and (2.58). The control law becomes

$$\mathbf{u}(t) = -R_e^{-1} B_e^T K \mathbf{x}_e(t)$$

where  $K$  is the positive solution of the algebraic Ricatti equation

$$K A_e + A_e^T K - (K B_e + N_e) R_e^{-1} (K B_e + N_e)^T + Q_e = 0$$

This is the outline of the design of FSLQ controllers. Further details regarding the FSLQ controller can be found in [50],[51].



For the lateral control problem, one can obtain a controller by utilizing the following performance index:

$$\begin{aligned}
 J = & \frac{1}{4\pi} \int_{-\infty}^{\infty} [a^*(j\omega) \frac{q_a^2}{1 + \lambda_a^2 \omega^2} a(j\omega) + y_s^*(j\omega) \left( \frac{q_y^2}{1 + \lambda_y^2 \omega^2} + \frac{q_i^2}{(j\omega)^2} \right) y_s(j\omega) \\
 & + (\dot{\epsilon}(j\omega) - \dot{\epsilon}_d(j\omega))^* \frac{q_\epsilon^2}{1 + \lambda_\epsilon^2 \omega^2} (\dot{\epsilon}(j\omega) - \dot{\epsilon}_d(j\omega)) \delta^*(j\omega) R \delta(j\omega)] d\omega \quad (2.59)
 \end{aligned}$$

where;

$$a = \ddot{y}_a - \frac{V^2}{\rho} \approx \ddot{y}_r$$

For the lateral control applications,  $R$  can be chosen as:

$$\begin{aligned}
 R = & \begin{bmatrix} 1 & 0 \\ 0 & \kappa \end{bmatrix} & 0.1 \leq \kappa \leq 10 & \text{4WS vehicles} & (2.60) \\
 R = & \begin{bmatrix} 1 & \mathbf{1} \\ 0 & \mathbf{0} \end{bmatrix} & \kappa \gg 1 & \text{FWS vehicles} \\
 R = & \begin{bmatrix} \kappa & \mathbf{1} \\ 0 & \mathbf{1} \end{bmatrix} & \kappa \gg 1 & \text{RWS vehicles}
 \end{aligned}$$

The coefficients  $\lambda_a, \lambda_y, \lambda_\epsilon$ , and  $\lambda_i$  are selected from the ride quality, high frequency robustness and steady state error considerations. After choosing the values of  $\lambda_a, \lambda_y, \lambda_\epsilon$ , and  $\lambda_i$ , the values for  $q_a, q_y, q_\epsilon$ , and  $q_i$  are selected by further tuning.

Simulations performed with this controller in place show that the car deviates to more than one meter after the tire burst occurs (see Fig. 2.17). This situation would be highly unacceptable because the vehicle would go in to the adjacent lane under the tire burst. In order to prevent this, several controller strategies were explored. Each one of them will be described in the following sections.

### 2.3.1 Designing a controller with modified performance index

One of the primary considerations in selecting the performance index for designing the nominal FSLQ controller was the ride quality. After a tire blow out, the ride quality and passenger comfort become secondary issues. Primary issue while

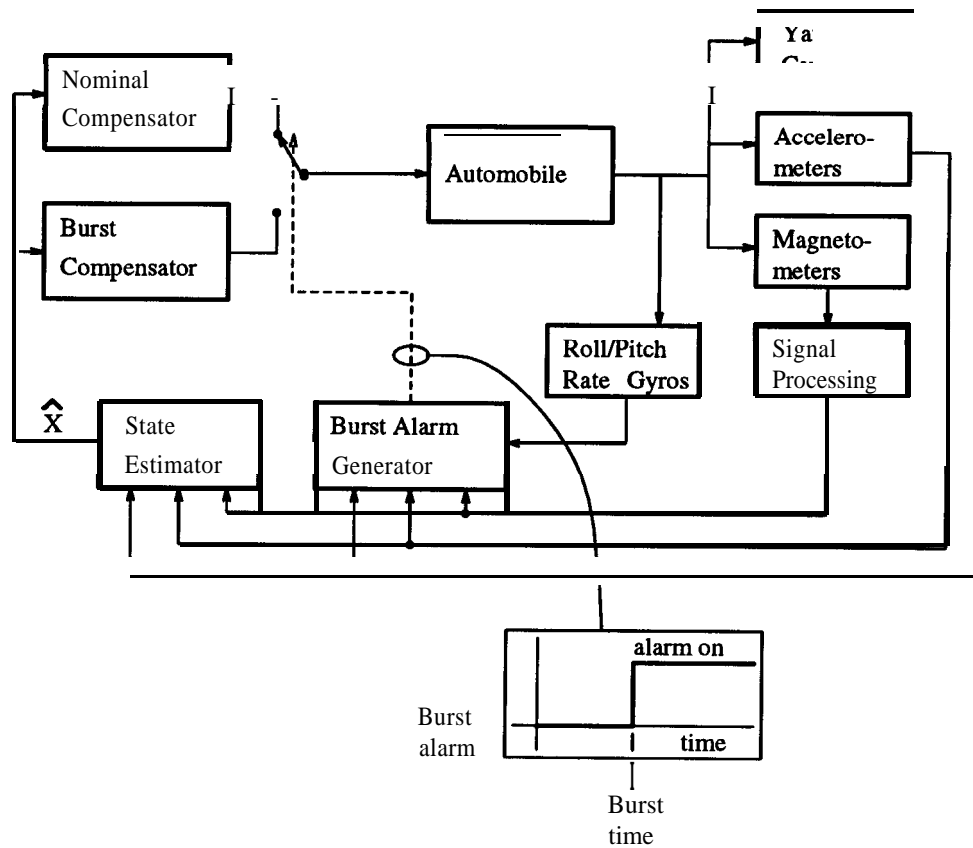


Figure 2.18: FSLQ burst controller structure

designing a tire burst controller is that the lateral deviation should be as small as possible. By properly selecting the coefficients  $q_a$ ,  $q_y$ ,  $q_e$ , and  $q_i$ , one can change the importance given to the ride quality, and in turn **improve** the performance of the FSLQ controller when operating with the tire burst. For example if  $q_a$  is decreased, the importance given to ride quality decreases. The controller will concentrate on the lateral error and yaw rate error. In addition, increase in  $q_i$  will improve steady state performance. This parameter scales the integrator gain, in the controller and its selection needs to be handled carefully in order that the system does not go unstable. The tuning of these parameters was done in simulations to obtain the best possible performance. Simulations performed with this idea are shown in Fig. 2.16 and 2.17. The structure of the controller is shown in Fig. 2.18.

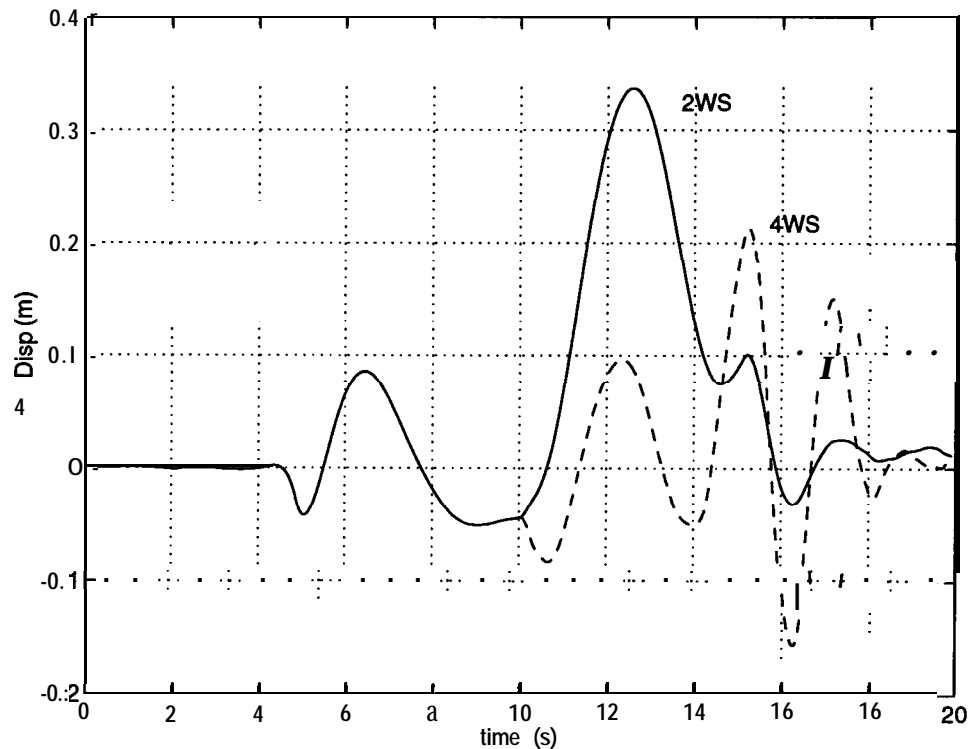


Figure 2.19: 4WS burst controller performance

### 2.3.2 Four wheel steering

If a car is equipped with four wheel steering, then one can exploit the additional steering capability that the car offers to the benefit in controlling the car after tire blow out. Equation (2.60) describes the  $\mathbf{R}$  matrix that can be used in the performance index while designing a FSLQ controller. When this matrix is used in conjunction with the FSLQ formulation as described earlier, one can get a controller utilizing the four wheel steering capability of the car. Performance of this controller is shown in Fig. 2.19. The performance definitely shows improvement over the 2WS car. The obvious reason for this to happen is that there are three steering wheels that can generate good amount of lateral force even under the tire burst condition as opposed to one or two steering wheels is the 2WS car. This kind of approach has limited practical value because it requires much more hardware to implement.

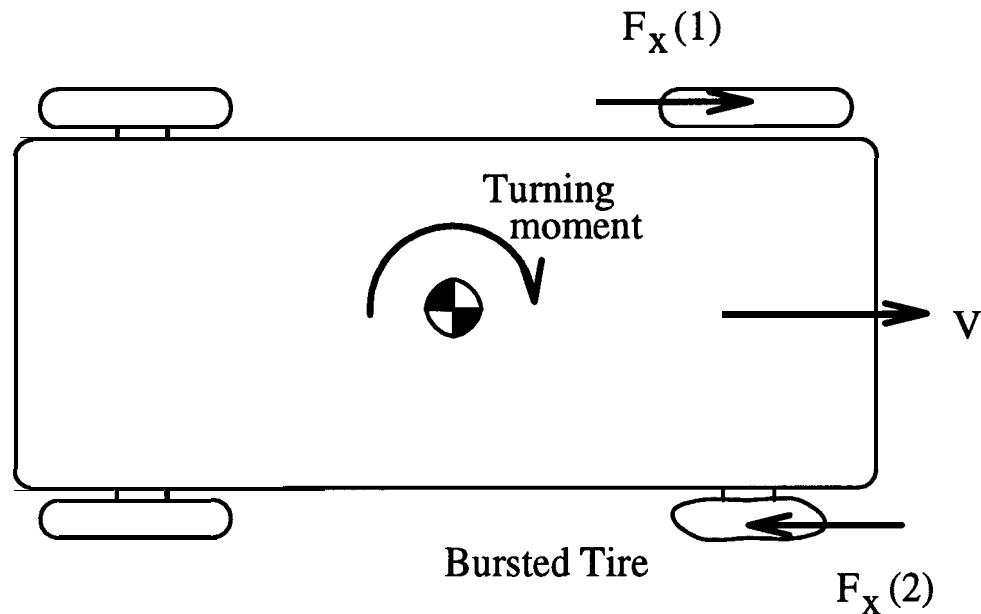


Figure 2.20: Force imbalance after a tire burst

Also this algorithm will not work with the traditional design of the cars.

### 2.3.3 Both tire burst

When a tire burst occurs, one of the effects is that there is imbalance of forces about the front-rear axis of the car that is created because of the different tire forces generated at right and left tires. This imbalance creates a turning moment that tends to rotate the car in the direction of the burst (see Fig. 2.20). This leads one to imagine that if one can successfully counteract this force imbalance, one can achieve better lane tracking performance. One of the obvious solutions to do this is to intentionally burst the symmetrically opposite tire, once a tire burst is detected. Conceptually, this could be achieved by a air release valve mounted on the wheel. Simulations performed to explore this possibility show that the overall steering capability of the car is lost, and the burst pair of tires can no longer support the lateral forces crucial for steering purposes. As a result, the car tends to go straight rather than tracking the curvature of the roadway center line (see Fig. 2.21).

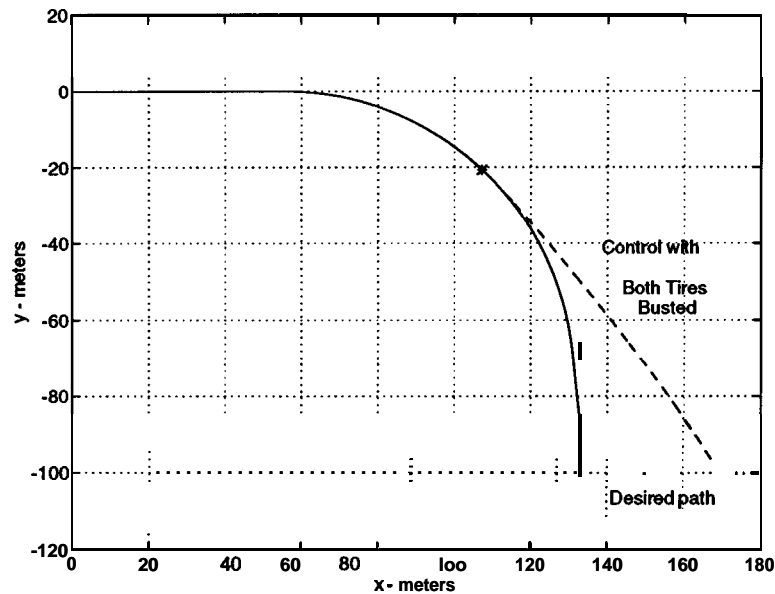


Figure 2.21: Both tires burst.

### 2.3.4 Better actuator

A key design parameter which will affect the performance of the burst controller is the bandwidth of the steering actuator. A sudden deflation of the tire air calls for quick action from the controller. This action needs to be transmitted to the car through the steering actuator faithfully. If these actuators have narrow bandwidth, they will fail to react quickly to the tire burst. In the simulations described until this point, the actuator time constant was 0.15 sec, with a rate limit of  $7.5^\circ/\text{sec}$ . When these actuator limitations were relaxed to 0.1 sec time constant and rate limit of  $30.0^\circ/\text{sec}$ , the car performance improves.

### 2.3.5 Feed-forward controller

#### Non linear model inversion

Consider a nonlinear system with affine inputs:

$$\begin{aligned}\dot{\mathbf{X}} &= \mathbf{f}(\mathbf{X}) + \mathbf{g}(\mathbf{X})u \\ y &= h(\mathbf{X})\end{aligned}$$

where  $\mathbf{X}$  is the state vector,  $u$  and  $\mathbf{y}$  are the input and output of the system respectively. Let the relative degree of the system be  $r$ . Then by successive differentiation of  $\mathbf{y}$  one gets,

$$\begin{aligned}
 \mathbf{y} &= h(\mathbf{X}) \\
 \dot{\mathbf{y}} &= L_f h(\mathbf{X}) \\
 &\vdots \\
 \mathbf{y}^{t-1} &= L_f^{r-1} h(\mathbf{X}) \\
 \mathbf{y}^r &= L_f^r h(\mathbf{X}) + L_g L_f^{r-1} h(\mathbf{X}) u
 \end{aligned} \tag{2.61}$$

If it is required that the output of the system tracks a desired output  $\mathbf{y}_d$ , that is differentiable up to  $r^{\text{th}}$  order, and also if it is assumed that the initial condition of the output lies on the desired trajectory, then Eq. (2.61) can be solved for  $u$  to give

$$\mathbf{u} = \frac{\mathbf{y}_d^r - L_f^r h(\mathbf{X})}{L_g L_f^{r-1} h(\mathbf{X})} \tag{2.62}$$

As a result, the output will become  $\mathbf{y} \equiv \mathbf{y}_d$ . If one wants to track  $\mathbf{y}_d \equiv 0$ , then the internal dynamics of the system becomes the zero dynamics, and it is the only dynamics that gets excited. If the internal dynamics of the system is stable, then one can successfully perform the inversion and the system will be stable when input (2.62) is injected into the system.

### Feed-forward controller for tire burst

In this section, the dynamic equations of car are considered for model inversion. The model inversion will be done for the specific case of tire burst conditions. Equations (2.31) to (2.37) describe the car dynamics. As can be seen from these equations, the inputs do not come in an affine manner. Still the model inversion can be performed by following steps similar to those in section 2.3.5.

Consider the vehicle dynamic equations (2.31) and (2.32).

$$\begin{aligned}
 & m[\ddot{x} - \dot{y}\dot{\epsilon} + \theta\dot{\gamma}\dot{y} - \theta\beta\dot{\Delta}\dot{y} - \Delta\theta\dot{y}\dot{\epsilon} + \phi\beta\dot{\gamma}\dot{y} \\
 & + \phi\dot{\Delta}\dot{y} + \phi\gamma\dot{\epsilon}\dot{y} + \dot{\theta}\dot{z} + \beta\dot{\gamma}\dot{z} + \dot{\Delta}\dot{z} + \gamma\dot{\epsilon}\dot{z} + \phi\dot{\epsilon}\dot{z}]
 \end{aligned}$$

$$\begin{aligned}
&= -K_{wx}\dot{x} + mg(\Lambda + \theta) - \sum_{i=1}^4 \theta F_{Pi} + \sum_{i=1}^4 F_{txi} \\
&\quad m[\ddot{y} + \dot{\epsilon}\dot{x} - \theta\dot{\gamma}\dot{x} + \theta\beta\dot{\Delta}\dot{x} + \Delta\theta\dot{\epsilon}\dot{x} - \phi\beta\dot{\gamma}\dot{x} \\
&\quad - \phi\dot{\Delta}\dot{x} - \phi\dot{\gamma}\dot{\epsilon}\dot{x} - \dot{\phi}\dot{z} - \dot{\gamma}\dot{z} + \beta\dot{\Delta}\dot{z} + \Delta\dot{\epsilon}\dot{z} - \theta\dot{\epsilon}\dot{z}] \\
&= -K_{wy}\dot{y} - mg(\gamma + \phi) + \sum_{i=1}^4 \phi F_{Pi} + \sum_{i=1}^4 F_{tyi}
\end{aligned}$$

These equations can be rewritten as

$$\ddot{x} = a_1(\mathbf{X}, S_P, S_x) \quad (2.63)$$

$$\ddot{y} = b_1(\mathbf{X}, S_P, S_y) \quad (2.64)$$

where :

$$\begin{aligned}
\mathbf{X} &= [x \ \dot{x} \ y \ \dot{y} \ z \ \dot{z} \ \phi \ \dot{\phi} \ \theta \ \dot{\theta} \ \epsilon \ \dot{\epsilon}]^T \\
S_P &= \sum_{i=1}^4 F_{Pi}, \quad S_x = \sum_{i=1}^4 F_{txi} \\
S_y &= \sum_{i=1}^4 F_{tyi}
\end{aligned}$$

The quantities  $F_{txi}$  and  $F_{tyi}$  are the tire forces in lateral and longitudinal direction. These are functions of state  $\mathbf{X}$ , steering command  $\delta = [\delta_1 \ \dots \ \delta_4]^T$ , time  $t$ , and the angular velocities  $\omega = [\omega_1 \ \omega_2 \ \omega_3 \ \omega_4]^T$  of the wheels [30][52]. Angular velocity  $w$  in turn depend on another input to the car, the engine torque  $\mathbf{T}_e = [T_{e1} \ \dots \ T_{e4}]^T$ .  $F_{Pi}$  is the suspension force at the  $i^{th}$  suspension,  $i = 1, \dots, 4$ . These are functions of  $\mathbf{X}$ , and time  $t$  [52]. The dependence on time  $t$  comes in because the tire stiffness  $K_{tyre_i}$ ,  $i = 1, \dots, 4$  changes as a function of time when one wants to model tire burst. As a result, Eqs. (2.63) - (2.64) will be modified to :

$$\ddot{x} = a_1(\mathbf{X}, S_P, S_x) = a(\mathbf{X}_B, t, \delta, \mathbf{T}_e) \quad (2.65)$$

$$\ddot{y} = b_1(\mathbf{X}, S_P, S_y) = b(\mathbf{X}_B, t, \delta, \mathbf{T}_e) \quad (2.66)$$

where,  $\mathbf{X}_B = [\mathbf{X}^T \ \omega^T]^T$ .

Now, consider Fig. 2.22. This figure defines the output of the lateral dynamics of the car. The output  $\mathbf{y}_r$  of the system is defined as the distance of the CG of the car

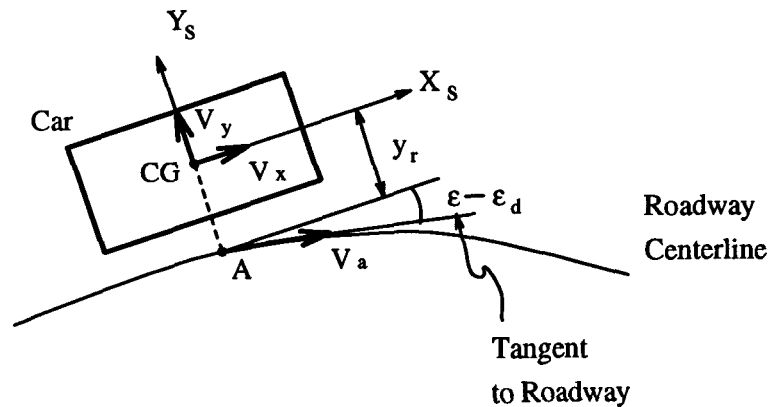


Figure 2.22: Definition of system output

from roadway center line. Point A is on the  $Y_s$  axis extended. In the figure,  $V_x \triangleq \dot{x}$ ,  $V_y \triangleq \dot{y}$ . Also,  $V_a \approx V_x$ . The velocity of point A with respect to the CG of the car is

$$\begin{aligned} \dot{y}_r &= V_y + V_a \sin(\epsilon - \epsilon_d) \\ &\approx \dot{y} + \dot{x}(\epsilon - \epsilon_d) \end{aligned} \quad (2.67)$$

The aim of any controller designed for the tire burst is to keep  $y_r$  as close to zero as possible. Note that the control input does not appear in the expression for  $y_r$  or  $\dot{y}_r$ . Differentiation of Eq. (2.67) gives:

$$\ddot{y}_r \approx \ddot{y} + \ddot{x}(\epsilon - \epsilon_d) + \dot{x}(\dot{\epsilon} - \dot{\epsilon}_d)$$

Substituting Eqs. (2.65) and (2.66) into this expression,

$$\begin{aligned} \ddot{y}_r &= b(\mathbf{X}_B, t, \delta, \mathbf{T}_e) + a(\mathbf{X}_B, t, \delta, \mathbf{T}_e)(\epsilon - \epsilon_d) \\ &\quad + \dot{x}(\dot{\epsilon} - \dot{\epsilon}_d) \end{aligned} \quad (2.68)$$

Here the control input appears through the functions  $S_x$  and  $S_y$ . If the desired output trajectory is  $y_r \equiv 0$ , then it also implies  $\dot{y}_r \equiv 0$  and  $\ddot{y}_r \equiv 0$ . When this value for  $\ddot{y}_r$  is substituted into Eq. (2.68),

$$b(\mathbf{X}_B, t, \delta) + a(\mathbf{X}_B, t, \delta)(\epsilon - \epsilon_d) + \dot{x}(\dot{\epsilon} - \dot{\epsilon}_d) = 0 \quad (2.69)$$

Solving Eq. (2.69) for  $\delta$  with the constraint,

$$\text{For 2WS} \quad \delta_1 = \delta_2, \quad \delta_3 = \delta_4 = 0 \quad (2.70)$$



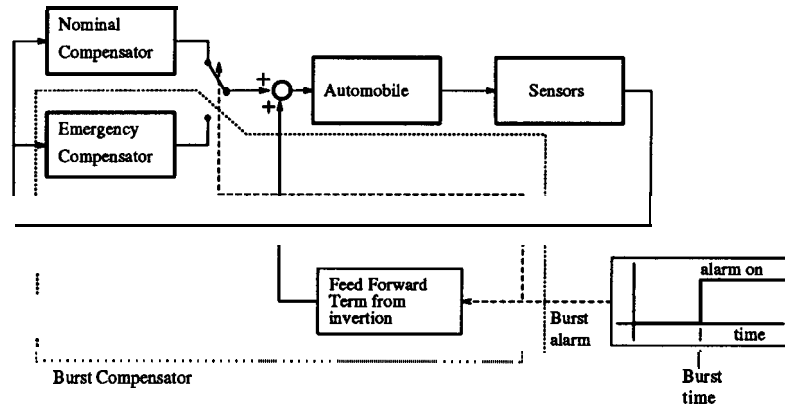


Figure 2.23: Feed-forward controller, structure

$$\text{For 4WS} \quad \delta_1 = \delta_2, \quad \delta_3 = \delta_4 \quad (2.71)$$

$$\text{For Front Wheel Drive} \quad T_{e1} = T_{e2} = T_{long}, \quad T_{e3} = T_{e4} = 0 \quad (2.72)$$

$$\text{For Rear Wheel Drive} \quad T_{e1} = T_{e2} = 0, \quad T_{e3} = T_{e4} = T_{long} \quad (2.73)$$

$$\text{For Four Wheel Drive} \quad T_{e1} = T_{e2} = T_{e3} = T_{e4} = T_{long} \quad (2.74)$$

gives the values of steering command that are required to follow the trajectory

$$\mathbf{y}_r \equiv 0, \quad \dot{\mathbf{y}}_r \equiv 0, \quad \ddot{\mathbf{y}}_r \equiv 0 \quad (2.75)$$

If such a solution of Eq. (2.69) is not possible, then one can find  $\delta$  that does the following minimization with constraint Eqs. (2.70)-(2.74)

$$\min_{\delta} [b(\mathbf{X}_B, t, \delta) + a(\mathbf{X}_B, t, \delta) (\epsilon - \epsilon_d) + \dot{\mathbf{x}}(\dot{\epsilon} - \dot{\epsilon}_d)]^2$$

Since the model inversion calls for solving transcendental equations, the computations can not be done on line. Fortunately for controlling tire burst, it is not required to perform these computations on line. Instead, one can run the inversion algorithm off line, and store the corresponding control input trajectory. This trajectory then will be fed in as a feedforward trajectory once a tire burst is detected. The structure of the controller is shown in Fig. 2.23. Simulation results of the feedforward controller are shown in Fig. 2.24. As seen in the simulations, the lane tracking accuracy is improved. The simulations were performed for a car traveling on a curve when the outer front tire bursts. During the simulations, the feedback controller used was a FSLQ controller.

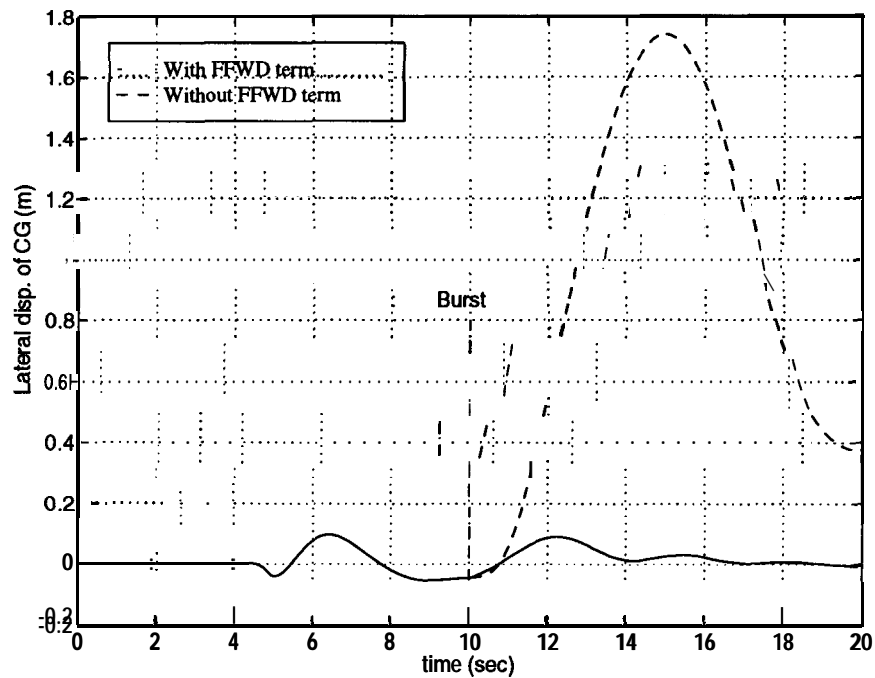


Figure 2.24: Feed-forward controller, performance

### Controller characterization

The controller presented above deals with the case when the vehicle is following a curve and the outer front tire bursts. The tire burst could happen at any place on the roadway, and the vehicle could be going on a straight road or on a curved road. Also depending upon which tire had burst, the feedforward terms will be different. This calls for characterization of the feedforward term based on road curvature  $\rho$  and the index  $k$  of the burst tire. Figure 2.25 shows the plots of the feedforward term for different radii of curvature for outer front tire burst. As a first step in characterization of the controller, it was proposed to approximate the feedforward term by the output of a second order filter, excited by a step input whose strength is a function of the radius of curvature of the roadway. Structure of this controller is shown in Fig. 2.26. Let us call this as the *simplified feedforward* controller. When the tire burst occurs, a burst alarm will be generated by the burst detection algorithm. This can be done simply by putting a threshold on the tire pressure measurement.

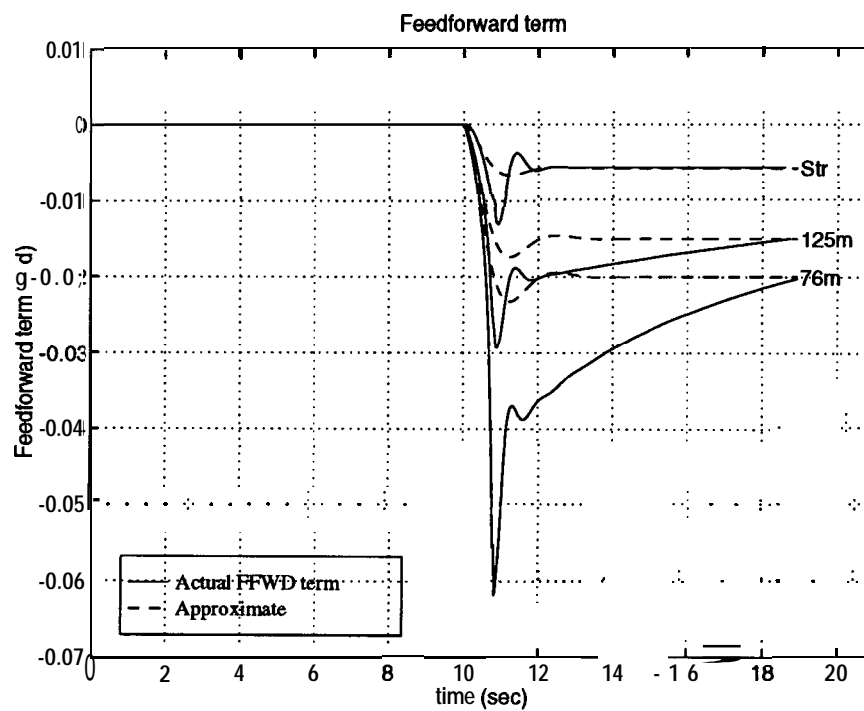


Figure 2.25: Feed-forward terms: actual & approximate

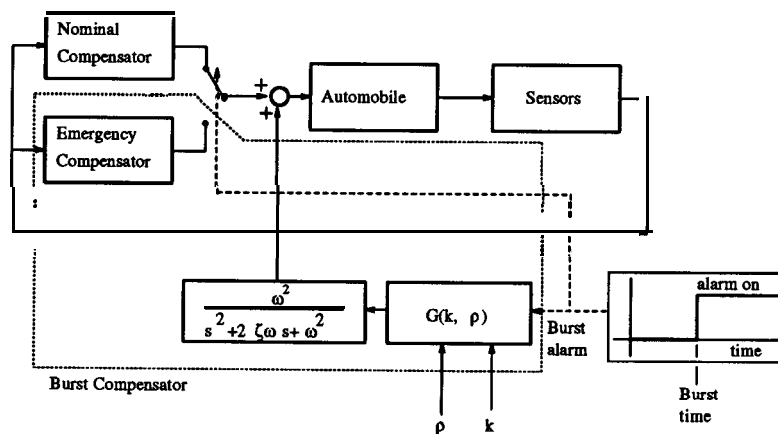


Figure 2.26: Simplified feed-forward controller, structure

$\rho$	$G$
-76m	0.02(rad)
-125m	0.015(rad)
$\infty$	0.0058(rad)

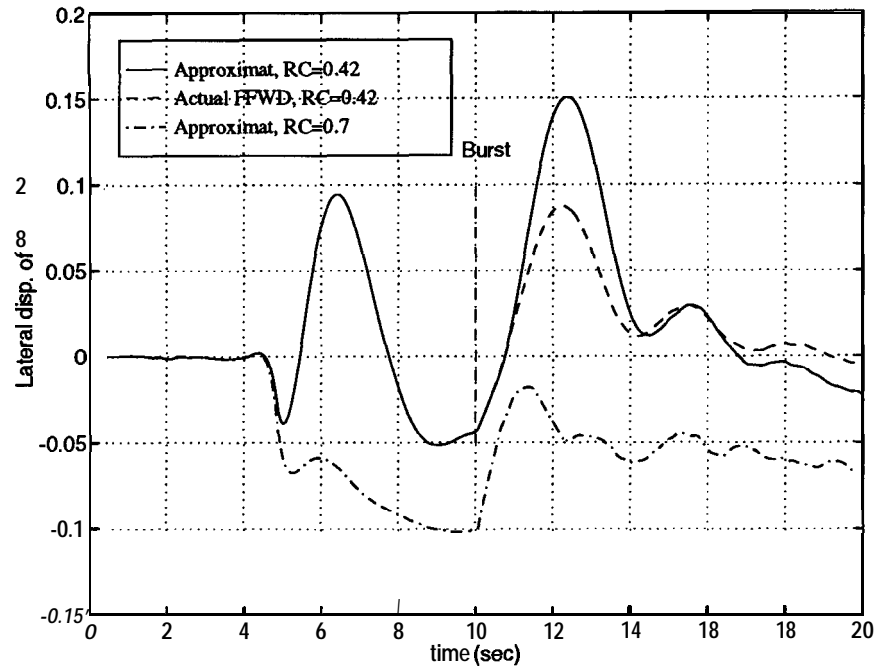
Table 2.2:  $G(k, \rho)$ ,  $k = 1$ 

Figure 2.27: Simplified feed-forward controller, performance

The burst alarm will then be scaled according to the current radius of curvature  $\rho$ . Radius of curvature is assumed to be known here, because in IVHS, this information can be encoded in the roadway [31]. The scaling block  $G(k, \rho)$  will be in the form of a lookup table. Table 2.2 shows such a lookup table for  $k = 1$  (front left tire burst). Results of simulations performed with the approximate feedforward term are shown in Figs. 2.27 and 2.28. Fig. 2.27 shows the performance degradation that occurs because of the approximation, and Fig. 2.28 compares the performance when tire bursts on different radii roadways. Figure 2.27 also shows the robustness of the simplified feedforward term to roadway condition.

The scheme of Fig. 2.26 also has the advantage of addressing the scenario of

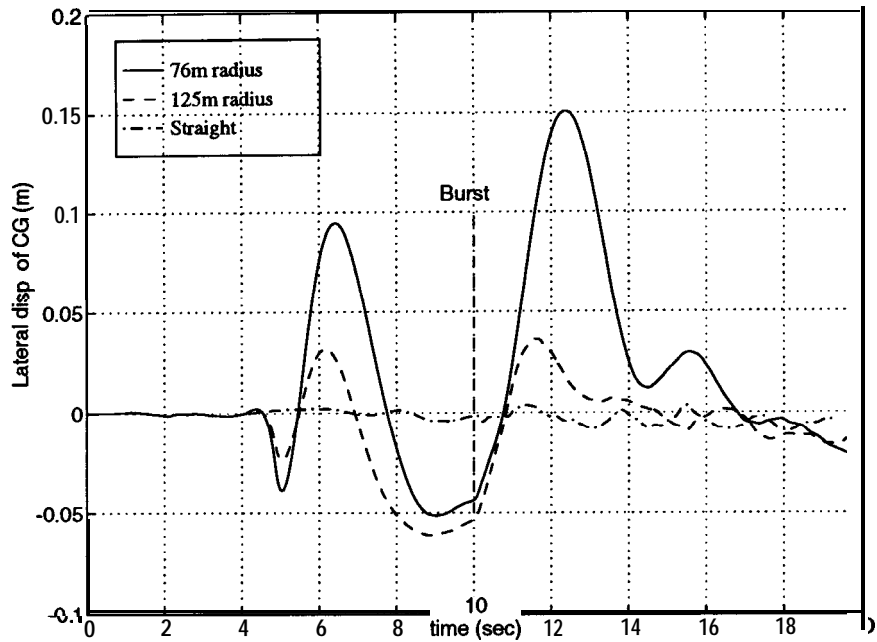


Figure 2.28: Simplified feed-forward controller, performance

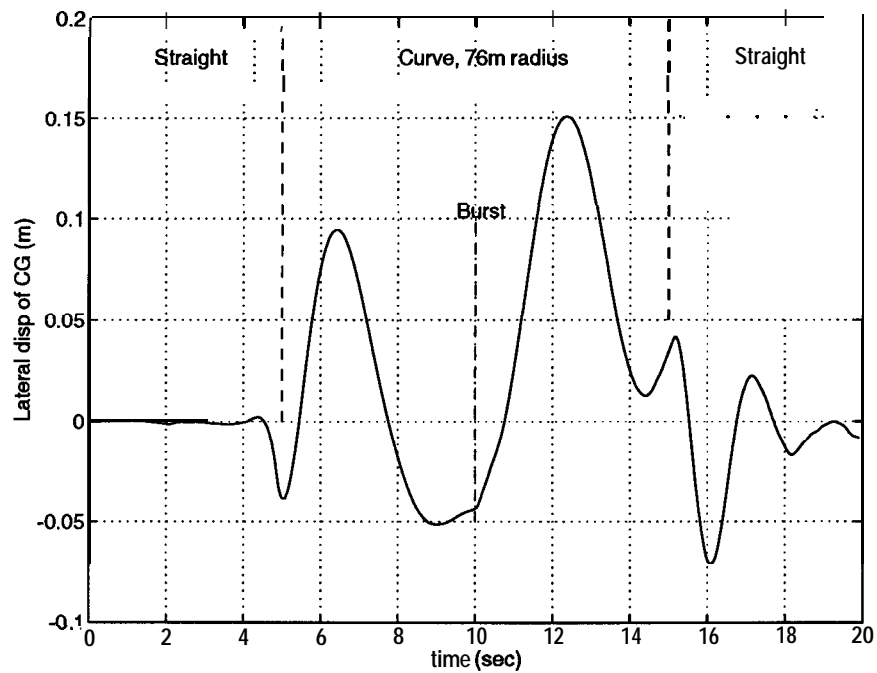


Figure 2.29: Simplified feed-forward controller, performance

road curvature change while one of the tires is burst. Under such a curvature change, the feedforward filter input will be changed to a different value, which is same as the value of the step if the burst had occurred on that patch of the roadway. Figure 2.29 shows the performance of the simplified feedforward controller when the car is traveling first on a straight road, followed by a curve that ends into a straight section. The outer front tire bursts midway through the curve.

### 2.3.6 Torque reduction

When a tire interacts with road, it produces forces in lateral as well as longitudinal direction. These forces are given by functions  $F_{ta}$  and  $F_{tb}$  of Eq. (B.1) and (8.2). Although these empirical relations are quite complex to get any idea from them, one can as a first approximation say that the net tire force generated in the horizontal plane is roughly proportional to the vertical load on that tire, when other factors are kept constant. Let the proportionality constant be  $\mu$ . So the maximum possible force that the tire can generate in horizontal plane is equal to  $\mu F_P$ , where  $F_P$  is the vertical load on the tire. Consider Fig. 2.30. The figure shows the circle with radius  $\mu F_P$  drawn about the point of tire force generation. This indicates that if the tire is generating longitudinal force  $F_{ta}$ , then the capacity of the tire to generate lateral force gets reduced to  $F_{tb}$ . **While** steering under tire burst condition, one needs as much lateral force as one can get. In order to achieve this, one can reduce the longitudinal force  $F_{ta}$  that the tire generates by reducing the engine torque. In other words, if tire burst is detected at time  $t = \tau$  then,

for front wheel drive

$$T_{e1} = T_{e2} = T_{long} f_B \quad T_{e3} = T_{e4} = 0 \quad (2.76)$$

for rear wheel drive

$$T_{e1} = T_{e2} = 0 \quad T_{e3} = T_{e4} = T_{long} f_B \quad (2.77)$$

for four wheel drive

$$T_{e1} = T_{e2} = T_{long} f_B \quad T_{e3} = T_{e4} = T_{long} f_B \quad (2.78)$$

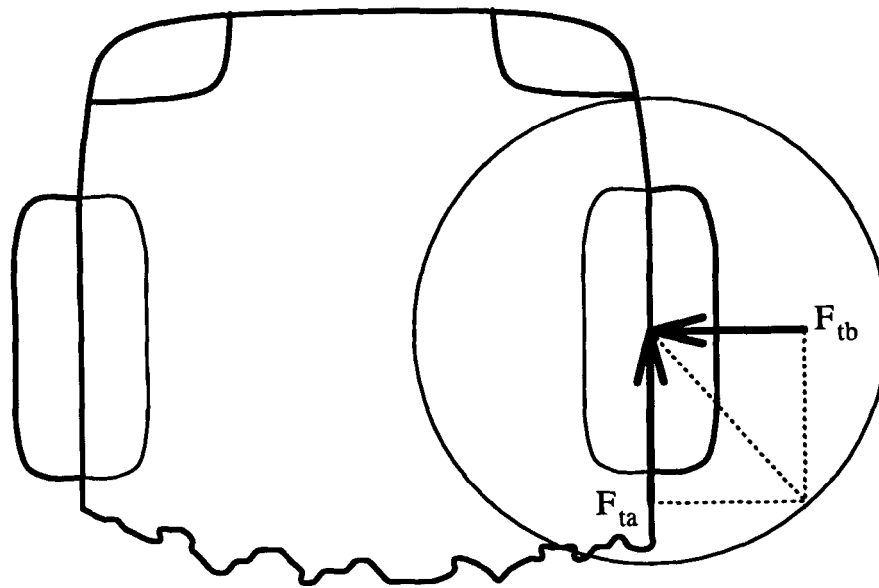


Figure 2.30: Tire force generation

where

$$f_B = 1 \quad \forall t < \tau$$

$$0 < f_B < 1 \quad \forall t \geq \tau$$

Simulations with the engine cut off from the wheels ( $f_B = 0 \quad \forall t \geq \tau$ , Fig. 2.31) indicate the corresponding performance improvement. In Fig. 2.31 the improvement in performance is also partly because of the fact that the longitudinal velocity of the car decreases as a result of the torque reduction,

### 2.3.7 Controller simulations

Several of the strategies discussed above lead to performance improvements of the burst controller. A combined strategy can be devised in order to get the best possible results. In particular, the feedforward controller and the torque reduction can work together to produce better performance shown in Fig. 2.32.

This figure also shows the performance when the burst is not detected instantaneously, but after a delay of 0.5 sec. It can be seen that the performance is still within

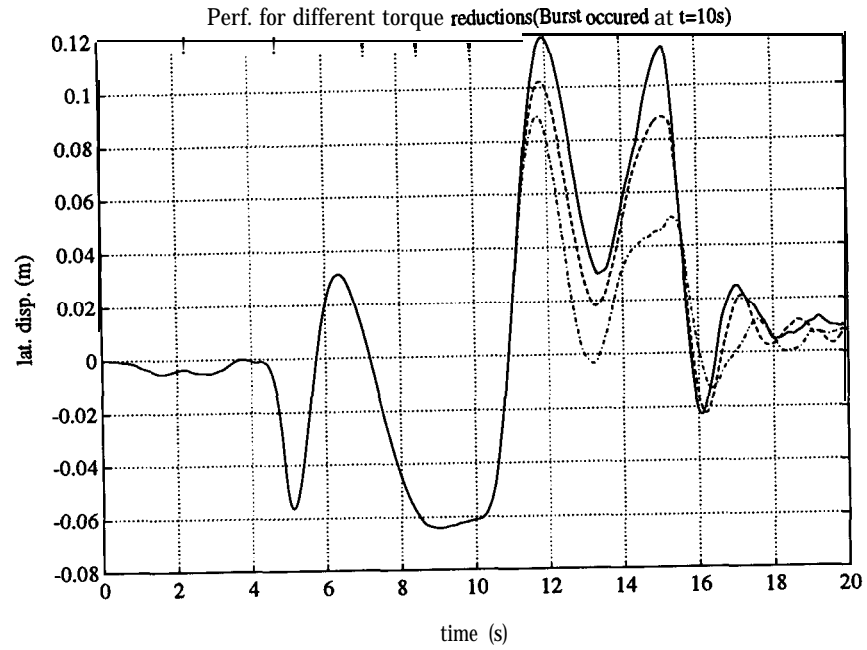


Figure 2.31: Performance improvement after engine torque reduction

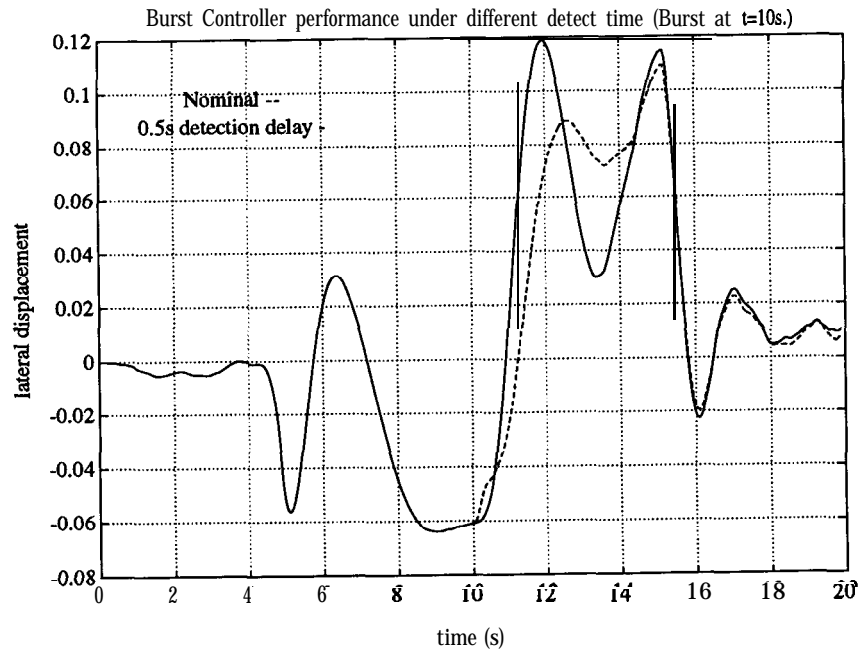


Figure 2.32: Performance of combined controller



reasonable limits. As seen in Fig. 2.28, the performance degradation is **within** acceptable level when road condition changes and affects the cornering stiffness of the tires.

## 2.4 Tire Burst Detection

When the tire burst occurs, tire pressure starts dropping. This is the very first effect of the tire blow-out. All other effects of tire burst follow the drop in pressure. Amongst the other effects, two of the most significant effects from burst detection viewpoint are the rolling and pitching of the vehicle. Consequently, there are two possible ways of detecting the tire burst and generating the burst alarm.

1. Tire pressure measurement: Tire pressure can be continuously monitored and whenever it drops below a certain threshold, the burst alarm can be generated. In fact, such alarm systems have already been developed [60]. In [60], the driver warning system consists of measuring the tire pressure once per revolution, on the other hand, **in** the experimental arrangement for the burst experiments (see section 2.5 for details), the tire pressure was monitored continuously.
2. Roll rate measurement: Consider a vehicle traveling at constant velocity  $\dot{x} = V$  and having front and rear cornering stiffnesses  $C_f$  and  $C_r$  respectively, such that  $F_{tyi} \approx C_f \alpha_i$  for  $i = 1, 2$  and  $F_{tyi} \approx C_r \alpha_i$  for  $i = 3, 4$ . Then, the Eqs. (2.32), (2.34) and (2.36) can be simplified to

$$\ddot{y} = -\frac{2C_m V 2C_r y}{m} - \left( \frac{2C_f l_m V 2C_r l_2}{+ V} \right) \dot{\epsilon} + \frac{2C_f}{m} \delta \quad (2.79)$$

$$\ddot{\epsilon} = -\frac{2C_f l_1 - 2C_r l_2}{I_x V} \dot{y} - \frac{2C_f l_1^2 + 2C_r l_2^2}{I_x V} \dot{\epsilon} + \frac{2C_f l_1}{I_x} \delta \quad (2.80)$$

$$\ddot{\phi} = -\frac{(2C_f + 2C_r)z_0}{I_x V} \dot{y} - \frac{(2C_f l_1 - 2C_r l_2)z_0}{I_x V} \dot{\epsilon} - \frac{kS_b^2}{2I_x} \dot{\phi} + \frac{bS_b^2}{2I_x} \phi + \frac{2C_f z_0}{I_x} \delta \quad (2.81)$$

where  $k$  is the sum of stiffnesses of right (or left) side suspension springs and  $b$  is the sum of damping coefficients of the same two suspension dampers.

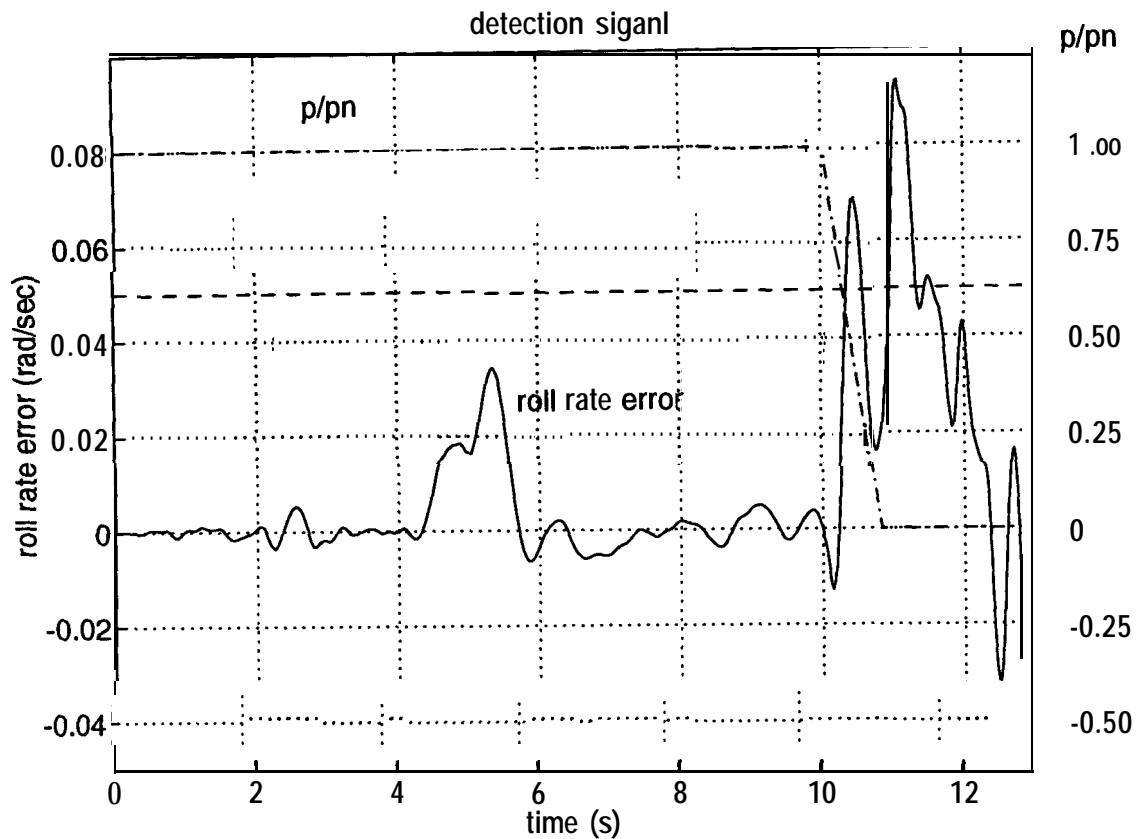


Figure 2.33: Tire burst detection

Notice that this dynamics includes the roll dynamics. In order to explore the possibility of building a model based tire burst detection scheme, an observer was built with Eqs. 2.79 - 2.81 as the plant. The observer designed was a simple pole placement observer using yaw rate feeding the observer. The preliminary simulation results are shown in Fig. 2.33. The figure shows the plots of roll rate error and the tire pressure ( as a fraction of the nominal tire pressure ) .

As far as the detection time is concerned, the two methods of burst detection compare quite well. The roll rate error measurement method suffers from following disadvantages.

- a. When the vehicle parameters such as vehicle speed, road condition change, the roll rate error becomes non zero. In order that the parameter variation

does not generate a false alarm, the detection threshold has to be increased. As a result of the higher detection threshold, the detection time would increase.

- b. Roll rate error tends to become non zero when car enters and leaves a curve. This also increases the detection threshold.
- c. Normal road elements such as bumps, potholes or superelevation angles would produce non zero roll rate errors.

Final method of burst detection can use either of these methods or combination of them. This can be done by sensor fusion techniques.

## **2.5 Experiments**

### **2.5.1 Experimental setup**

Experiments were designed to verify the tire burst model. These experiments were conducted on an AMC-Concord sedan. The plan for the experiment was to run the car with it's steering fixed, and to burst one of the tires once a preselected speed is achieved. The car was equipped with a water jet at the front bumper that would leave a trail on the pavement of the test site. After each run of the experiment, the water trail was measured from the reference marked on the test site. These measurements then were recorded and compared with the simulation outputs (see Fig. 2.34).

One of the biggest hurdle in doing this was how to rupture the tire or to create an effect close enough to that. Three proposals were under consideration.

Very first proposal was to install a valve on the tire/wheel and to operate this valve with a remote controlled device powered by a small battery. Important consideration of this proposal is to have a valve of about an inch diameter opening in order to ensure that the air in the tire gets released within a short time span, characteristic of a typical tire blow out (see Sec. 2.2.2). In other words, the area of the opening of the valve should be such that it is slightly greater than a typical rupture area in case of a burst. As the opening area of a valve increases, the force required to keep it shut will increase. To reduce the valve actuator requirements, it

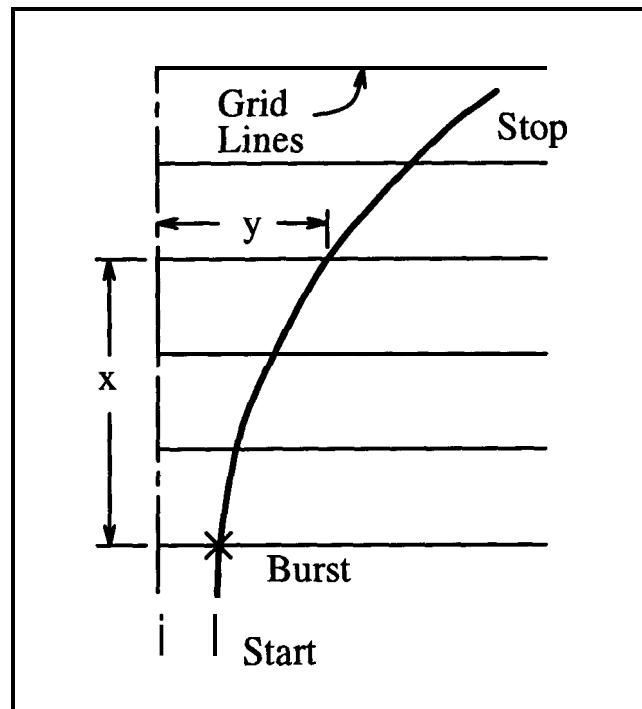


Figure 2.34: Experiment site

was proposed to have a release valve only. This approach would create a situation close to the tire burst, without actually rupturing the tire. In turn, one tire can be used more than once for the experiment.

The second proposal consisted of a retractable/extendable knife edge on the road. For experiments with front tire burst, the knife edge would be first in the extended position. It would retract once the ruptured front wheel passes the knife edge. This retraction could be triggered by a switch *S*, that the passing ruptured tire would activate. For rear tire burst experiments, the arrangement would be reversed. The knife edge in this case would be in retracted position to begin with. Once the front tire passes the switch *S* (see Fig. 2.35), the knife edge would extend and rupture the rear tire. This experimental arrangement would require digging the road pavement and installing the retractable knife arrangement. The proposal was discarded on the basis that it would involve quite a bit more work and it would be unwise to disturb the road pavement.

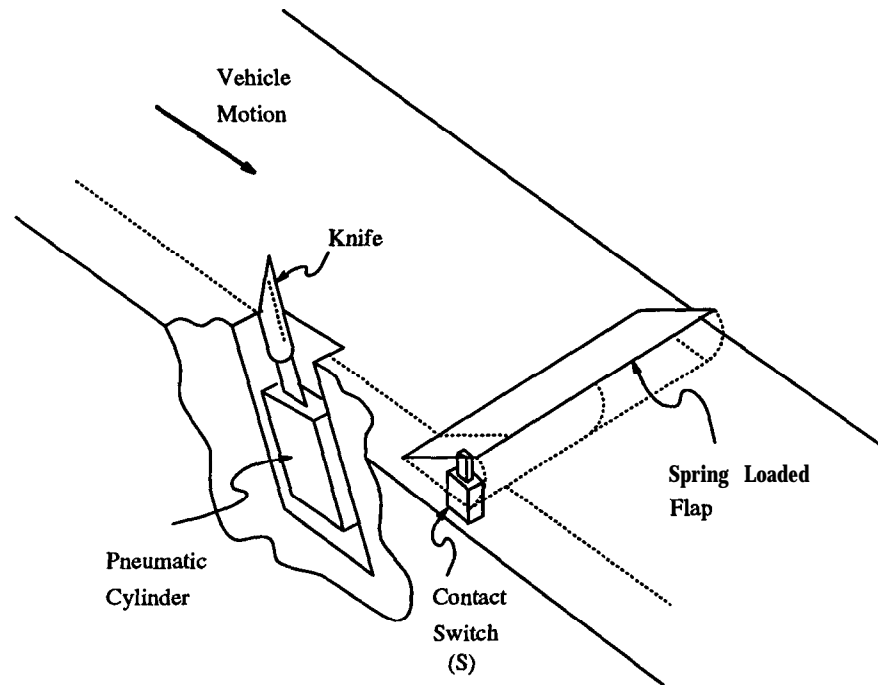


Figure 2.35: Tire burst, experimental arrangement

In the last proposal, the knife blade would be installed on the car chassis. This would eliminate the requirement of digging the road pavement (see Fig. 2.36). The disadvantage of this approach is that firstly, it would require quite an elaborate yet portable knife activation device. Secondly, the knife after rupturing the tire, would be still in contact with the tire and would exert a braking torque on the wheel. In turn, it would not represent the tire burst situation realistically.

Finally the first proposal of having an air release valve in the wheel was pursued. As shown in the Fig. 2.37, eight holes were drilled in the rim of the wheel, that opened to the air in the tire. The area of each drilled hole was such that the sum total of the area of these eight holes was slightly more than the area of an one inch diameter hole. A bunch of flexible tubing connected these openings to the release valve at the center of the wheel. The valve was designed as a two stage release valve: the first stage was a solenoid pneumatic valve that was bought off the shelf, and the second stage was a pneumatic cylinder that operated on the air from the tire itself. This cylinder in turn operated the latch of the valve flap. The

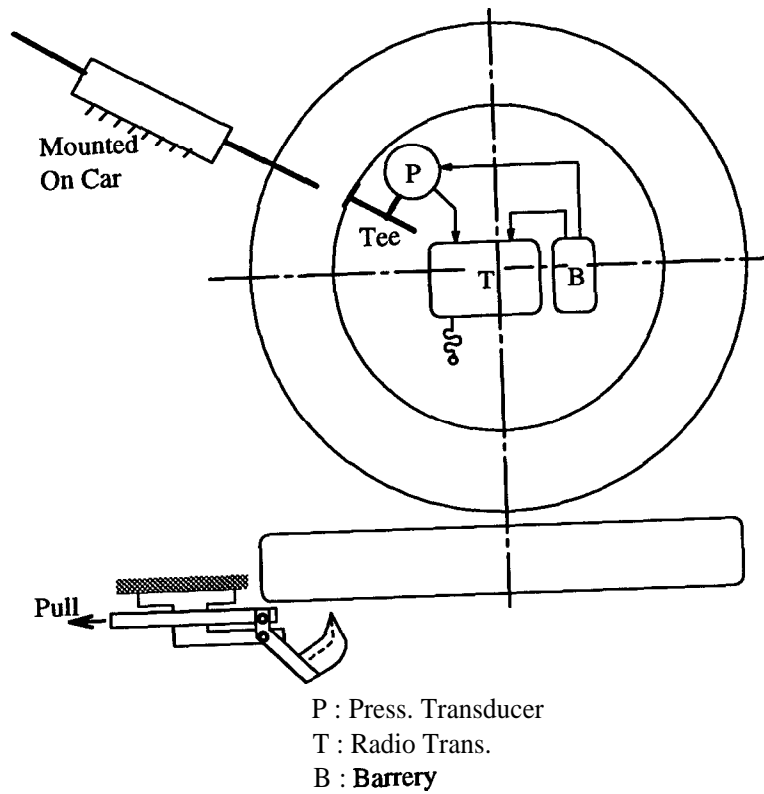


Figure 2.36: Tire burst, experimental arrangement

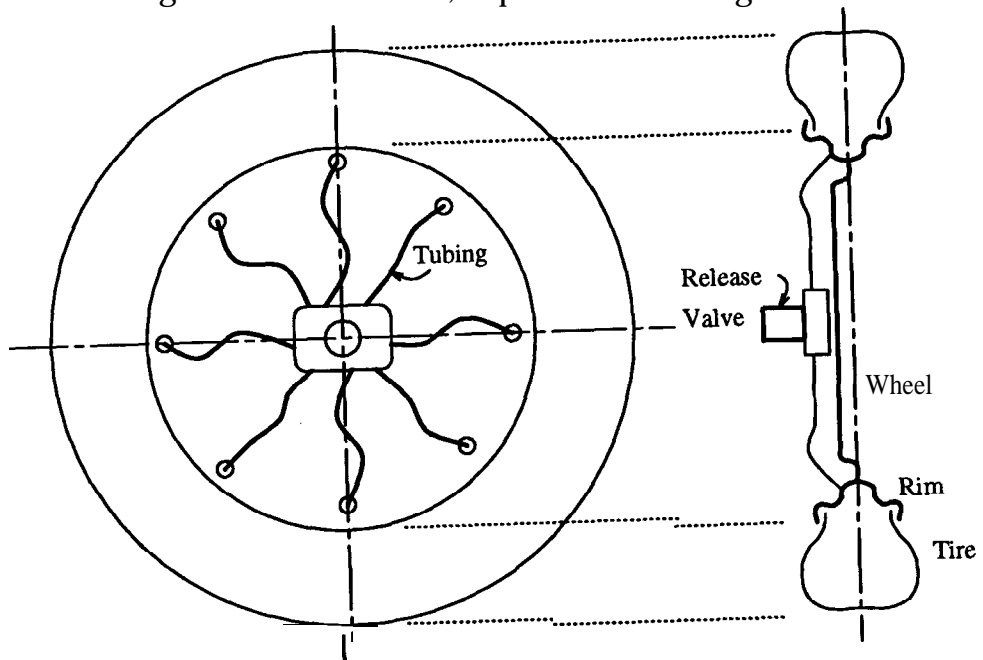
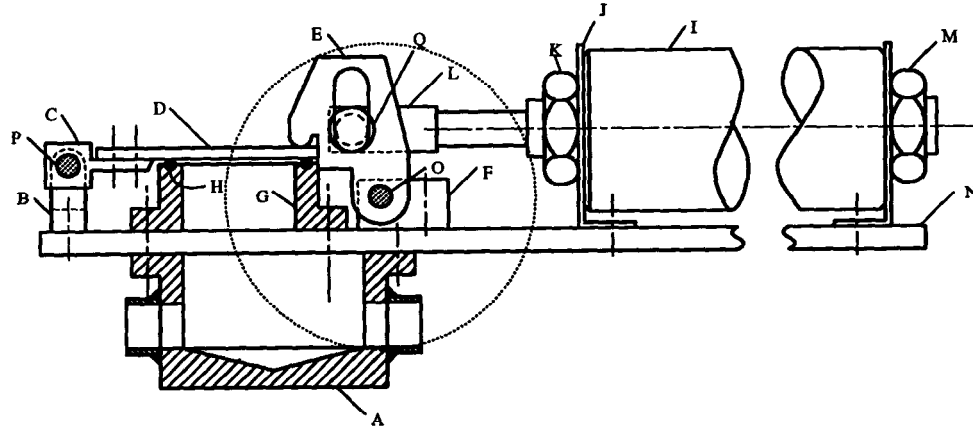


Figure 2.37: Tire burst, experimental arrangement



ASSEMBLY DRAWING

Figure 2.38: Tire burst, experimental arrangement

arrangement was devised from the viewpoint of reducing the power requirements for operating the valve. See Fig. 2.38 for details. The first stage solenoid valve was powered by a small battery on the wheel, and triggered by a radio receiver that would receive trigger signals from a radio transmitter operated by the driver. This is the transmitter receiver pair A in Figs. 2.39 and 2.40.

For the tire burst detection purposes, the tire pressure was also measured during each run of the experiment. For doing this, a pressure transducer was installed on the wheel. This pressure transducer output was passed to a signal conditioner and then to a radio transmitter on the wheel. The pressure signal then would be received by a radio receiver inside the car, and then subsequently read by the computer. This is the transmitter receiver pair B in Fig. 2.39 and 2.40. The photographs in Figs. 2.41 and 2.42 show the final form of the experimental setup. In Fig. 2.41, the wheel rim and the burst valve assembly can be seen. The flexible, transparent tubes connecting the tire air to the valve chamber are visible in the picture. The horizontal block behind the pneumatic cylinder is the first stage solenoid valve. The flap sealing the valve chamber, the slotted latch of the flap and the pneumatic cylinder make the second stage of the burst valve. Also partly visible is the tire pressure sensor and the attached wiring. Figure 2.42 shows the full burst assembly

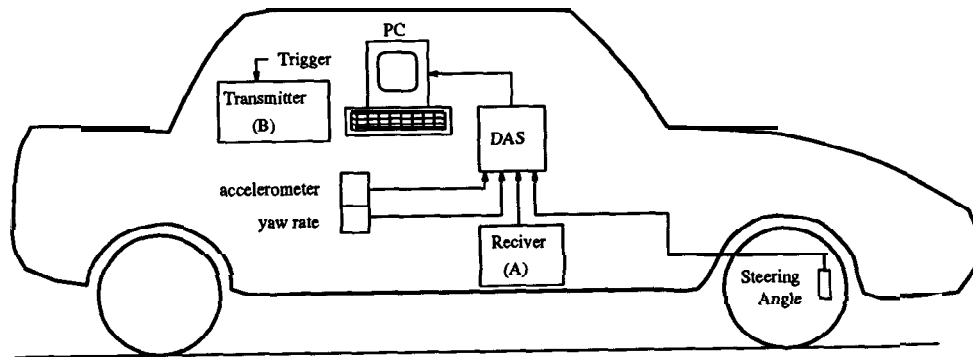


Figure 2.39: Tire burst, experimental arrangement

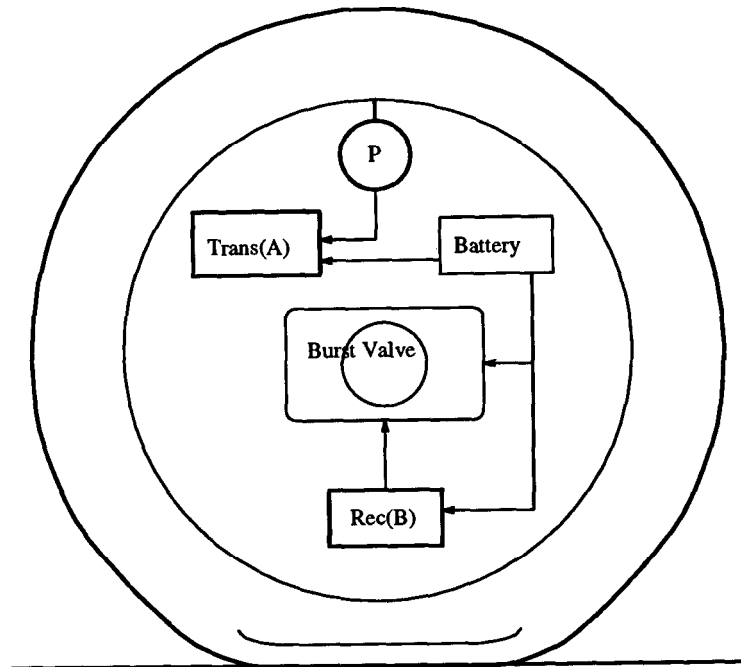


Figure 2.40: Tire burst, experimental arrangement



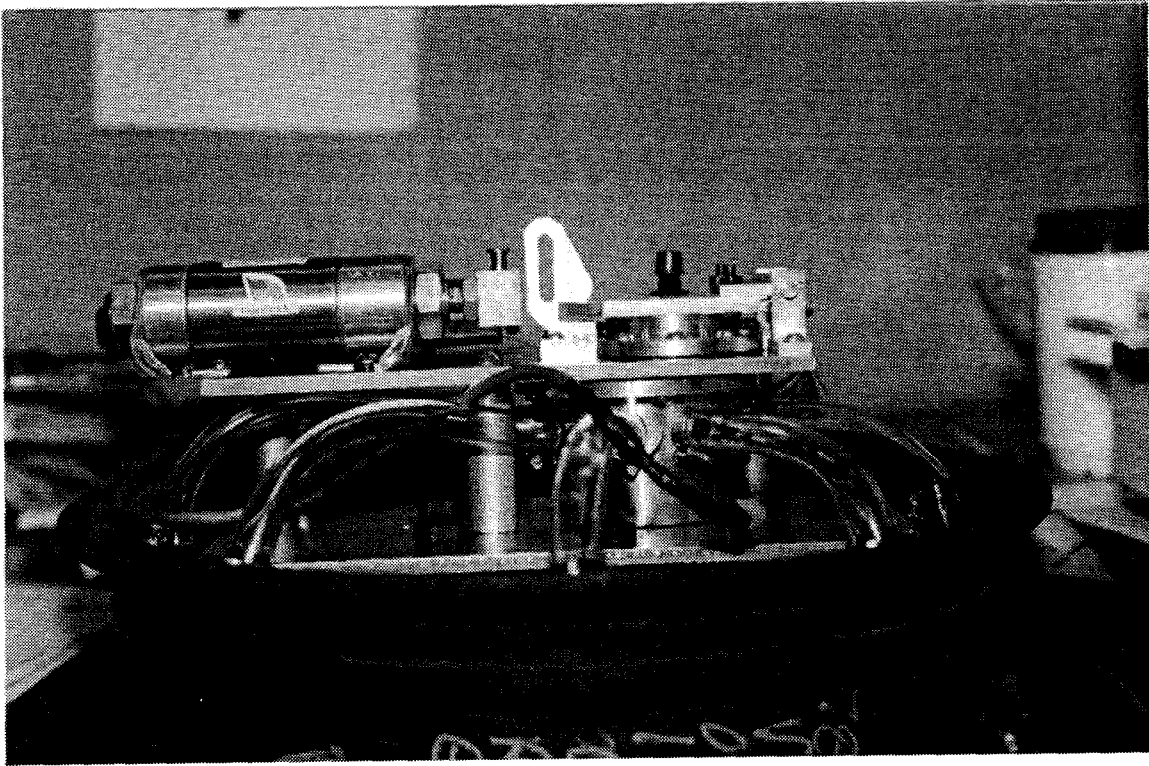


Figure 2.41: Tire burst, experimental arrangement

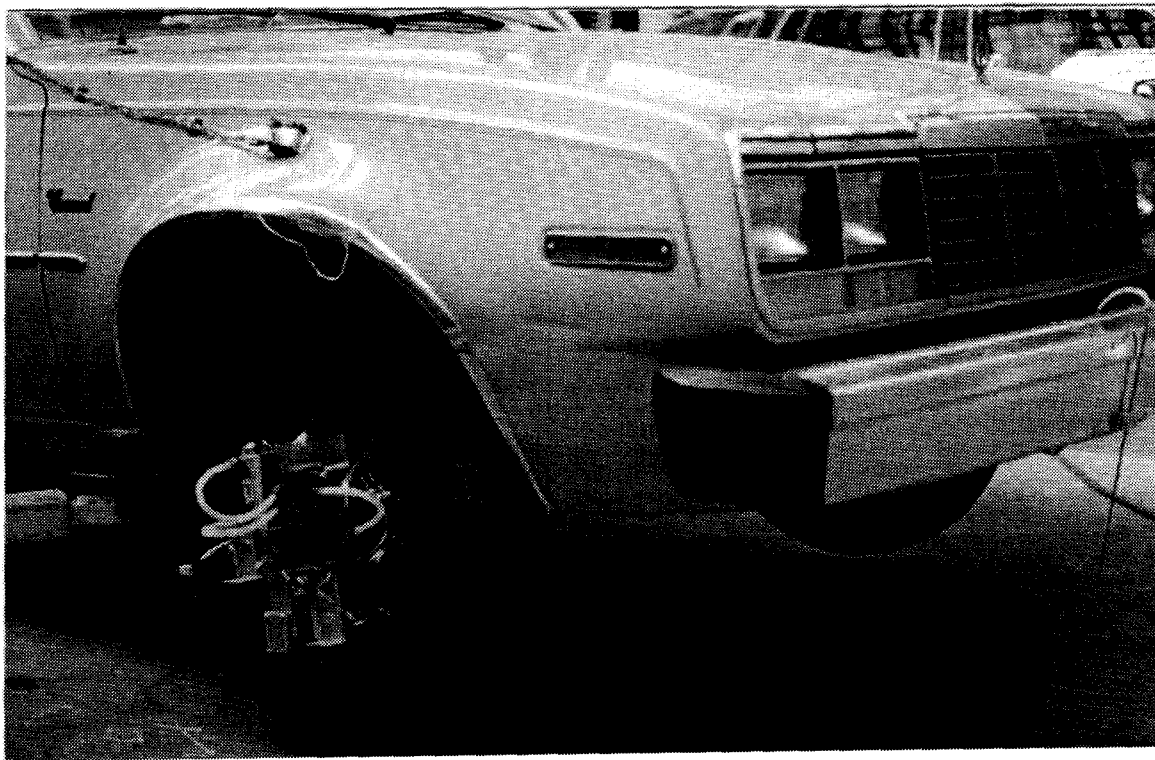


Figure 2.42: Tire burst, experimental arrangement

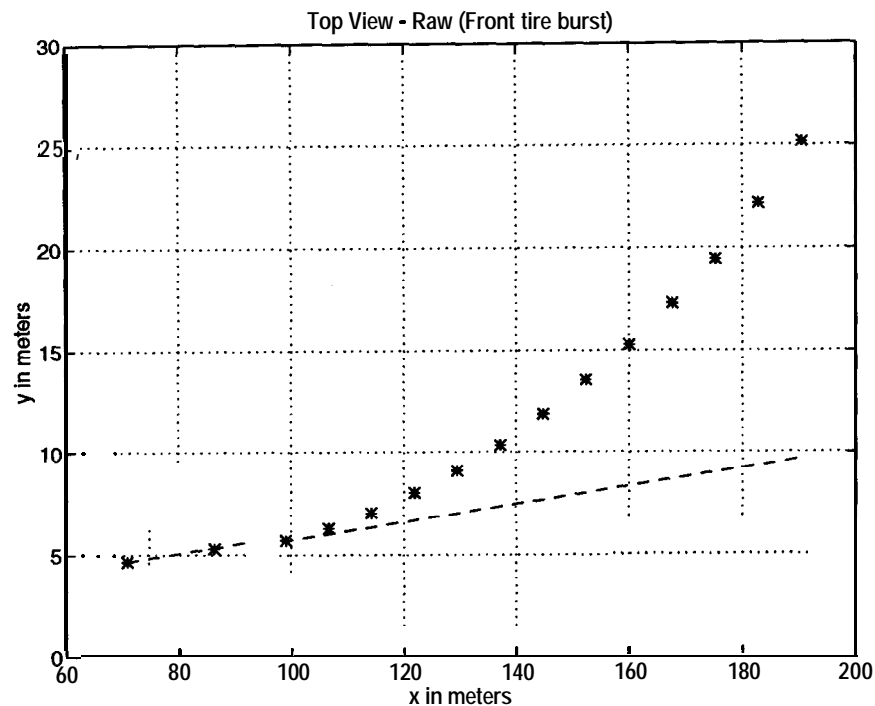


Figure 2.43: Tire burst, experimental results

mounted on the front wheel of the experimental car. The receiver B is seen with its antenna, mounted on the car body vertically above the tire. This way, the receiver could effectively catch the radio reception from the transmitter B on the wheel (not seen in the photograph).

## 2.5.2 Experimental results

Results of the experiments come in the form  $x$ - $y$  coordinates of points at which the car trail cuts the grid on the pavement. Fig. 2.43 shows one such data set plotted. The dotted line represents the initial inclination of car with respect to the pavement reference. This data set needs to be compensated for the initial inclination so that the dotted line of Fig. 2.43 becomes the  $x$ -axis of the graph. On this graph, the simulation outputs can be superimposed to compare with the experiments. Fig. 2.44 shows such a plot for the front wheel burst experiments. Plot for rear wheel burst experiments is shown in Fig. 2.45. The lateral displacements predicted

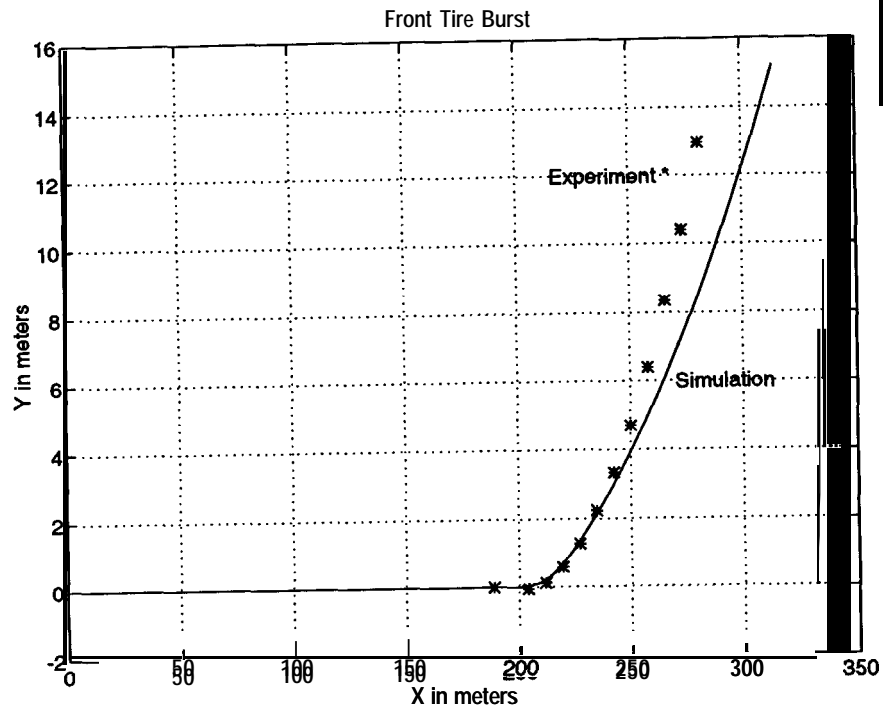


Figure 2.44: Tire burst, experimental results

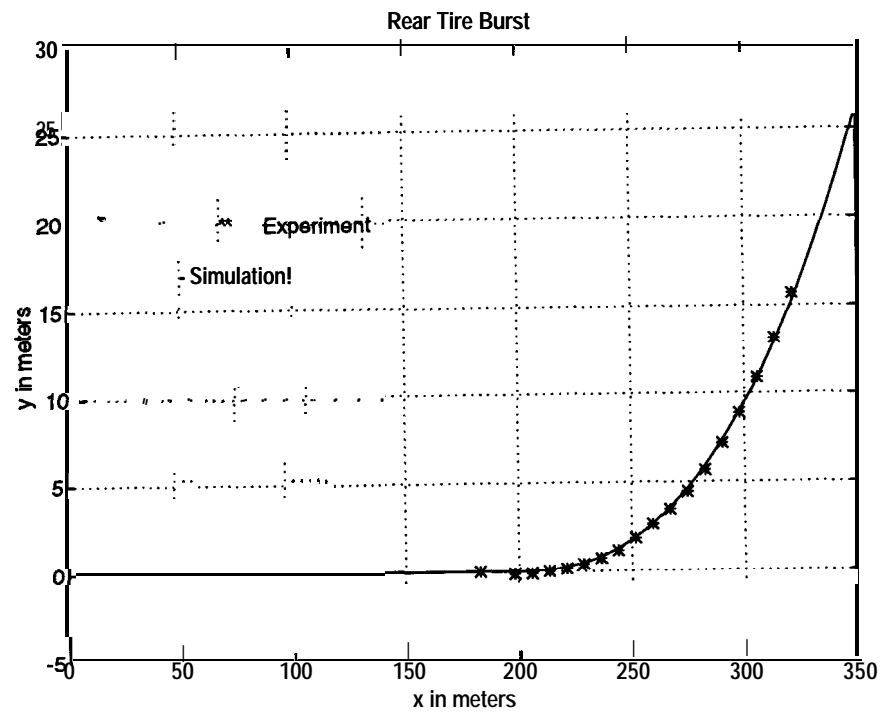


Figure 2.45: Tire burst, experimental results

by the burst model are within 20% of the actual displacements. The experimental results can be seen to be close enough to the simulations to conclude the validity of the model.

## **2.6 Conclusions**

In this chapter, we investigated the problem of tire burst and how it affects the performance of the car. The problem was approached by first modelling the tire burst in the form of nonlinear differential equations. It was demonstrated that the nominal controller would not perform well under the tire burst conditions. A controller was designed for operation after tire burst. A feedforward controller was designed for controlling the car after tire burst. The feedforward term was designed by inverting the nonlinear car dynamics. A way of approximating this term was presented. The approximation also provided a way to characterize the feedforward term for different road curvature and different tires (front/rear, left/right). Simulations were conducted to test effectiveness of the controller designed. The simplified feedforward term proved to be robust to parameter changes such as road condition change also. This was followed by the tire blow-out detection algorithm design. Finally the tire burst model was verified by experiments performed on a car.

# Chapter 3

## Sensor Fault Detection

### 3.1 Introduction

This chapter concentrates on identification of sensor faults in the car. Some of the important measurements required to control the lateral position of a car on roadway are lateral position, yaw rate, and lateral acceleration. Effective control of the car depends on the validity of these measurements. Having redundant sensors for validation has its disadvantages. Additional sensors add to the cost and space requirements. Also similar sensors generally have similar life expectancy. This means that if one of the sensors fails, there is a good chance that others will also go down soon. To avoid these problems, analytical redundancy methods are pursued for application. The basic idea is to build three observers, each of which uses two out of three measurements. If the observers are insensitive to model uncertainties, and if one of the sensors fails, then error **output**<sup>1</sup> of only one of the observers will be zero. For example, in Fig. 3.1, if sensor for  $\dot{e}$  fails, then output estimates of observer #2 and #3 will go wrong. This will make the error outputs of observer #2 and #3 to be non zero and that of #1 to be zero. Thus by knowing which error output is zero and which is not, one can identify the faulty sensor. This methodology needs observers that are insensitive to model uncertainties. If observers were not insensitive to model uncertainties, then any changes in plant, which do not

---

<sup>1</sup>error output = difference between actual measurements and their estimates

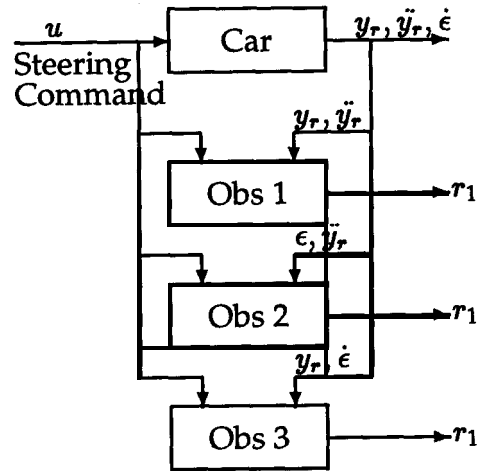


Figure 3.1: Sensor fault detection

necessarily correspond to faulty conditions, would signal fault alarm, when there is actually no fault. The theory and design of these observers is given in section 3.3.

Above discussion tells that observers and their outputs should be designed in such a way that one sensor influences only a small group of observer outputs, and does not influence others. In section 3.3, a single observer (using all the three measurements) will be designed such that each of its residue<sup>2</sup> channel is influenced by only one sensor fault.

While designing the observers, a simplified linear model of the car was used. This model was derived from the sixteen state nonlinear car model given in section 2.2.1. The simplified model is described in section 3.2. Simulations performed on the complex nonlinear model are detailed in section 3.4. For experimental investigation, a four wheel steering, four wheel drive model car was used. Experimental results and the model car details are given in section 3.5. Conclusions are presented in section 3.6.

---

<sup>2</sup>residue is a function of error output, and decisions regarding faults will be based on this vector quantity

## 3.2 System Description and Modelling

Input to the lateral control system of the car is the steering command, either from a steering wheel or by a computer. Output of the system is measured by the three sensors: lateral position sensor ( $y_r$ ), lateral acceleration sensor ( $\ddot{y}$ ), and yaw rate sensor ( $\dot{\epsilon}$ ). For lateral guidance purposes, lateral position is the output that is being regulated. The other two outputs are required for successful control of lateral position [30].

This system can be described by two different models [30]. One is a six degree of freedom nonlinear model that represents the vehicle as realistically as possible. Another is a simplified model, obtained by linearizing the complex model and retains the lateral and yaw motion dynamics. The observer used for failure detection is designed based on simplified model. Then the complex model is used for simulation purposes. Both models can describe four wheel steering vehicle.

### 3.2.1 Simplified model

The simplified model includes only the lateral and yaw motions. This model is obtained from complex model. For this purpose, cornering stiffness is defined as

$$C_s = \frac{F_y}{\alpha}$$

where  $F_y$  is the lateral force generated from the tire, and  $\alpha$  is the tire slip angle. In state space, the system can be expressed as

$$\dot{\bar{x}} = \begin{bmatrix} 0 & 1 & 0 & 0 \\ 0 & \frac{A_1}{V} & -A_1 & \frac{A_2}{V} \\ 0 & 0 & 0 & 1 \\ 0 & \frac{A_3}{V} & -A_3 & \frac{A_4}{V} \end{bmatrix} \bar{x} + \begin{bmatrix} 0 \\ B_1 \\ 0 \\ B_2 \end{bmatrix} \delta \quad (3.1)$$

$$\bar{x} = \left[ y_r \quad \dot{y}_r \quad (\epsilon - \epsilon_d) \quad (\dot{\epsilon} - \dot{\epsilon}_d) \right]^T \quad (3.2)$$

where the variables and symbols are defined in Appendix C. Lateral position  $y_r$  of the vehicle is the distance of center of mass of the vehicle from the road center line.

Table 3.1: Parameters of simplified model

Symbol	Nominal Value	min	max
$m$	1500( $kg$ )	0.85	1.15
$I_z$	3100( $kg\ m^2$ )	0.85	1.15
$C_s$	42000( $N/rad$ )	0.2	2.0
$V$	70( $mi/hr$ )	25	85
$l_1\ l_2$	1.15, 1.51( $m$ )	.	.
$d_s$	1( $m$ )	.	.

If measurement of the lateral position is done by a sensor located at a distance  $d_s$  ahead of the mass center, then the measured quantity  $y_s$  can be written as

$$y_s = y_r + d_s(\epsilon - \epsilon_d) \quad (3.3)$$

Also, the lateral acceleration in terms of state variables can be written as

$$\ddot{y} = \ddot{y}_r - V(\dot{\epsilon} - \dot{\epsilon}_d) \quad (3.4)$$

Equations (3.3) and (3.4) can be written in terms of  $\bar{x}$  as

$$\begin{aligned} \bar{y} &= \begin{bmatrix} y_s \\ \ddot{y}_r \\ \dot{\epsilon} - \dot{\epsilon}_d \end{bmatrix} \\ &= \begin{bmatrix} 1 & 0 & d_s & 0 \\ 0 & \frac{A_1}{V} & -A_1 & \frac{A_2}{V} - V \\ 0 & 0 & 0 & 1 \end{bmatrix} \bar{x} + \begin{bmatrix} 0 & 0 \\ B_1 & B_2 \\ 0 & 0 \end{bmatrix} \begin{bmatrix} \delta_1 \\ \delta_2 \end{bmatrix} \end{aligned} \quad (3.5)$$

The parameters of the simplified model are given in table 3.1. The measurement  $y_s$  is obtained by the discrete marker scheme [31]. The vehicle dynamics depends on four parameters, viz. cornering stiffness ( $C_s$ ), longitudinal velocity ( $V$ ), vehicle mass ( $m$ ), and moment of inertia about vertical axis ( $I_z$ ). Frequency response and open loop simulations show that cornering stiffness  $C_s$  and the velocity  $V$  are the dominant parameters. They vary and change the response of the system drastically. In order that the fault detection algorithm does not give false alarms, it is necessary that the algorithm is insensitive to these parameter changes.



### 3.3 Robust Fault Detector

Equation (3.1) can be written in the following form:

$$\begin{aligned}\dot{\bar{\mathbf{x}}} &= \mathbf{A}\bar{\mathbf{x}} + \mathbf{B}\mathbf{u} + \mathbf{E}\mathbf{d} \\ \bar{\mathbf{y}} &= \mathbf{C}\bar{\mathbf{x}} + \mathbf{D}\mathbf{u} + \mathbf{f}_s\end{aligned}\quad (3.6)$$

where the term  $\mathbf{E}\mathbf{d}$  accounts for the parameter and model uncertainties.  $\bar{\mathbf{x}}$  and  $\bar{\mathbf{y}}$  are state and output vectors of dimensions  $\mathbf{n} \times 1$  and  $\mathbf{m} \times 1$  respectively. The matrix  $\mathbf{E}$  describes the structure of the uncertainty, and the signal  $\mathbf{d}$  tells the magnitude of the uncertainty. The vector  $\mathbf{f}_s$  is the sensor fault vector and is of dimension  $\mathbf{m} \times 1$ .

Let the observer states be  $\hat{\mathbf{x}}$  and the dynamic equations be:

$$\begin{aligned}\dot{\hat{\mathbf{x}}} &= \mathbf{A}\hat{\mathbf{x}} + \mathbf{B}\mathbf{u} + \mathbf{K}(\bar{\mathbf{y}} - \hat{\mathbf{y}}) \\ \hat{\mathbf{y}} &= \mathbf{C}\hat{\mathbf{x}} + \mathbf{D}\mathbf{u}\end{aligned}\quad (3.7)$$

where  $\mathbf{K}$  is observer gain. Define the state error vector  $\mathbf{e} = \bar{\mathbf{x}} - \hat{\mathbf{x}}$ . The error dynamics becomes

$$\dot{\mathbf{e}} = (\mathbf{A} - \mathbf{K}\mathbf{C})\mathbf{e} + \mathbf{E}\mathbf{d} + \mathbf{K}\mathbf{f}_s\quad (3.8)$$

Define residue  $\tau$  as  $\tau = \mathbf{H}\mathbf{e}$ . Transfer function from uncertainties  $\mathbf{d}$  to  $\tau$  becomes:

$$\mathbf{G}_{rd}(s) = \mathbf{H}(s\mathbf{I} - \mathbf{F})^{-1}\mathbf{E}\quad (3.9)$$

where  $\mathbf{F} = \mathbf{A} - \mathbf{K}\mathbf{C}$  is the close loop matrix. Here,  $\mathbf{K}$  and  $\mathbf{H}$  matrices will be determined later. The structure of the fault detection scheme is shown in Fig. 3.2. Note that  $\mathbf{H}$  should be such that  $\mathbf{H} = \mathbf{W}\mathbf{C}$  for some suitable  $\mathbf{W}$ .  $\mathbf{H}$  should not have non-zero elements in a column if corresponding column of  $\mathbf{C}$  matrix has all zero elements. For the residue to be insensitive to uncertainties,  $\mathbf{G}_{rd}(s)$  should be zero.

$$\mathbf{H}(s\mathbf{I} - \mathbf{F})^{-1}\mathbf{E} = \mathbf{W}\mathbf{C}(s\mathbf{I} - \mathbf{F})^{-1}\mathbf{E} = \mathbf{0}\quad (3.10)$$

The problem now reduces to choosing  $\mathbf{K}$  and  $\mathbf{W}$  matrices to satisfy Eq. (3.10). This can be done by eigenstructure assignment[19]. If  $\mathbf{H}\mathbf{E} = \mathbf{0}$  and  $\mathbf{H}$  is such that rows

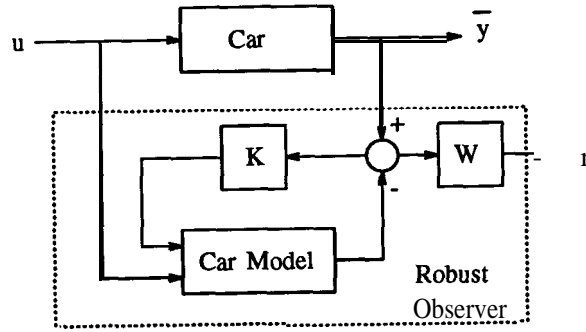


Figure 3.2: Robust observer

of  $\mathbf{H}$  are left eigenvectors of  $\mathbf{F}$ , then  $G_{rd}(s)$  becomes zero. This can be seen from the following:

$$H(sI - F)^{-1}E = H\left(\sum_{i=1}^n \frac{v_i l_i^T}{s - \lambda_i}\right)E$$

where  $v_i$  and  $l_i^T$  are right and left eigenvectors of  $\mathbf{F}$  and  $\lambda_i$  are eigenvalues of  $\mathbf{F}$ . Let,  $H = [l_1 \dots l_p]^T$ . Since right and left eigenvectors are orthogonal to each other,  $Hv_i = 0 \forall i = p+1, \dots, n$ . Then

$$H(sI - F)^{-1}E = H\left(\sum_{i=1}^p \frac{v_i l_i^T}{s - \lambda_i}\right)E$$

Also,  $\mathbf{H}\mathbf{E} = \mathbf{W}\mathbf{C}\mathbf{E} = \mathbf{0}$  implies that  $l_i^T E = 0 \forall i = 1, \dots, p$ ; giving  $G_{rd}(s) = 0$ .

The overall design procedure then consists of first determining  $\mathbf{H}$  (or  $\mathbf{W}$ ) such that  $\mathbf{H}\mathbf{E} = 0$ , and then choosing  $\mathbf{K}$  such that rows of  $\mathbf{H}$  are left eigenvectors of  $\mathbf{F}$ . This can be done as follows.

Let  $\lambda_i$  and  $l_i$  be corresponding eigenvalue and left eigenvector of  $\mathbf{F}$ . Then

$$(\lambda_i I - A^T)l_i + C^T K^T l_i = 0 \quad (3.11)$$

Consider the matrix  $[\lambda_i I - A^T : C^T]$ , and let  $[P_i^T T_i^T]^T$  be the basis for its null space. Then for any vector  $z$ ,

$$\begin{aligned} [\lambda_i I - A^T : C^T] \begin{bmatrix} P_i \\ T_i \end{bmatrix} z &= 0 \\ \Rightarrow (\lambda_i I - A^T)P_i z + C^T T_i z &= 0 \end{aligned} \quad (3.12)$$

Comparison of Eqs. (3.11) and (3.12) gives,

$$l_i = P_i z_i \quad (3.13)$$

$$K^T l_i = T_i z_i \quad (3.14)$$

Procedure for finding  $\mathbf{K}$  will be first choosing  $\lambda_i$ 's corresponding to  $l_i$ 's that need to be assigned. The selection of  $\lambda_i$  's is done arbitrarily, although it is possible to choose a set of  $\lambda_i$  's that are best for assigning the given  $l_i$ 's. This optimization problem is not attempted here. Then find the matrices  $P_i$  and  $T_i$ . From Eq. (3.13),  $z_i$  can be found. When these  $z_i$  's are plugged into Eq. (3.14) give

$$K^T [ l_1 \cdots l_p ] = [ T_1 z_1 \cdots T_p z_p ] \quad (3.15)$$

If the matrix  $[ l_1 \cdots l_p ]$  is invertible, then  $\mathbf{K}$  can be found by direct inversion. Otherwise,  $\mathbf{K}$  will be non unique.  $P_i$  may not be always square or full column rank. In that case, Eq. 3.13 should be solved in the least square sense. If  $\mathbf{P}$  is not square, then  $z$  can be found by  $z_i = (P_i^T P_i)^{-1} P_i^T l_i$ . Moreover, if  $P_i$  is not full column rank, then one can rearrange columns of  $[ P_i^T \ T_i^T ]^T$  so that  $P_i$  can be partitioned as  $[ P_{I_i} \ P_{N_i} ]^T$  with  $P_{I_i}$  being full column rank. After the rearrangement,

$$\left[ \begin{array}{c} (P_{I_i}^T P_{I_i})^{-1} P_{I_i}^T (l_i - P_{N_i} z_N) \\ z_N \end{array} \right] \quad (3.16)$$

where  $z_N$  is a free vector.

It can be noticed that  $f_{si}$  ( $i^{th}$  component of  $f_s$ ) is related to  $r_i$  ( $i^{th}$  component of  $r$ ) as:

$$r_i(s) = \frac{h_i^T k_i}{s + \lambda_i} f_{si}(s) \quad (3.17)$$

where  $h_i^T$  is  $i^{th}$  row of  $\mathbf{H}$ , and  $k_i$  is  $i^{th}$  column of  $\mathbf{K}$ . Thus if it is possible to get  $\mathbf{HK}$  product with larger terms along diagonal and off-diagonal terms close to zero, one can have separation of faults occurring in different channels of measurements[20]. This way, fault in  $i^{th}$  channel will appear in  $r_i$ , and not in other channels of  $r$ . If all the eigenvalues of  $\mathbf{F}$ , corresponding to eigenvectors in  $\mathbf{H}$  are chosen to be same, then performing rows operations on  $\mathbf{H}$  will not affect  $\mathbf{K}$ . This fact comes from the

reasoning that if all corresponding eigenvalues are equal, then linear combination of the eigenvectors is again an eigenvector of the same eigenvalue. Alternatively, the freedom available while solving Eqs. 3.13 and 3.15 can be exploited to achieve diagonal dominance of  $\mathbf{HK}$  product.

### 3.3.1 Application to lateral control problem

Notice that the uncertainties in the  $\mathbf{A}$  matrix of Eq. (3.1) are concentrated in the second and fourth row. This indicates that  $\mathbf{E}$  matrix of Eq. (3.6) would have its first and third rows to be zero and second and fourth rows to be non zero. Let the nominal plant matrix be  $\mathbf{A}$ , and the corresponding matrix under parameter variation be  $\mathbf{A}_{,,} + \Delta\mathbf{A}$ . Then the error  $e$  can be written as

$$\mathbf{e}(s) = -(sI - \mathbf{A}_c)^{-1} \mathbf{K}f(s) + (sI - \mathbf{A}_c)^{-1} \Delta\mathbf{A}(sI - \mathbf{A}_{,,} - \Delta\mathbf{A})^{-1} \mathbf{B}u(s) \quad (3.18)$$

$$\equiv -(sI - \mathbf{A}_c)^{-1} \mathbf{K}f(s) + (sI - \mathbf{A}_c)^{-1} \mathbf{E}d(s) \quad (3.19)$$

$$\Rightarrow \Delta\mathbf{A}(sI - \mathbf{A}_{,,} - \Delta\mathbf{A})^{-1} \mathbf{B}u(s) \equiv \mathbf{E}d(s) \quad (3.20)$$

where  $\mathbf{A}_{,,} = (\mathbf{A}_{,,} - \mathbf{K}\mathbf{C})$ . Figure 3.3 shows the frequency response of  $\Delta\mathbf{A}(sI - \mathbf{A}_{,,} - \Delta\mathbf{A})^{-1} \mathbf{B}u(s)$  when the velocity of the car is changed from  $V = 40\text{mi/hr}$  to  $V = 70\text{mi/hr}$ . The lines marked E(1) ... E(4) are the transfer functions of the form  $E_{,}^1$  that approximate the frequency response of  $\Delta\mathbf{A}(sI - \mathbf{A}_{,,} - \Delta\mathbf{A})^{-1} \mathbf{B}u(s)$ . From this, the estimated value of  $\mathbf{E}$  comes out to be

$$\mathbf{E} = \begin{vmatrix} 0.0461 \\ 4.5551 \\ 0.0044 \\ .4283 \end{vmatrix} \quad (3.21)$$

This confirms the intuition that the first and third row of  $\mathbf{E}$  are close to zero.

## 3.4 Simulations

Simulations were performed with the plant represented by the complex nonlinear model with the parameters of the full size car and the fault detection algorithm

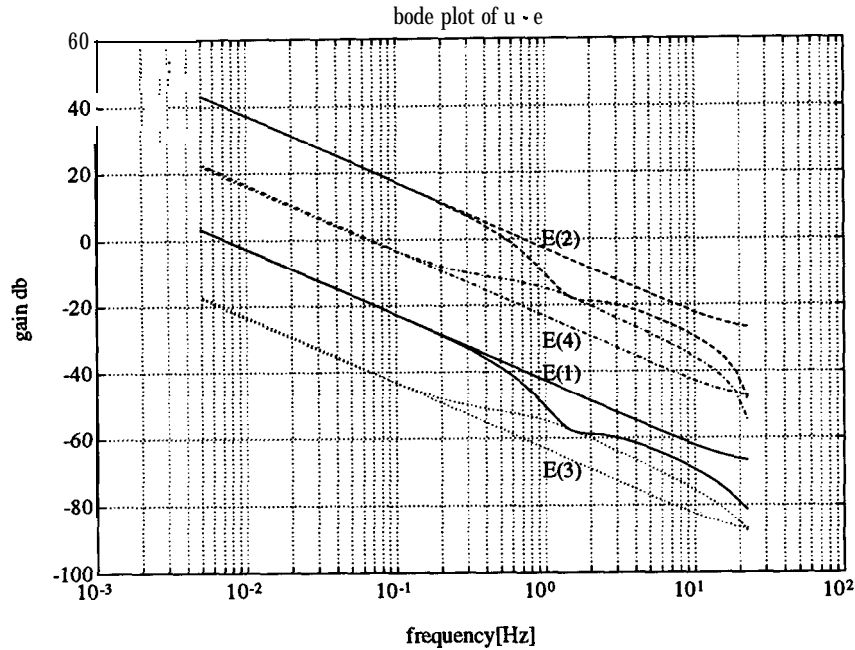


Figure 3.3: Frequency response of uncertainties

designed using the four state linear model with nominal plant parameters. The fault detection algorithm was simulated in discrete time and the plant was simulated in continuous time. First simulation (Figs. 3.4-3.7) was performed with noise in measurements and inputs. Artificial faults in measurements were introduced in these simulations. It can be seen that  $r_1$ ,  $r_2$  and  $r_3$  are sensitive to  $y_s$ ,  $\ddot{y}$ , and  $\dot{e}$  sensor faults respectively. Note that although the plant is working under nominal conditions, cornering stiffness is varying as shown in Fig. 3.7. In order to detect the faults, a threshold is required, so that when residue increases beyond the threshold, a fault alarm can be generated. The information about the covariance of residue and probability of false alarms can be combined to find out the threshold.

The next set of simulations were performed with an icy patch on roadway. Icy patch is not a faulty condition and one should expect that it produces little effect on the residue of the fault detection observer. As can be seen from Figs. 3.8-3.11, the residues are insensitive to road condition changes.

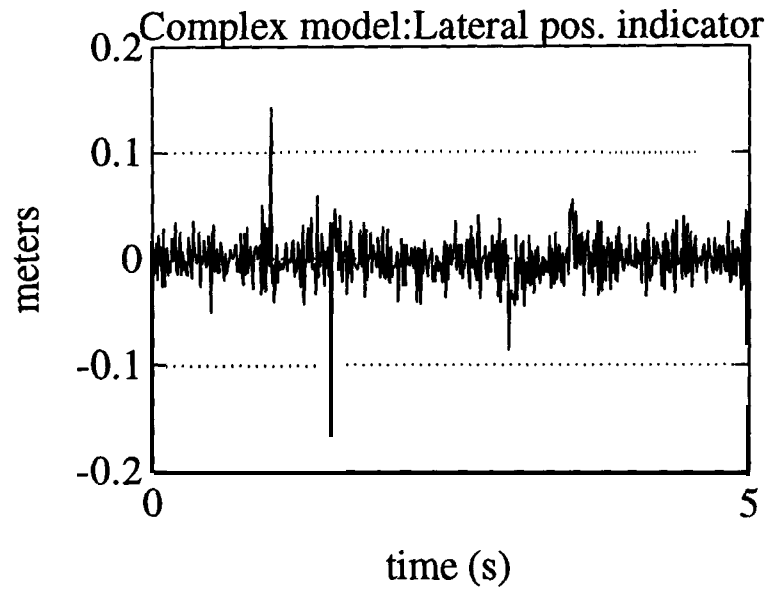


Figure 3.4: Lateral position fault indicator

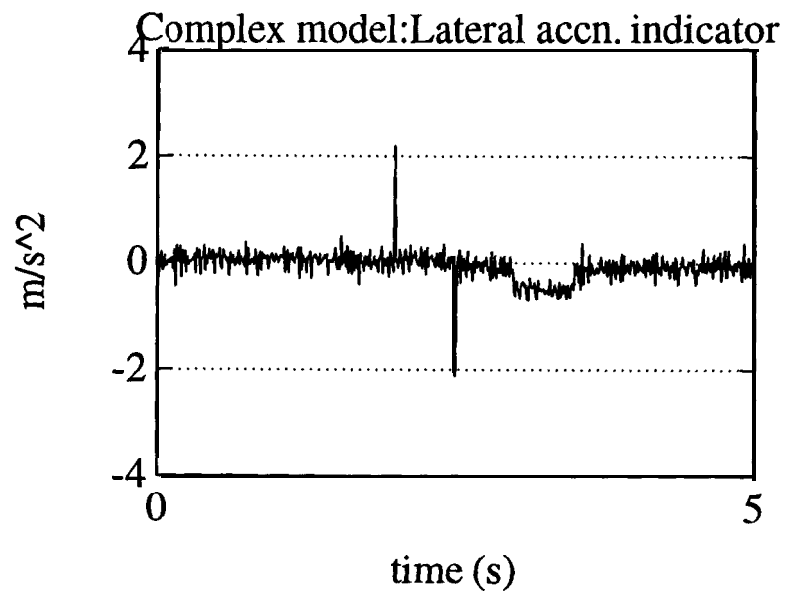


Figure 3.5: Lateral acceleration fault indicator

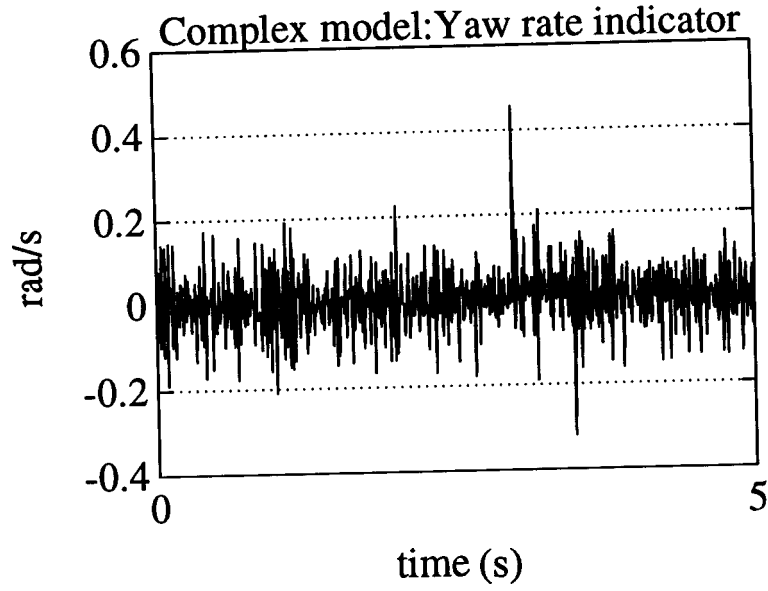


Figure 3.6: Yaw rate fault indicator

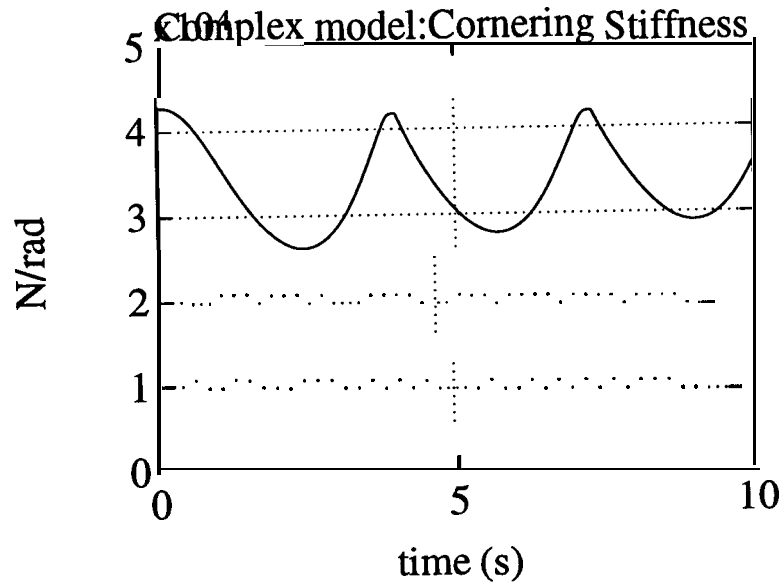


Figure 3.7: Cornering stiffness variation

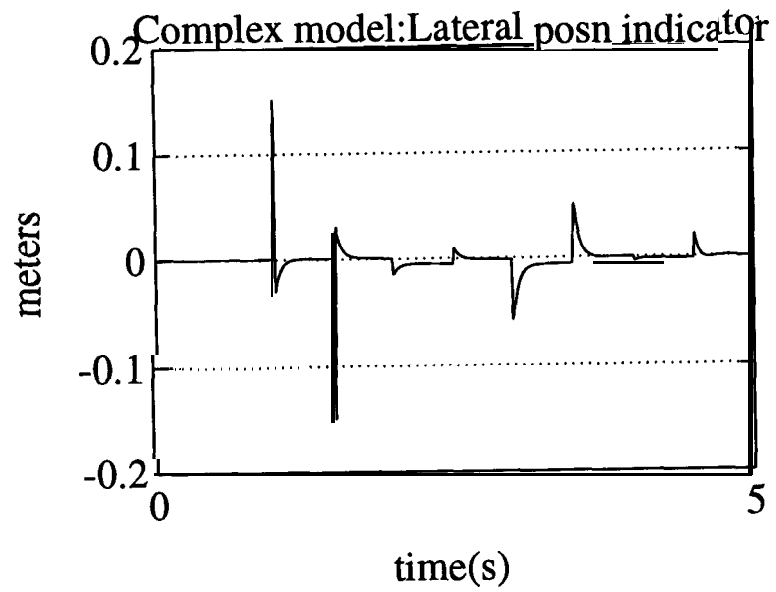


Figure 3.8: Lateral position fault indicator: icy roadway

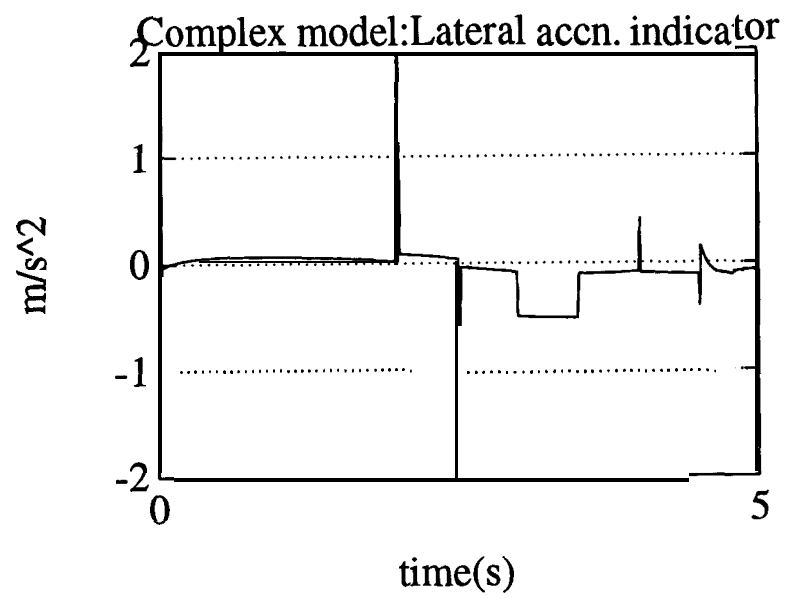


Figure 3.9: Lateral acceleration fault indicator: icy roadway



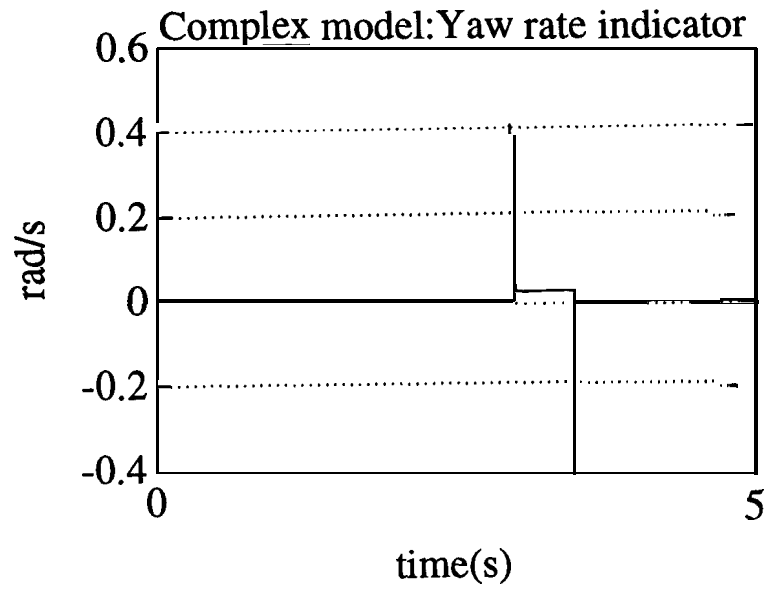


Figure 3.10: Yaw rate fault indicator: icy roadway

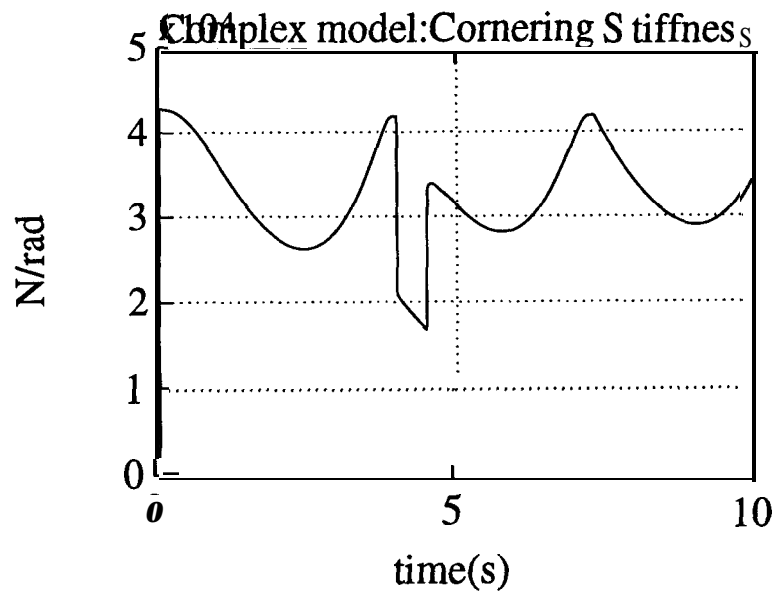


Figure 3.11: Cornering stiffness: icy roadway

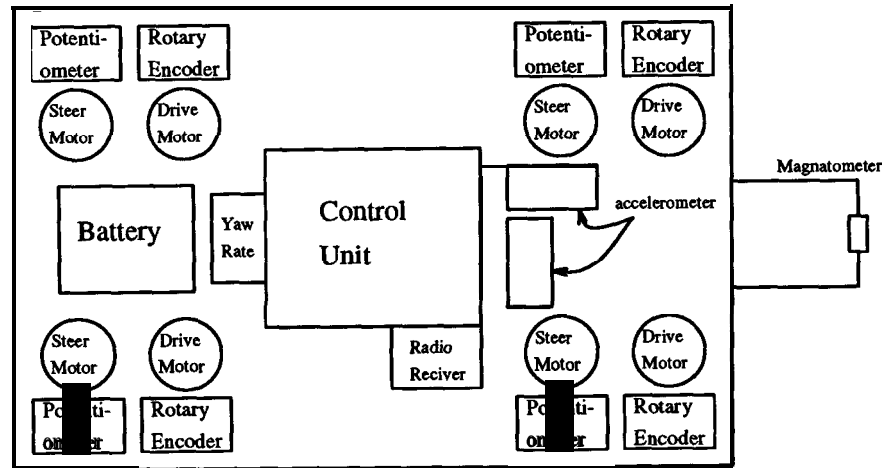


Figure 3.12: Schematic of experimental vehicle

### 3.5 Experiments

Laboratory level experimental car was used to investigate the performance of the fault detection filter. The experimental car was provided by Nippondenso Co., Ltd. for feasibility studies of vehicle control systems such as 4WS control system or four wheel drive control system and for the analysis of vehicle dynamics.

Fig. 3.12 show the schematic diagram of the experimental car. Each wheel is equipped with a driving motor and a steering motor so that the driving force and the steering angle of each wheel are controlled independently. A DC torque motor is used for the driving motor and a DC servo motor is used as the steering motor.

An optical rotary encoder is used to measure the rotational speed of each wheel and a potentiometer is used to measure the steering angle of each wheel. The car is equipped with an angular velocity sensor, a longitudinal acceleration sensor, a lateral acceleration sensor and a magnetometer. The angular velocity sensor is used for measuring the yaw rate of the car. The lateral acceleration sensor is used for measuring lateral velocity of the car and magnetometer for the lateral deviation from the magnetic markers on the roadway.

The control unit is composed of an on-board computer, where a Motorola 68020 processor and a 68881 floating point coprocessor are used for the control of the

Table 3.2: Specifications of experimental car.

<b>Chassis</b>	
Length	<b>1042mm</b>
Width	<b>630 mm</b>
Height	<b>420 mm</b>
Wheel base	<b>864 mm</b>
Tread	<b>504 mm</b>
Weigh	<b>50 kg</b>
<b>Sensor</b>	
Acceleration sensor	<b>JAE MC100</b>
Angular velocity sensor	<b>Watson ARS C141-1A</b>
Magnetometer	<b>MEDA u-MAG</b>
<b>Control Unit</b>	
CPU	<b>68020, 68881</b>
UPP	<b>HD63140*2</b>
ROM	<b>128kbytes</b>
RAM	<b>512kbytes</b>
Interface	<b>GPIB, RS232</b>
maximum speed	<b>3.0 m/s</b>

car and Hitachi universal pulse processor (UPP) is used for input sensor signals and output actuator driving signals. The control unit also has a data acquisition function that can be interfaced to a personal computer. The experimental car can be operated by a radio control unit. The electrical power of all components is supplied from a 12V battery. Table 3.2 shows the specification of the experimental car.

Experimental results are shown in Figs. 3.13-3.15. Fault in the lateral position sensor was introduced by offsetting the magnetic markers in a patch of roadway, as shown in the right side box in Fig. 3.13.  $r_1$  easily identifies this fault. Additional faults in yaw rate and lateral acceleration sensors are introduced at  $t=6.0$  and  $t=7.0$  respectively. Faults in lateral acceleration sensor are not easily detected. The reason for this is that the sensor is quite noisy as compared to other two sensors.

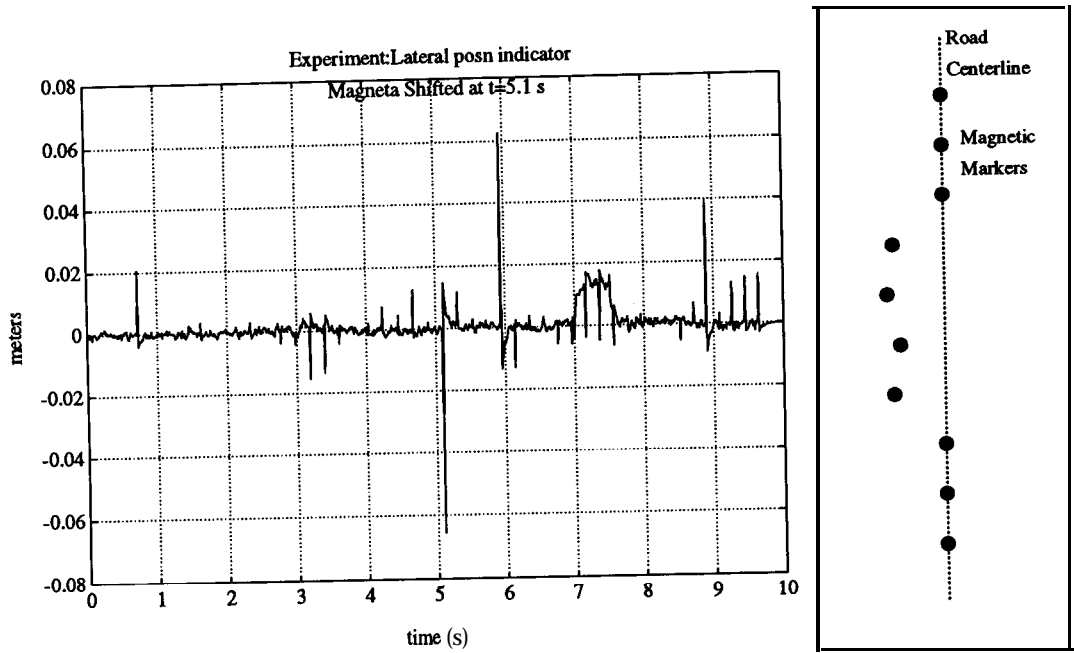


Figure 3.13: Lateral position fault indicator: experiment

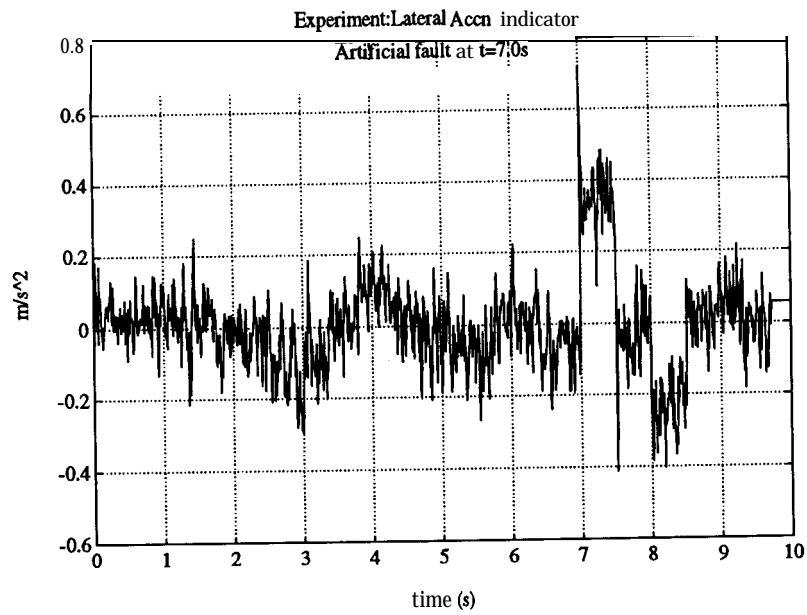


Figure 3.14: Lateral acceleration fault indicator: experiment

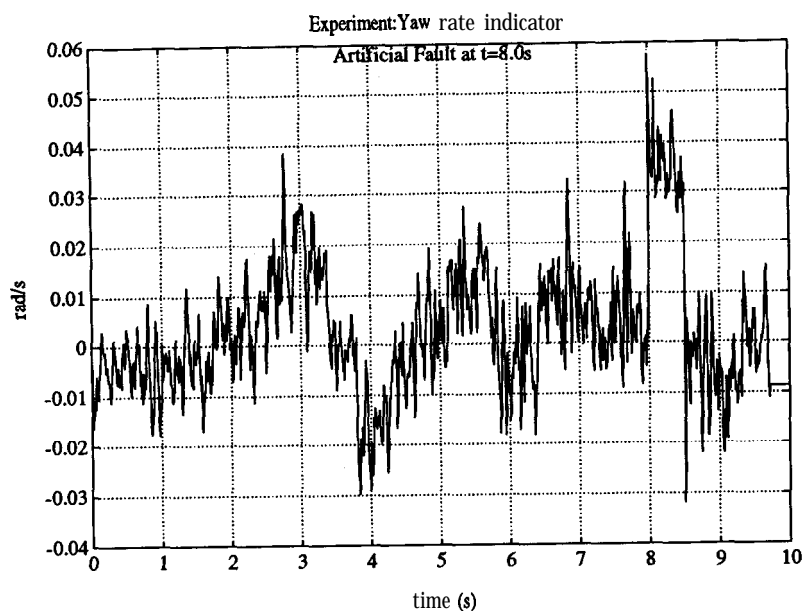


Figure 3.15: Yaw rate fault indicator: experiment

## 3.6 Conclusions

Robust fault detection algorithms have been presented for sensor fault detection. An observer is built to estimate the output variables measured by these sensors. The failure detection decisions were based on the residue, a linear function of output errors. Nonlinear vehicle model was linearized and simplified for the designing the detection algorithms. The biggest problem of counteracting the variations in cornering stiffness was handled by eigenstructure assignment approach. Also the separation of the effects of the sensor faults was achieved by making transfer function from faults to residues, diagonally dominant. Finally, the feasibility of the algorithms was verified on an experimental car.

## Chapter 4

# Enhancing Performance of Direction Sensitive Filters

### 4.1 Introduction

This chapter addresses the fault detection in a general sense. Schemes to improve the performance of direction sensitive filters will be discussed in the chapter. Direction sensitive filters or Beard Jones filters is a class of observers with some special properties. These filters were first introduced by Beard and Jones for dealing with the fault detection problem.

The additive type of failures that can be identified by the *Beard Jones* (BJ) filter are modeled by the following state space representation

$$\dot{\mathbf{x}} = \mathbf{A}\mathbf{x} + \mathbf{B}\mathbf{u} + \sum_{i=1}^r \mathbf{f}_i \rho_i \quad (4.1)$$

$$\mathbf{y} = \mathbf{c}\mathbf{x} \quad (4.2)$$

where  $\mathbf{x} \in \mathfrak{R}^n$ ,  $\mathbf{y} \in \mathfrak{R}^m$ ,  $\mathbf{u} \in \mathfrak{R}^p$  are state, output and input vectors respectively. Matrices  $\mathbf{A}$  and  $\mathbf{B}$  are of suitable dimensions.  $\mathbf{f}_i \in \mathfrak{R}^n$  are constant vectors, called failure event vectors.  $\rho_i$ 's are scalars such that  $E[\rho_i] = \mathbf{0}$  under no failure condition and  $E[\rho_i] \neq \mathbf{0}$  when  $i^{\text{th}}$  failure occurs. This model is quite suitable for representing actuator failures. For example, if the actuator corresponding to  $j^{\text{th}}$  channel of  $\mathbf{u}$

fails and makes associated component of  $u$  zero, then the failure can be represented by  $f = B_j$ , where  $B_j$  is the  $j^{\text{th}}$  column of  $B$ .

The BJ filter is a linear observer with the gain matrix  $D$ .

$$\dot{\hat{x}} = A\hat{x} + Bu + D(y - C\hat{x}) \quad (4.3)$$

Section 4.2 describes the relevant details regarding the design of  $D$  matrix. To identify more failures than the capacity of one BJ filter, a bank of such filters is proposed in section 4.3. Failure identification is based on the behavior of the output *error*<sup>1</sup> in the *output error* space. Expectation of output error (also called residue) is zero under no fail conditions, and grows in a particular direction when one of the failures occurs. The direction of growth is characteristics of the failure that has occurred. As the number of failures detected by BJ filter increases, the output error space becomes crowded with characteristic directions of failures. When noise is present in the system, it becomes difficult to recognize the direction of growth when residue magnitude is small. To detect the failure as early as possible, it becomes imperative to process the residue coming out of the filters by some additional means. Sections 4.4, 4.5 and 4.6 describe the regression and likelihood ratio[3] tests that can be used for this purpose. Section 4.7 gives derivations of some of the interesting properties of the outputs of the likelihood ratio tests. Simulations performed for testing the algorithms are presented in section 4.8, and conclusions in section 4.9.

## 4.2 Detection Filter

The detection filter has the form (4.3). Define the state error  $e = x - \hat{x}$  and output error (or residue in this case)  $\epsilon = Ce$ . Then from Eqs. (4.1) and (4.3),

$$\dot{e} = Ge + \sum_{i=1}^r f_i \rho_i \quad (4.4)$$

$$\epsilon = Ce \text{ where } G = A - DC \quad (4.5)$$

---

<sup>1</sup>difference between measurements and their estimates

The filter gain  $D$  is selected such that when one particular failure occurs, the output error becomes non-zero, as well as, it maintains one specific direction for each failure. Then the direction in which this error grows becomes the indicator of the failure that has occurred.

The basic idea behind the design can be stated as follows:

Let,

$$f_i = \sum_{j=1}^{n_i} \alpha_i^j v_i^j \quad (4.6)$$

for some  $n_i \leq n$ , where,  $v_i^j$  are eigenvectors of  $G$  and  $\alpha_i^j$  are some coefficients. This means that  $f_i$  can be represented as a linear combination of some of the eigenvectors of the close loop matrix  $G$ . Whenever,  $\rho_i$  jumps from zero to a non zero value, its effect is that the system of Eqs. (4.4) - (4.5) is excited in the direction of  $v_i^j$  eigenvectors of  $G$ . The state space response of the system can then be written as linear combination of  $v_i^j$ , with time varying linear combination coefficients. That is the state vector  $e(t)$  will be in  $sp[v_i^j]$  and the output vector  $\epsilon(t)$  will be in  $sp[Cv_i^j]$ . In order that the output vector maintains a fixed direction, one should have  $rank(sp[Cv_i^j]) = 1$ . This imposes a constraint on the eigenvectors of the close loop matrix. This constraint just says that  $Cv_i^j$ 's for all  $j$ 's should be parallel. In light of Eq. (4.6), all these  $Cv_i^j$  vectors should be also parallel to  $Cf_i$ .

It is shown in[17] that if certain conditions called mutual detectability conditions are satisfied, then a solution for  $D$ , which will assign eigenvalues of  $G$  arbitrarily; is possible. Finally, for each failure  $f_i$ , there will be a set of eigenvectors  $v_i^j$  that satisfy

$$Cv_i^1 = Cv_i^2 \dots = Cf_i \quad (4.7)$$

The subspace formed by  $v_i^1, v_i^2, \dots$  is called the detection space of  $i^{\text{th}}$  failure. In[17] it has been proved that it is impossible to design a single  $D$  matrix for more than  $m$  failures.

---

<sup>2</sup>here,  $sp[\cdot]$  stands for the subspace spanned by its argument vectors. In this case, it is the subspace spanned by  $v_i^1, \dots, v_i^{n_i}$



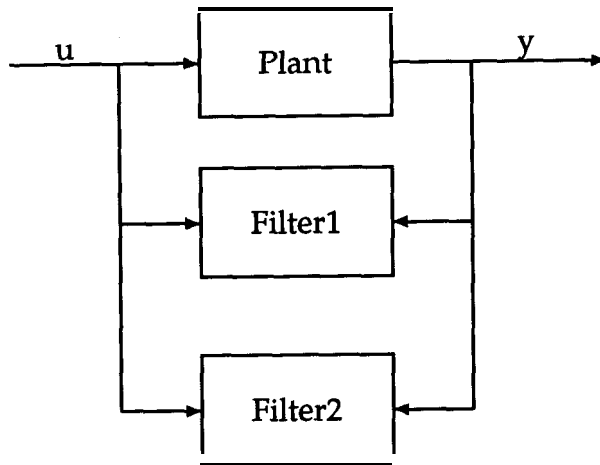


Figure 4.1: Bank of filters

When a failure occurs, the residue magnitude grows. When residue magnitude becomes sufficiently large, it generates the fault alarm. This is the failure detection phase. The fault alarm in turn triggers the failure *identification* algorithm, which identifies the direction of the residue growth to ascertain which fault has occurred. Failure identification is thus a two stage process, involving failure detection and identification.

### 4.3 Adding Additional Failures

In general, in a control system, it is required that one identifies a larger number of failures with a fewer number of sensors. There is a requirement to increase the failure identification capability. For this purpose, a bank of filters (Fig. 4.1) will be used. Filter 1 will be designed (using concepts of section 4.2) for first  $m$  failures, then Filter 2 will be designed for next  $m$  failures ( $f_i: i = m + 1, \dots, 2m$ ) and so on. When a failure occurs, and gets detected by the detection test, there will be a multiple number of directions in *output error space* to which one will have to match the residue growth direction. To do this efficiently, three methods of increasing

complexity are proposed. They are regression, likelihood ratio test with failure time known from the failure detection test and lastly, likelihood ratio test without the knowledge of failure time. The last method will not need the intermediate step of detecting the failure.

## 4.4 Regression

Once it is known that some failure has occurred at time  $t = \theta$ , the error outputs at times  $t_1, \dots, t_{n_p}$  ( $\theta < t_1 < \dots < t_{n_p}$ ) are collected and an attempt to fit a line (in  $\mathfrak{R}^m$ ) to this data is made. General equation of a line in  $\mathfrak{R}^m$  is

$$\epsilon_1 = \frac{a}{h_1} = \dots = \frac{\epsilon_m}{h_{m-1}} \quad (4.8)$$

where the parameters  $h_i$ 's will be estimated by minimizing the mean squared error. Here there are  $m - 1$  parameters to be estimated. For two output case, this becomes:

$$h_1 = \frac{\sum_{i=1}^{n_p} \epsilon_1(t_i) \epsilon_2(t_i)}{\sum_{i=1}^{n_p} (\epsilon_1(t_i))^2} \quad (4.9)$$

The design parameter for this test is the number of data points  $n_p$  that are collected. Small  $n_p$  value will yield poor convergence for  $h_i$ 's. On the other hand, larger  $n_p$  values will need longer processing time.

## 4.5 Ratio Test (*known failure time*)

This is essentially, a hypothesis test. As in section 4.4, after detecting failure at time  $t = \theta$ , the samples of *output error* are collected at times  $t_1, \dots, t_{n_p}$  ( $\theta < t_1 < \dots < t_{n_p}$ ). Hypothesis that are tested are:

- $H_0$ : No failure has occurred
- $H_i$ :  $i^{th}$  failure has occurred at  $t = \theta$ , with  $E[\rho_i(t > \theta)] = \mu_i$ .

$\mu_i$  will be estimated as a by-product of the test.

Define

$$\begin{aligned} \mathbf{e}_B &= \left[ \begin{array}{c} e^T(t_1) \cdots e^T(t_{n_p}) \end{array} \right]^T \\ \boldsymbol{\epsilon}_B &= \left[ \begin{array}{c} \epsilon^T(t) \cdots \epsilon^T(t_{n_p}) \end{array} \right]^T \end{aligned}$$

and a  $m n_p \times m n_p$  matrix,

$$C_B = \begin{bmatrix} 0 & C & \cdots & 0 \\ 0 & 0 & \cdots & C \end{bmatrix} \quad (4.10)$$

With the gaussian assumption, and under the assumption that  $H_i$  is true, the probability distribution of  $\mathbf{e}_B$  is given by following mean and variance equations[18].

$$\frac{d}{dt}(E[e(t)]) = G(E[e(t)]) + f_i \mu_i \quad (4.11)$$

$$\begin{aligned} \mathbf{0} &= GM(t, t) + M(t, t)G^T \\ &+ \left[ \begin{array}{ccc} f_1 & \cdots & f_r \end{array} \right] W \left[ \begin{array}{ccc} f_1^T & \cdots & f_r^T \end{array} \right]^T \end{aligned} \quad (4.12)$$

where,

$$M(t, s) = E[\tilde{e}(t)\tilde{e}^T(s)] \quad (4.13)$$

$$\tilde{e}(t) = \mathbf{e}(t) - E[e(t)]$$

$$M(t, t + s) = M(t, t)\exp\{sG^T\} \quad (4.14)$$

and,  $W$  is the covariance of the vector  $[\rho_1 \cdots \rho_r]^T$ . In Eq. (4.12), it is assumed that the covariance matrix  $W$  does not change because of the fault and that the noise in  $[\rho_1 \cdots \rho_r]^T$  is affecting the system for sufficiently long time. In turn Eq. (4.12) describes the steady state behavior of  $M(t, t)$ . Also note that above quantities are a function of  $\mu_i$  which is the jump occurred in the expectation of  $\rho_i$  because of failure.

The probability distribution function  $p_{\epsilon_B}(\cdot)$  of  $\boldsymbol{\epsilon}_B$  can be easily calculated by Eqs. (4.11)-(4.14) and the relation  $\boldsymbol{\epsilon}_B = C_B \mathbf{e}_B$ . Let  $Q = E[\boldsymbol{\epsilon}_B]$  and  $R = \text{Cov}[\boldsymbol{\epsilon}_B]$ . Then,

$$p_{\epsilon_B}(\boldsymbol{\epsilon}_B) = \left( \frac{1}{\sqrt{2\pi}} \right)^{m n_p} \frac{1}{\sqrt{|R|}} \exp\left[-\frac{1}{2}(\boldsymbol{\epsilon}_B - Q)^T R^{-1}(\boldsymbol{\epsilon}_B - Q)\right] \quad (4.15)$$

Now,  $p_{\epsilon_B}(\epsilon_B)$  depends on the quantity  $\mu_i$ . The probability that the hypothesis  $H_i$  is true is given by the maximum of  $p_{\epsilon_B}(\epsilon_B)$  over all  $\mu_i$  [61]: i.e.

$$\begin{aligned} p_{H_i} &= P(H_i \text{ is true}) \\ &= \max_{\mu_i} p_{\epsilon_B}(\epsilon_B) \\ &= \max_{\mu_i} \left\{ \left( \frac{1}{\sqrt{2\pi}} \right)^{m \cdot n_p} \frac{1}{\sqrt{|R|}} \exp\left[-\frac{1}{2}(\epsilon_B - Q)^T R^{-1}(\epsilon_B - Q)\right] \right\} \end{aligned} \quad (4.16)$$

The maximization problem can be solved by taking logarithm and then equating the derivative to zero. The maximization problem is not affected by taking the logarithm because logarithm is a monotonically increasing function. Now,  $Q$  is a linear function of  $\mu_i$  and one can write  $Q = q\mu_i$ , where  $q$  is unit step response of Eq. 4.11 This gives the optimum value of  $\mu_i$  that maximizes  $p_{\epsilon_B}(\epsilon_B)$  to be

$$\mu_i^* = \frac{\epsilon_B^T R^{-1} q}{q^T R^{-1} q} \quad (4.17)$$

and the corresponding probability will be

$$p_{H_i} = \left( \frac{1}{\sqrt{2\pi}} \right)^{m \cdot n_p} \frac{1}{\sqrt{|R|}} \exp\left[-\frac{1}{2}(\epsilon_B - q\mu_i^*)^T R^{-1}(\epsilon_B - q\mu_i^*)\right] \quad (4.18)$$

The probability number  $p_{H_i}$  by itself is of little significance. This number has to be compared with the probability that no fault has occurred. The probability that no fault has occurred ( $p_{H_0}$ ) can be computed by substituting  $\mu_i = 0$  in the expression for  $p_{\epsilon_B}(\epsilon_B)$ .

$$p_{H_0} = \left( \frac{1}{\sqrt{2\pi}} \right)^{m \cdot n_p} \frac{1}{\sqrt{|R|}} \exp\left[-\frac{1}{2}\epsilon_B^T R^{-1}\epsilon_B\right] \quad (4.19)$$

Comparison of  $p_{H_i}$  and  $p_{H_0}$  is done in order to ascertain if the  $i^{\text{th}}$  fault has occurred.

$$p_{i0} = \log \frac{p_{H_i}}{p_{H_0}} = \frac{1}{2} \frac{(\epsilon_B^T R^{-1} Q)^2}{Q^T R^{-1} Q}$$

One can imagine  $p_{i0}$  to be normalized version of  $p_{H_i}$ . Thus the failure corresponding to the largest  $p_{i0}$  will be the best guess for which failure has occurred,

## 4.6 Ratio Test (*unknown failure time*)

When the failure time  $\theta$  is unknown, the output error samples will be collected from a time window  $t_1 < t_2 < \dots < t_{n_p}$  that goes on shifting forward as time progresses. In fact the end point  $t_{n_p}$  of the window will be the current time. The hypothesis that are tested for this sample are exactly same as the ones in section 4.5. The only difference is that the expectations of the output error (used for finding the probability distribution of output error) is also a function of the time of failure. In turn, the number  $p_{\epsilon_B}(\epsilon_B)$  is a function of both  $\theta$  (failure time) and  $\mu_i$ . The dependence of  $p_{\epsilon_B}(\epsilon_B)$  on  $\mu_i$  is similar to the case handled in section 4.5. Its dependence on failure time can be considered as follows. Consider Eq. (4.6) where  $\alpha_i^j$  is written as  $\alpha_j$  for convenience.

$$f_i = \sum_{j=1}^{n_i} \alpha_j v_i^j = \begin{bmatrix} v_i^1 & \dots & v_i^{n_i} \end{bmatrix} \begin{bmatrix} \alpha_1 \\ \vdots \\ \alpha_{n_i} \end{bmatrix}$$

Thus when  $i^{\text{th}}$  fault occurs at time  $t = \theta$ , the state error expectation becomes,

$$E[\epsilon(t_k - \theta)] = \begin{bmatrix} C f_i & \dots & C f_i \end{bmatrix} \begin{bmatrix} \frac{\alpha_1}{-\lambda_1^i} (1 - e^{\lambda_1^i(t_k - \theta)}) \\ \vdots \\ \frac{\alpha_{n_i}}{-\lambda_{n_i}^i} (1 - e^{\lambda_{n_i}^i(t_k - \theta)}) \end{bmatrix} \mu_i$$

If,  $\lambda_i$  are chosen to be equal to  $\lambda$ , then

$$\begin{aligned} E[\epsilon(t_k - \theta)] &= -C f_i \left[ \frac{\alpha_1}{\lambda} + \dots + \frac{\alpha_{n_i}}{\lambda} \right] \mu_i \\ &\quad + C f_i \left[ \frac{\alpha_1}{\lambda} e^{\lambda t_k} + \dots + \frac{\alpha_{n_i}}{\lambda} e^{\lambda t_k} \right] e^{-\lambda \theta} \mu_i \end{aligned}$$

Let  $J = -C f_i \left[ \frac{\alpha_1}{\lambda} + \dots + \frac{\alpha_{n_i}}{\lambda} \right]$  and  $K(t_k) = C f_i \left[ \frac{\alpha_1}{\lambda} e^{\lambda t_k} + \dots + \frac{\alpha_{n_i}}{\lambda} e^{\lambda t_k} \right]$ . Then,

$$Q = \begin{bmatrix} E[\epsilon(t_1 - \theta)] \\ \vdots \\ E[\epsilon(t_{n_p} - \theta)] \end{bmatrix} = \begin{bmatrix} J \\ \vdots \\ J \end{bmatrix} \mu_i + \begin{bmatrix} K(t_1) \\ \vdots \\ K(t_{n_p}) \end{bmatrix} e^{-\lambda \theta} \mu_i \quad (4.20)$$

$$\text{Let } H = \begin{bmatrix} J \\ \vdots \\ J \end{bmatrix}, N = \begin{bmatrix} \mathbf{1} \\ \vdots \\ \mathbf{1} \end{bmatrix} = \begin{bmatrix} K(t_1) \\ \vdots \\ K(t_{n_r}) \end{bmatrix} \text{ and } \mathbf{r} = e^{-\lambda\theta} \mu_i. \text{ Then,}$$

$$Q = H\mu_i + Nr$$

The probability distribution  $p_{\epsilon_B}(\epsilon_B)$  of  $\epsilon_B$  can be obtained from Eqs. (4.20), (4.12) and from the relation  $\epsilon_B = C_B e_B$ . Here again the probability that  $H_i$  is true is given by

$$p_{H_i} = \max_{\mu_i, \theta} p_{\epsilon_B}(\epsilon_B)$$

The maximization problem can be solved by taking logarithm and then equating the partial derivatives with respect to  $\mu_i$  and  $\theta$  to zero. This gives the optimum values of  $\mu_i$  and  $\mathbf{r}$  as

$$\begin{bmatrix} \mu_i^* \\ \mathbf{r}^* \end{bmatrix} = \begin{bmatrix} H^T R^{-1} H & H^T R^{-1} N \\ H^T R^{-1} N & N^T R^{-1} N \end{bmatrix}^{-1} \begin{bmatrix} \epsilon_B^T R^{-1} H \\ \epsilon_B^T R^{-1} N \end{bmatrix}$$

It can be noted that the estimated failure occurrence time  $\theta^*$  is obtained as a by-product of this test ( $\theta^* = \frac{1}{\lambda} \log(\frac{\mu_i^*}{\mathbf{r}^*})$ ). The values of  $\mu_i^*$  and  $\mathbf{r}^*$  can be substituted in the expression for  $p_{\epsilon_B}(\epsilon_B)$  to get  $p_{H_i}$ . Equation 4.19 can be combined with this to get the value of  $p_{i0}$ .

## 4.7 Some Properties

- Case where  $\theta$  is known; under correct hypothesis:

Let the failure be such that  $E[\rho_i(t > \theta)] = \mu$ . Then

$$\begin{aligned} E[\mu_i^*] &= \frac{E[\epsilon_{i0}^T] R^{-1} Q}{Q^T R^{-1} Q} \\ &= \frac{Q^T R^{-1} Q}{Q^T R^{-1} Q} \mu \\ &= \mu = \text{actual jump in variable } \rho_i \end{aligned}$$

- Case where  $\theta$  is known; under incorrect hypothesis:

Let  $n_p = 1$  and let there be only two failures. The results can be similarly proved when these assumptions are not made. Consider Eq. (4.12) for finding covariance of  $\epsilon_B$ . Let  $\sigma_1$  and  $\sigma_2$  be the variances of  $\rho_1$  and  $\rho_2$  respectively Then,

$$0 = GM + MG^T + \begin{bmatrix} f_1 & f_2 \end{bmatrix} \begin{bmatrix} \sigma_1 & 0 \\ 0 & \sigma_2 \end{bmatrix} \begin{bmatrix} f_1^T \\ f_2^T \end{bmatrix} \quad (4.21)$$

Let  $V = [v_1 \dots v_n]$  be the matrix of eigenvalues of  $G$  with corresponding eigenvectors being  $\lambda_1, \dots, \lambda_n$ . Now, the eigenvectors and the corresponding eigenvalues of the map  $g(M) = GM + MG^T$  are given by  $(v_i; v_i^*)$  and  $(\lambda_i + \bar{\lambda}_i)$  respectively Thus, the solution of Eq. (4.21) for  $M$  can be written as linear combination of eigenvectors of the map  $g(m)$ . The final solution for  $M$  can be written in the form

$$M = V \begin{bmatrix} M_{11} & \mathbf{0} \\ 0 & \underline{M_{22}} \end{bmatrix} V^*$$

The special structure of the  $M$  matrix comes from the fact that  $V$  can be written as

$$V = \left[ \begin{array}{ccc|ccc} v_1^1 & v_1^2 & \dots & v_2^1 & v_2^2 & \dots \end{array} \right]$$

Thus under incorrect hypothesis, the expectation of  $\mu_i^*$  becomes,

$$E[\mu_i^*] = \frac{\begin{bmatrix} 0 \\ \vdots \\ 0 \\ x \\ \vdots \\ x \end{bmatrix}^T \begin{bmatrix} M_{11} & \mathbf{0} \\ 0 & \underline{M_{22}} \end{bmatrix}^{-1} \begin{bmatrix} x \\ \vdots \\ x \\ 0 \\ \vdots \\ 0 \end{bmatrix}}{Q^T R^{-1} Q} = \frac{0}{Q^T R^{-1} Q} = 0$$

where  $x$  represent non-zero entries. Moreover, one can see that  $p_{i0} = 0$  for this case.

- Third failure such that  $Cf_3 = \alpha_1 Cf_1 + \alpha_2 Cf_2$  occurred, with  $E[\rho_1(t > \theta)] = 1$  and  $E[\rho_2(t > \theta)] = 1$

Hypothesis test for  $f_1$  will yield:

$$\begin{aligned}
 E[\mu_3^*] &= \left[ \begin{array}{c} \gamma_1 \\ \vdots \\ \gamma_{n_1} \\ \mathbf{0} \\ \vdots \\ \mathbf{0} \end{array} \right]^T V^* \alpha_1 + \left[ \begin{array}{c} 0 \\ \vdots \\ 0 \\ \gamma_{n_1+1} \\ \vdots \\ \gamma_n \end{array} \right]^T V^* \alpha_2 V^{-*} \begin{bmatrix} M_{11} & 0 \\ 0 & M_{22} \end{bmatrix}^{-1} \\
 &= V^{-1} V \left[ \begin{array}{c} \gamma_1 \\ \vdots \\ \gamma_{n_1} \\ \mathbf{0} \\ \vdots \\ \mathbf{0} \end{array} \right]^T \left[ \begin{array}{c} \gamma_1 \\ \vdots \\ \gamma_{n_1} \\ \mathbf{0} \\ \vdots \\ \mathbf{0} \end{array} \right]^T V^{-*} \begin{bmatrix} M_{11} & 0 \\ 0 & M_{22} \end{bmatrix}^{-1} V^{-1} V \left[ \begin{array}{c} \gamma_1 \\ \vdots \\ \gamma_{n_1} \\ 0 \\ \vdots \\ 0 \end{array} \right]^{-1} \\
 &= \alpha_1 + 0
 \end{aligned}$$

where,  $\gamma$ 's represent non-zero quantities.

It can be seen from the three properties that the hypothesis test for  $i^{\text{th}}$  failure detects the components of any failure in the detection space of the  $i^{\text{th}}$  failure. If a failure event vector is having components in more than one detection spaces, the hypothesis tests on all those detection spaces will indicate smaller strength failures. In summary, the decision table 4.1 can be used for detecting faults.

## 4.8 Simulations

The theory was applied in simulations to a dynamic system with following state space representation.

$$A = \begin{bmatrix} -56.7253 & 1 \\ -17.5848 & 0 \end{bmatrix} \quad (4.22)$$



For  $n = 4, m = 2, \# \text{ of faults} = 4$

which fault $\rightarrow$	$f_1$	$f_2$	$f_3$	$f_4$
test perf. on Obs #1	$p_{10}$	$\times$ 0 $\times$	$\times$	$\times$
	$p_{20}$	0 $\times$ $\times$	$\times$	$\times$
test perf. on Obs #2	$p_{30}$	$\times$ $\times$ $\times$	0	$\times$
	$p_{40}$	$\times$ $\times$ 0	$\times$	$\times$

x indicates non zero elements.

Table 4.1: Fault detection decision table

$$c = \begin{bmatrix} 1 \\ 0 \end{bmatrix} \mathbf{1} \quad (4.23)$$

$$f = \begin{bmatrix} f_1 & \cdots & f_4 \end{bmatrix} \quad (4.24)$$

$$= \begin{bmatrix} -4.68 & 4.68 & -4.38 & 4.68 \end{bmatrix}$$

Two different filters were designed for  $f_1, f_2$  and  $f_3, f_4$ . When  $f_1$  occurred, the regression tests performed on filter #1 are shown in Fig. 4.2. Figure shows the convergence of  $h_1$ . Fig. 4.3 shows the values of  $p_{10}-p_{20}$  (known failure time problem) when failure # 1 occurred at time  $t = 3.59$ . It can be seen that value of  $p_{10}$  is larger than  $p_{20}$ . In Fig. 4.4 and Fig. 4.5, values of  $\mu_1^*$  and  $\mu_2^*$  are shown. It can be noticed that  $\mu_1$  converged to 1, whereas  $\mu_2$  is close to 0 all the time (see section 4.7). Fig. 4.6 shows the values of  $p_{i0}$  (unknown failure time problem) when failure #1 occurred at time  $t = 3.59$ . The estimate of the time of failure is shown in Fig. 4.7.

## 4.9 Conclusions

Failure detection and identification was done using Beard-Jones filters combined with likelihood ration test. The scheme facilitates the detection of failures when the output error space is clustered with characteristic failure directions. It is demonstrated that the probability tests are in general better than regression. It was possible to find a close form solution to the maximization problem in likelihood ratio test, even when the time of failure is unknown. This approach eliminates the

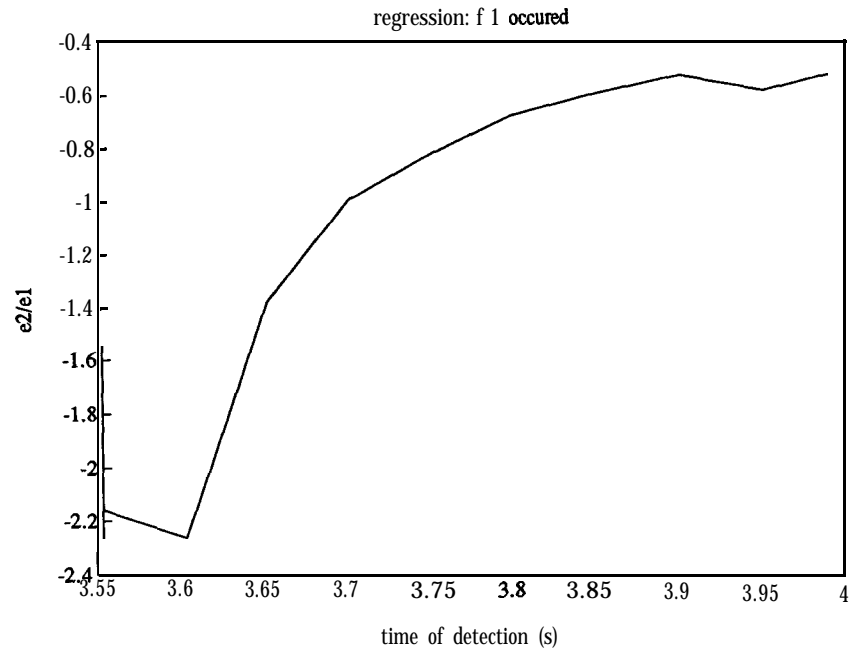


Figure 4.2: Regression

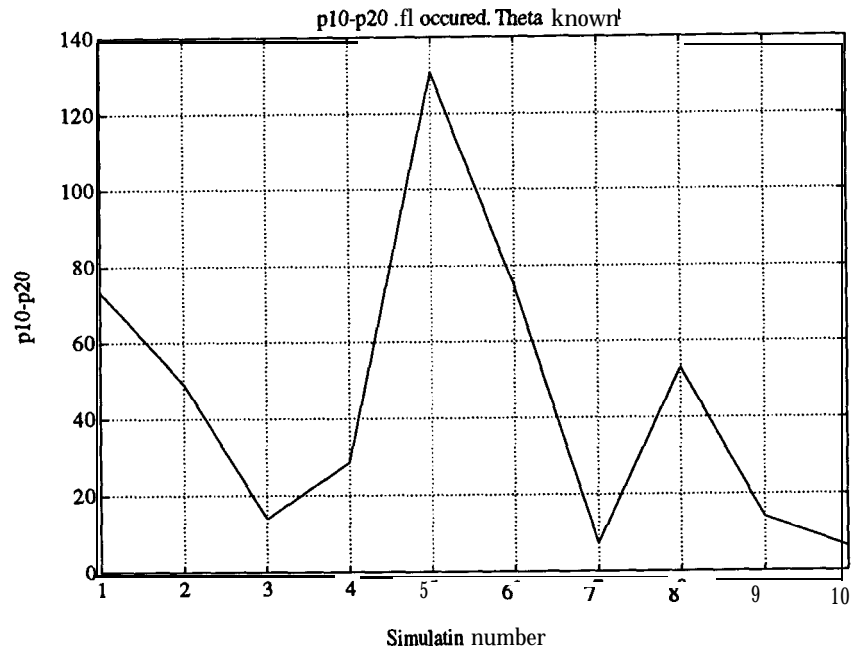


Figure 4.3: Known failure time

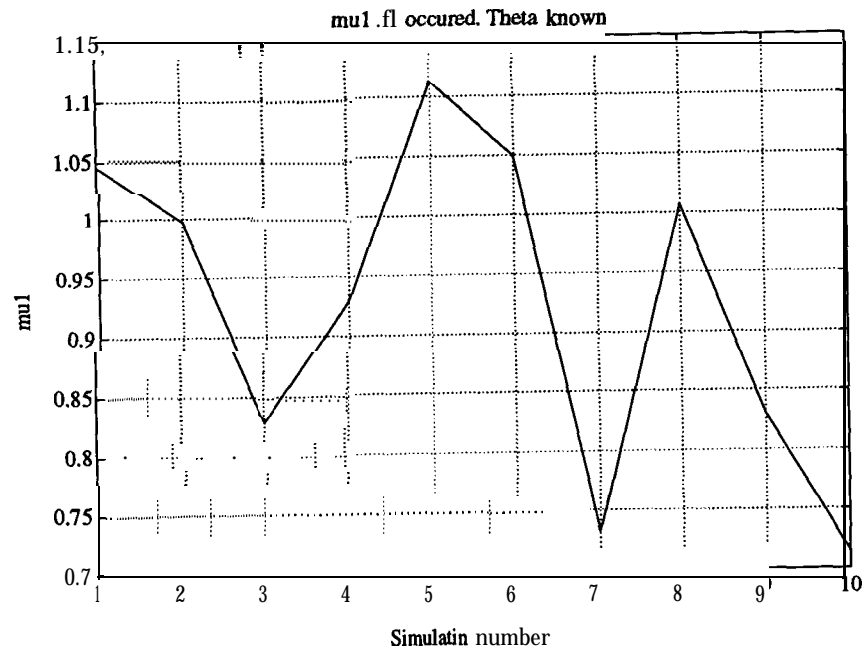


Figure 4.4: Known failure time

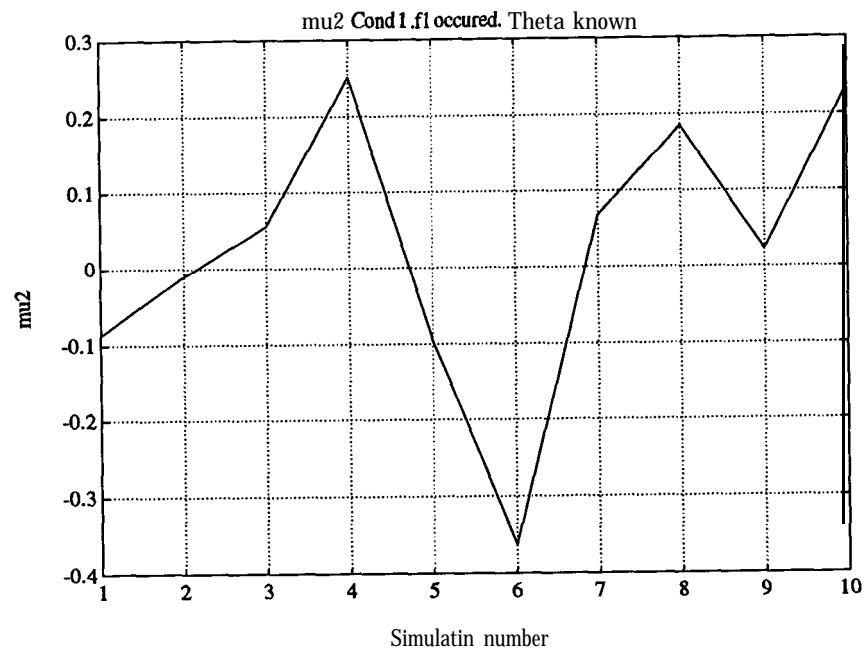


Figure 4.5: Known failure time

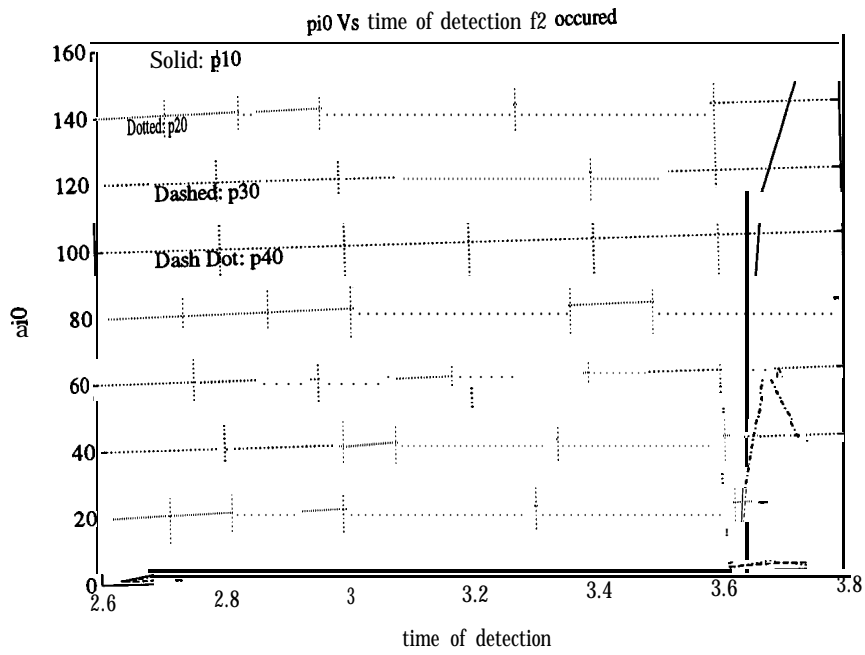
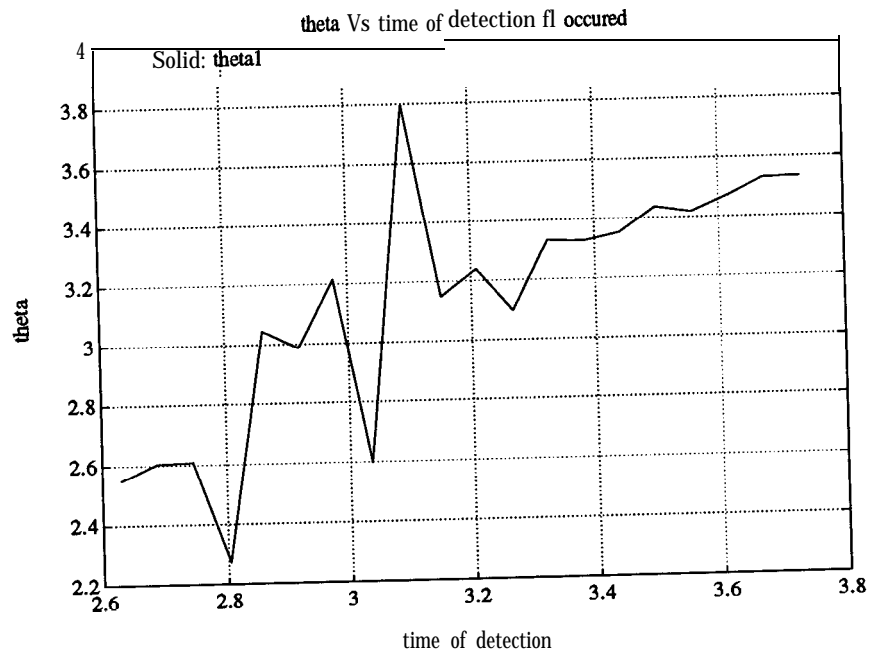


Figure 4.6: Unknown failure time

Figure 4.7: Unknown failure time, estimate of  $\theta$

need for threshold tests on norm of residue to detect the failure. Detection and identification capabilities are combined in one.

## Chapter 5

# Slip Angle Control

### 5.1 Introduction

Slip angle ( $\alpha$ ) is the angle between the plane of a tire and the linear velocity vector of the coincident point of the car. Tire-road interaction characteristics indicate that the lateral force generated at the tire is a nonlinear function of slip angle. A typical tire-road interaction characteristics is shown in Fig. 5.1. It can be seen from the figure that the tire-road characteristics has a peak around  $\alpha = \alpha^* \approx 7^\circ$ . This indicates that if the steering commands are such that the slip angle exceeds  $\alpha^*$ , then no additional lateral force can be generated by the tire. In turn, the steering commands that make slip angle larger than  $\alpha^*$  are no more effective than those that produce slip angle equal to  $\alpha^*$ . This observation leads to the concept of controlling the slip angle so that it never exceeds the value  $\alpha^*$ . In the previous lateral control work in PATH, lane following under no emergency situation has been considered. In this case, the slip angles rarely exceed  $4^\circ$  and the approximation of the characteristics in Fig.B.2 by a straight line with a slope coefficient called the cornering stiffness has been adequate. Consideration on non-linear nature of the curve in Fig.B.2 and possibility of  $\alpha$  exceeding  $\alpha_{max}$ , however should be studied for at least two reasons. Firstly, tighter radius curves can be negotiated since the slip angle will be maintained at its optimum value when the maximum steering is required, for example, in emergency maneuvers like obstacle avoidance

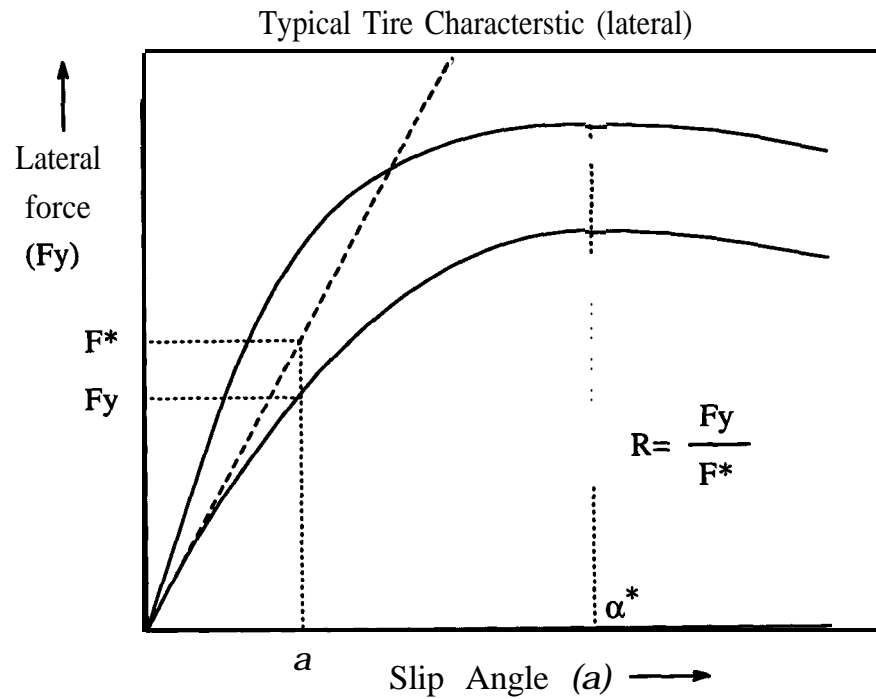


Figure 5.1: Typical tire-road interaction characteristics

or during control of vehicle under tire burst scenario. Secondly, similar curves can be negotiated with smaller steering command. Consequently, the steering actuator requirements can be relaxed.

## 5.2 Definitions

As defined in section 5.1, slip angle is the angle between the wheel plane and the linear velocity vector of the coincident point of the car.

See Fig. 5.2 for the definition of slip angle. If the velocity  $\dot{z}$  is neglected, then the equations that describe the slip angle for each of the four wheels can be rewritten as

$$\alpha_1 = \delta_1 - \tan^{-1} \left( \frac{\dot{y} + l_1 \dot{\epsilon}}{\dot{x} - \frac{a_{b1} \dot{\epsilon}}{2}} \right) \quad \alpha_2 = \delta_2 - \tan^{-1} \left( \frac{\dot{y} + l_1 \dot{\epsilon}}{\dot{x} + \frac{a_{b1} \dot{\epsilon}}{2}} \right) \quad (5.1)$$

$$\alpha_3 = \delta_3 - \tan^{-1} \left( \frac{\dot{y} - l_1 \dot{\epsilon}}{\dot{x} - \frac{a_{b2} \dot{\epsilon}}{2}} \right) \quad \alpha_4 = \delta_4 - \tan^{-1} \left( \frac{\dot{y} - l_2 \dot{\epsilon}}{\dot{x} + \frac{a_{b2} \dot{\epsilon}}{2}} \right) \quad (5.2)$$

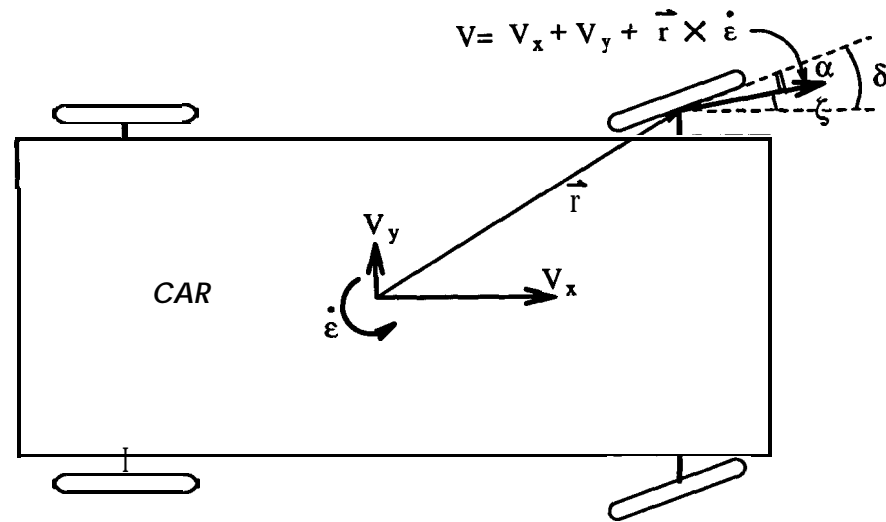


Figure 5.2: Slip angle definition

where all the variables are defined in table 2.1.

### 5.3 Slip Angle Estimation

There is no direct way of measuring the slip angle. For the purpose of controlling slip angle, one has to estimate the slip angle. Three methods for estimating the slip angle are described in this section.

Method # 1 and #2 make use of only on board sensors to estimate the slip angles, and can be used even in the absence of IVHS concepts. Method #3 on the other hand can only be applied in IVHS scenario and needs the measurement of vehicle lateral displacement.

#### 5.3.1 Method #1

In this section, we will only distinguish the slip angles as either front or rear. Thus the following discussion refers to either the inner or outer side wheels of the car, where inner and outer refer to the pairs of wheels closer to the center of curvature and farther from the center of curvature respectively. Let  $\alpha_f$ , and  $\alpha_r$  be



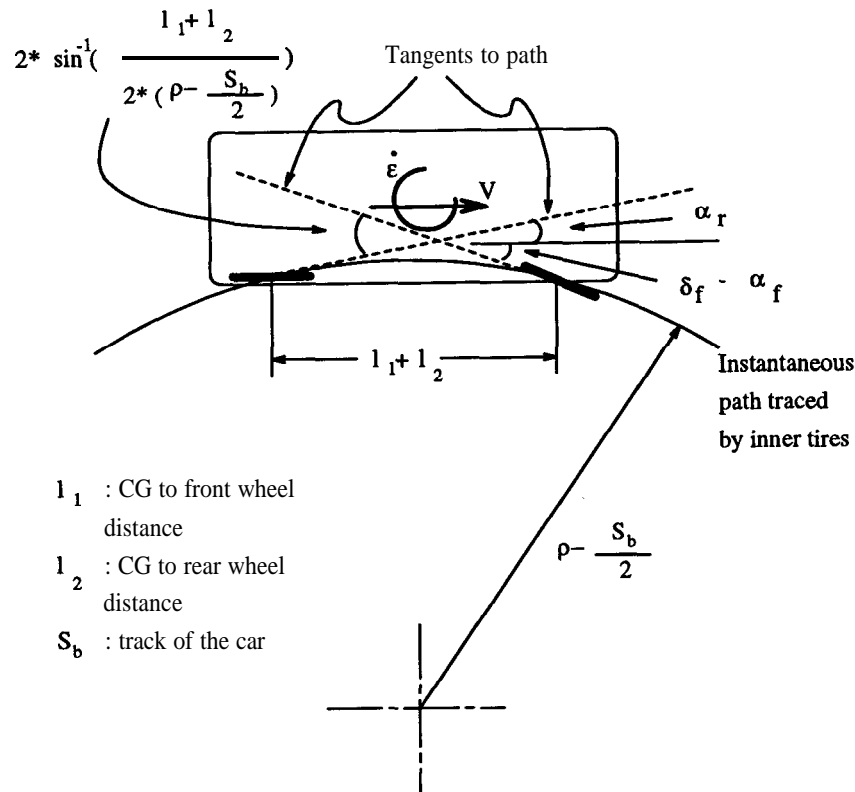


Figure 5.3: Vehicle kinematics

the slip angles at front and rear wheels respectively. Note that each point of the car will have a different velocity, because the vehicle undergoes a rigid body motion with translation as well as rotation.

Angle between the velocity vectors at the front and rear tires can be found if the instantaneous radius of curvature of the path traced by the corresponding wheels is estimated (see Fig. 5.3). This angle is in turn related to the difference  $\alpha_f - \alpha_r$ , giving one equation for estimating  $\alpha_f$  and  $\alpha_r$  as

$$\delta_f - \alpha_f + \alpha_r = 2 \sin^{-1} \left( \frac{l_1 + l_2}{2\rho^*} \right) \quad (5.3)$$

where

$$\rho^* = \rho - \frac{S_b}{2} \quad \text{for left two wheels}$$

$$\rho^* = \rho + \frac{S_b}{2} \quad \text{for right two wheels}$$

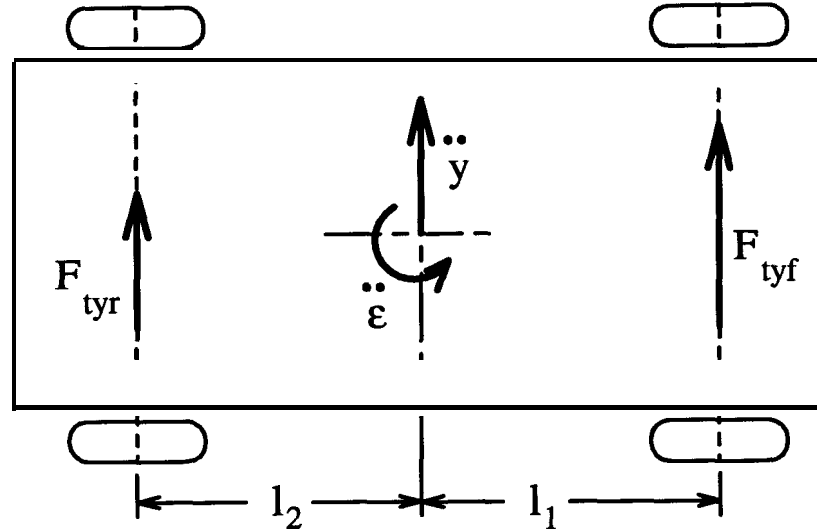


Figure 5.4: Vehicle top view, free body diagram

and  $\rho$  is the radius of curvature of the path traced by the CG of the car, given by

$$\rho = \frac{V}{\dot{\epsilon}} \quad (5.4)$$

For estimating slip angles, one more equation relating  $\alpha_f$  and  $\alpha_r$  is required. This can be obtained by several ways.

Firstly, one can argue that the ratio  $\frac{\alpha_f}{\alpha_r}$  is constant and is equal to the ratio of static component of the suspension forces. This gives

$$\frac{\alpha_f}{\alpha_r} = \frac{l_2}{l_1} \quad (5.5)$$

Solving Eqs. 5.3 and (5.5) will give the values of  $\alpha_f$  and  $\alpha_r$  as

$$\alpha_f = \frac{l_2(\delta_f - 2 \sin\gamma \frac{l_1+l_2}{2\rho^*})}{l_2 - l_1}$$

$$\alpha_r = \frac{l_1(\delta_f - 2 \sin\gamma \frac{l_1+l_2}{2\rho^*})}{l_2 - l_1}$$

Note that a good estimate of the ratio  $\frac{\alpha_f}{\alpha_r}$ , improves the estimates of the slip angles. A better estimate of ratio  $\frac{\alpha_f}{\alpha_r}$  comes from the free body diagram of the automobile (see Fig. 5.4). If one can measure lateral acceleration ( $\ddot{y}$ ) and angular

acceleration ( $\ddot{\epsilon}$ ) about  $Z$  axis, one can write

$$F_{tyf} + F_{tyr} \approx m\ddot{y} \quad (5.6)$$

$$F_{tyf}l_1 - F_{tyr}l_2 \approx I_z\ddot{\epsilon} \quad (5.7)$$

Here,  $F_{tyf}$  and  $F_{tyr}$  are the front and rear lateral forces respectively. Equations (5.6) and (5.7) can be solved to get

$$\frac{F_{tyf}}{F_{tyr}} = \frac{l_2m\ddot{y} + I_z\ddot{\epsilon}}{l_1m\ddot{y} + I_z\ddot{\epsilon}} \quad (5.8)$$

The assumptions made while deriving Eq. (5.8) are that the angular acceleration generated by the longitudinal forces is negligible as compared to the ones generated by the lateral forces (inner and outer side longitudinal forces have opposite direction moments about CG.), and that the lateral forces generated by the tires dominate over the side wind forces.

From the characteristics of Fig. B.1, one can see that as a first approximation, one can write:

$$\frac{\alpha_f}{\alpha_r} = \frac{F_{Pr}(l_2m\ddot{y} + I_z\ddot{\epsilon})}{F_{Pf}(l_1m\ddot{y} + I_z\ddot{\epsilon})} \quad (5.9)$$

where the lateral force was assumed to be proportional to the product of slip angle and the vertical force ( $F_{Pf}, F_{Pr}$ ) on the tires.

### 5.3.2 Method #2

In section 5.3.1, the distinction about slip angles was only up to front and rear. In this section, we will be dealing with slip angles at the four wheels separately ( $\alpha_i, i = 1, \dots, 4$ ). Four simultaneous equations will be written for the four slip angles.

Consider Eqs. (5.1) - (5.2). These equations can be simplified to:

$$\alpha_1 \approx \delta_1 - \frac{\dot{y} + l_1\dot{\epsilon}}{\dot{x}} \quad (5.10)$$

$$\alpha_2 \approx \delta_2 - \frac{\dot{y} + l_1\dot{\epsilon}}{\dot{x}} \quad (5.11)$$

$$\alpha_3 \approx \delta_3 - \frac{\dot{y} - l_2\dot{\epsilon}}{\dot{x}} \quad (5.12)$$

$$\alpha_4 \approx \delta_4 - \frac{\dot{y} - l_2\dot{\epsilon}}{\dot{x}} \quad (5.13)$$

Subtracting Eq. (5.12) from Eq. (5.10) gives:

$$\alpha_1 - \alpha_3 = \delta_1 - \delta_3 - \frac{(l_1 + l_2)\dot{\epsilon}}{\dot{x}} \quad (5.14)$$

Similarly, by subtracting Eq. (5.11) from Eq. (5.10) and Eq. (5.13) from Eq. (5.12) give:

$$\alpha_1 - \alpha_2 = \delta_1 - \delta_2 \quad (5.15)$$

$$\alpha_3 - \alpha_4 = \delta_3 - \delta_4 \quad (5.16)$$

Finally, the last equation for solving the slip angles comes from an argument similar to the one used in deriving Eq. (5.9). The empirical equations describing the lateral force generation characteristics of the tire indicate that the lateral force is approximately proportional to the vertical load on the tire. Moreover, the lateral force characteristics get scaled up and down, depending on the road condition number  $r_c$ . Thus,  $F_{tyi}$  the lateral force generated by  $i^{th}$  tire can be written as:

$$F_{tyi} = C_s \alpha_i R(\alpha_i) F_{P_i} r_c \quad (5.17)$$

Here,  $R(\cdot)$  is a function that is independent of the road condition and vertical loading on the tire. In other words,  $R(\cdot)$  remains same whether the car is traveling on various surfaces such as dry asphalt and ice. See Fig. 5.1 for definition of  $R(\cdot)$ . Combining Eq. (5.8) and Eq. (5.17) gives:

$$\frac{\alpha_1 R(\alpha_1) F_{P1} + \alpha_2 R(\alpha_2) F_{P2}}{\alpha_3 R(\alpha_3) F_{P3} + \alpha_4 R(\alpha_4) F_{P4}} = \frac{l_2 m \ddot{y} + I_z \ddot{\epsilon}}{l_1 m \ddot{y} + I_z \ddot{\epsilon}} \quad (5.18)$$

Equations (5.14), (5.15), (5.16), and (5.18) can be solved to get the slip angles  $\alpha_i, i = 1, \dots, 4$ .

### 5.3.3 Method #3

In Eqs. (5.1) and (5.2), the only quantity that can not be usually measured is the lateral velocity  $\dot{y}$  of the vehicle. However in the PATH-IVHS scenario, lateral displacement  $y_r$  of the CG of the car from the roadway centerline can be measured. In addition, it is possible to measure the inclination of the car with respect to the

roadway centerline by having lateral displacement sensors at front and rear ends of the car. This inclination is nothing but  $(\epsilon - \epsilon_d)$ , where  $\epsilon$  is the inclination of the car from a fixed reference and  $\epsilon_d$  is inclination of roadway centerline at the current place from the same fixed reference. The lateral velocity of the car can be calculated to be

$$\dot{y} = \dot{y}_r - \dot{x}(\epsilon - \epsilon_d)$$

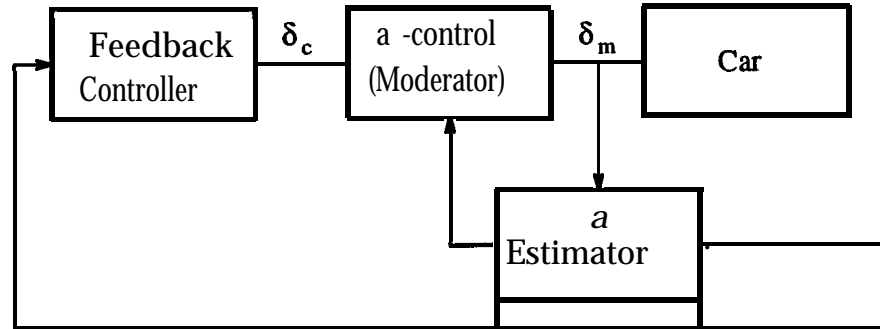
The lateral velocity thus measured can be directly used in Eqs. (5.1) and (5.2) to get the slip angle for each of the four wheels.

This method of slip angle estimation can be used in the PATH-IVHS scenario where measurement of  $y_r$  is available. Moreover, this method involves differentiation of lateral displacement, and could lead to noise amplification.

## 5.4 Slip Angle Controller

The basic aim of slip angle controller is to ensure that the slip angle does not exceed the peak point of lateral tire force characteristics. In addition the slip angle controller should not hinder the vehicle operation when the slip angle is less than  $\alpha^*$ . In reality, there are four slip angles and one control input ( front wheel steering command ). It is impossible to control all four slip angles at the same time. This problem will be solved by controlling the weighted average of the slip angles instead of the slip angles themselves.

A controller structure shown in Fig. 5.5 will be considered for  $\alpha$ -control. The controller will consist of an  $\alpha$ -estimator block to estimate the slip angle. Based on the value of this estimate with respect to the saturation point  $\alpha_{max}$ ; the moderator block will either let the steering commands pass as it is ( $\delta_1 = \delta_2$ ) when  $\alpha_{estimate}$  is less than  $\alpha_{max}$  or it will block them. This type of action will tend to improve the lateral stability of the vehicle. If slip angles are permitted to exceed  $\alpha_{max}$ , the lateral forces generated will saturate and consequently lesser accelerations and velocities will be produced. This in turn will tend to increase the slip angles, creating a positive feedback loop. The positive feedback is potentially hazardous and should



$\delta_c$  : Steering Command

$\delta_m$  : Modified Steering Command

Figure 5.5:  $\alpha$ -control structure

be avoided. Slip angle control will address this issue by not permitting the slip angle to exceed the saturation point.

Let us define a quantity  $q$  as follows:

$$q = \alpha_f - \alpha^*$$

When  $q$  is less than zero, the slip angle is less than  $\alpha^*$ , and the slip angle control does not have to be active. When  $q$  is greater than zero, slip angle is more than  $\alpha^*$ . By blocking the steering commands going to the car in such a way that  $q$  is reduced, the slip angle control will be able to produce more lateral force than would be produced without the slip angle control. The slip angle controller will be dormant when  $q \leq 0$  and will be blocking the steering commands when  $q > 0$ .

Since the lateral force produced by a tire is proportional to the vertical load on the tire, each of the slip angles produced are only as important as the corresponding vertical force in generating the lateral force. This leads to redefinition of the quantity ( $q$ ) as:

$$q = \frac{1}{S_P} \sum_{i=1}^4 F_{P_i} (\alpha_i - \alpha^*) \quad (5.19)$$

Based on this quantity  $q$ , the a-control block of Fig. 5.5 would become,

$$\delta_m = \delta_c - kq \text{ for } q > 0$$

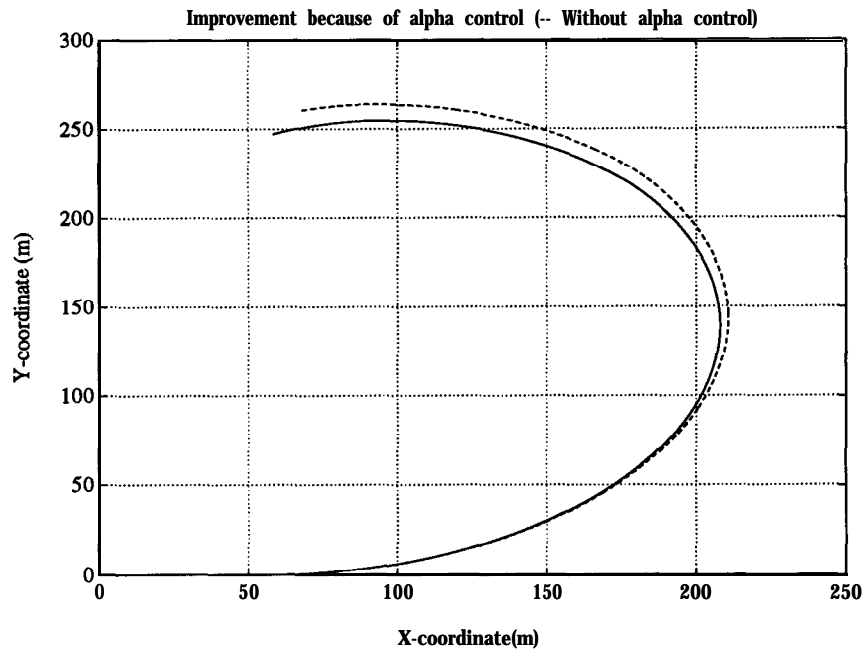


Figure 5.6: Slip angle controller performance: trajectory

$$= \delta_c \quad \text{for } q \leq 0$$

In addition to the proportional control of Eq. (5.20), lead controller was also pursued for possible application for slip angle control.

$$\begin{aligned} \delta_m &= \delta_c - k \frac{1 + T_s}{1 + aT_s} q \quad \text{for } q > 0 \\ &= \delta_c \quad \text{for } q \leq 0 \end{aligned}$$

Figures 5.6 - 5.7 show the simulation results with proportional control when the car was commanded to negotiate a 'J' curve. The car steering angle was kept zero till time  $t = 2.09$  and then a step of  $7^\circ$  was given to the steering input. The trajectory of the car with and without slip angle control is shown in Fig. 5.6. The corresponding steering angles are shown in Fig. 5.7. As can be seen from the figure, after applying the slip angle control, one can achieve tighter curves. There is also a significant reduction in control effort required to perform the maneuver under the slip angle control. It can be noticed that the slip angle tends to overshoot during the transition from the straight to the curved section of the 'J' curve, and

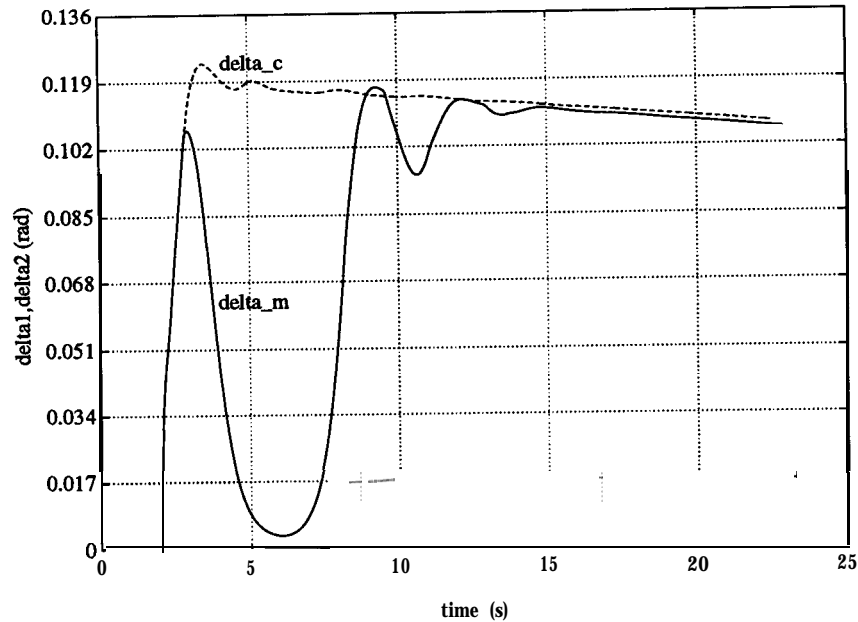


Figure 5.7: Slip angle controller performance: steering command

that the slip angle controller creates more lateral accelerations during the transition period. This leads to shifting of the curve traced by the vehicle towards the center of curvature.

## 5.5 Conclusions

The idea of slip angle control to improve the cornering performance of cars was presented in this chapter. Three schemes for estimating the slip angle were presented. This was followed by a controller structure for controlling the slip angle. Finally, simulations were conducted to show the performance improvement because of the slip angle control. The performance improvement is of two kinds. Firstly, tighter curves become possible under the slip angle control. Secondly, similar curves can be negotiated by much smaller steering commands.



## 5.6 Future Research

In addition to the proportional and lead control (Eqs. (5.20) and (5.20)) used in the *slip* angle control *block*, one could use fancier algorithms. This control block starts moderating the steering command when  $q$  crosses zero, and is increasing at some finite non zero rate. This introduces sudden action on the part of slip angle controller. It is possible to use  $\dot{q}$  to get some sort of preview information of  $q$ , to improve the performance of the slip angle controller. Since this is a nonlinear system with a lot of uncertainties, it is a good place for applying the sliding mode controller.

In order to improve the slip angle estimate, one can build an observer to estimate  $\dot{y}$ . The estimate can be directly used in Eqs. (5.1) - (5.2).

Equations B.1 and B.2 indicate that the tire forces generated are functions of slip angle ( $\alpha$ ) as well as slip ratio ( $A$ ). In order to maximize the lateral/longitudinal force, one has to really consider controlling both of the slip ratio and slip angle. The detailed investigation of combining the different control strategies for slip ratio and slip angle control are left for future research.

## Chapter 6

# Conclusions and Future Research

### 6.1 Conclusions

The problem of fault tolerant control of automobiles was addressed in this dissertation. The ultimate goal of fault tolerant control was to improve the safety and reliability of the cars when operating under the IVHS scenario. In the IVHS scenario, a close-loop controller replaces human driver. For achieving the safety/reliability goals, fault detection algorithms were applied. The controller structure was designed to get rearranged when a fault alarm is generated. The rearrangement would replace the nominal controller by emergency controller to handle the fault effectively.

A specific failure considered in this dissertation was tire blow out. The tire burst and its effects on the behavior were modelled in the form of differential equations. Modelling of tire burst involves the modelling of several effects like changes in the operating conditions, vehicle geometry and tire characteristics. Based on the tire burst model, the behavior of the car after the tire blow out was studied. The study showed the importance of developing emergency controllers to handle the tire burst effectively.

The emergency controller consists of two parts. First is a feedback part that was essentially a FSLQ controller, redesigned by ignoring passenger comfort. The second part consists of a feedforward term, that is triggered by the tire burst

alarm. This term was designed using non-linear model inversion technique. The feedforward term was generated off-line and was approximated by the output of a second order filter. The parameterization of the feedforward term was done for the different radii of curvature of the roadway on which burst happens and for different tires (eg. front, rear, right, left). The controller was tested in simulation study and the lateral displacements of the vehicle were controlled within  $\pm 0.15m$ . Finally the tire burst model was verified by experiments. During the experiments, the tire burst was created by rapidly releasing the air from the tire by a two stage release valve that was mounted on the tire and triggered by a remote controlled device. The model developed was found to predict the behavior of the car quite well.

For sensor fault detection, model based fault detection scheme was pursued. In the model based fault detection scheme essentially a set of observers was designed to estimate the quantities that were measured by the sensors. The decisions regarding the sensor faults were based on the comparison of the sensor output and the corresponding estimates. Linearized car model was used for designing the sensor fault detection scheme. Eigen-structure assignment was used for making the fault detector insensitive to road condition changes. The algorithm was successfully used to detect sensor faults in a laboratory experimental car.

In order to improve the performance of the direction sensitive filters, a likelihood ratio test was proposed. In the likelihood ratio test the probability that a specific failure has occurred was calculated and compared with the probability that no failure has occurred to detect if the failure has occurred or not.

Finally the idea of slip angle control to improve the emergency cornering performance of the vehicles was developed. The slip angle controller essentially controls the tire slip angle by modulating the steering commands so that the slip angle never goes beyond the desired range. The structure of slip angle controller consisted of slip angle estimator and a moderator block. The slip angle controller was demonstrated to improve the cornering performance of the vehicle by producing larger lateral accelerations.

## 6.2 Future Research

The future research topics in the area of fault tolerant lateral control of vehicles are,

- (1) Closed loop experimentations of the tire burst controllers: In this dissertation, the tire burst model was verified in open loop. The controllers designed for tire burst operation should be tested in the close loop tire burst experiments.
- (2) Slip angle controller: Sliding mode, FLC and feedforward controllers can be investigated for possibility of application to the slip angle control problem.
- (3) Improvement of slip angle estimate by estimation of the lateral velocity can be explored.
- (4) Slip angle control ( which is concerned with lateral force generation characteristics) and slip ratio control ( which is concerned with longitudinal force generation characteristics) can be integrated. Since the total tire force depends both on the slip angle and the slip ratio it is logical to combine the two approaches in order to control the total tire force.
- (5) Integration of lateral/longitudinal fault detection schemes: The sensor fault detection schemes developed for longitudinal / lateral control problems need to be integrated.

## Bibliography

- [1] M. Frank, "Fault Diagnosis in Dynamic Systems Using Analytical and Knowledge-based Redundancy- A Survey and Some New Results", *Automatica*, vol 26, No 3, pp459-474, 1990.
- [2] Deyst, Jr., J.J., et al., "Fault Detection, Identification and Reconfiguration of Spacecraft Systems", *J of Astronautical Sciences*, XXIX(2), pp113-126, 1981.
- [3] A.S.Willsky, H.L. Jones, "A Generalized Likelihood Ratio Approach to State Estimation in Linear Systems Subject to Abrupt Changes", *Proc.1974 IEEE Conf. Decision and Control*, Nov.1974.
- [4] Varaiya, S. Shladover, "Sketch of an IVHS Architecture", *Proc. of Vehicle Navigation and Information Systems Conference*, Dearborn, MI, p.909-922,1991
- [5] A. Hitchcock, "Intellegent Vehicle Highway System Safety: Problems of Requirement Specification and Hazard Analysis", *Transportation Redearch Board No. 1318*, pp98-103, 1991.
- [6] L. Segel, "Theoretical Prediction and Experimental Substantiation of the Response of the Automobile to Steering Control", automobile division, The Institute of Mechanical Engineers, pp26-46, 1956.
- [7] D. W. Whitcomb, W. F. Milliken, "Design Implications of a General Theory of Automobile Stability and Control", automobile division, The Institute of Mechanical Engineers, pp83-107, 1956.

- [8] R. E. Fenton, G. C. Melocik, K. W. Olson "On the Steering of Automated Vehicles: Theory and Experiment", *IEEE Trans. on Automatic Control*, Vol. AC-21, No.3, pp306-315, June 1976.
- [9] P. Lugner, "Horizontal Motion of Automobiles- Theoretical and Practical Investigations.", *Dynamics of High Speed Vehicles*, New York, Springer-Verlag, 1982.
- [10] P. Lugner, "The Influence of Structure of Automobile Models and Tyre Characteristics on the Theoretical Results of Steady-state and Transient Vehicle Performance", *The Dynamics of Vehicles, Proceedings of the 5th VSD-2nd IUTAM Symposium*, Vienna, Austria, 1977.
- [11] R. E. Fenton, I. Selim "On the Optimal Design of an Automotive Lateral Controller", *IEEE Trans. on Vehicle Technology*, Vol. 37, No. 2, pp108-113, May 1988.
- [12] K. Gardels, "Automatic Car Controls for Electronic Highways", GMR, General Motors Corp., Warren, MI, Report GMR-276, June 1960.
- [13] K. H. F. Cardew, "The Automatic Steering of Vehicles- An Experimental System Fitted to a DS 19 Citroen Car", *Road Research Lab., Crowthorne, Berkshire*, 1970.
- [14] J. Ackermann, "Parameter Space Design of Robust Control Systems", *IEEE Trans. on Automatic Control*, Vol. AC-25, No. 6, Dec. 1980, pp1058-1072.
- [15] J. Ackermann, "Sampled-data Control Systems", Springer, Berlin, 1985.
- [16] H. L. Jones, "Failure Detection in Linear Systems", Ph.D. Thesis, MIT, Cambridge, MA., 1973.
- [17] J.E.White, J.L.Speyer, "Detection Filter Design: Spectral Theory and Algorithms", *IEEE Transactions on Automatic Control*, Vol.AC-32, No.7, July 1987.

- [18] R.F.Stengel, "Stochastic Optimal Control: Theory and Applications", John Wiley, NY 1986.
- [19] R.J.Patton, J.Chen, "Robust Fault Detection of Jet Engine Sensor Systems Using Eigenstructure Assignment", AIAA Journal of Guidance, Control, and Dynamics, pp1666-1675, 1991.
- [20] R.Patton, P.Frank, R.Clark, "Fault Diagnosis in Dynamic Systems: Theory and Applications", Prentice Hall International (UK) Ltd, 1989.
- [21] R. K. Mehra, I. Peshon, "An Innovation Approach to Fault Detection and Diagnosis in Dynamic Systems", Automatica, 7, pp637-640, 1971.
- [22] P. Frank "Fault Diagnosis in Dynamic systems via state estimation-A Survey". In Tzafestas, S., Singh, M. and Schmidt, G. System Fault Diagnostics, Reliability and Related Knowledge-Based Approaches. Vol. 1 pp35-98. Reidel, Dordrecht.
- [23] J. C. Deckert, M. N. Desai, J. J. Deyst, A. S. Willsky "DFBW Sensor Failure Detection Using Analytic Redundancy", IEEE Trans. on Automatic Control, AC-22, pp795-809, 1977.
- [24] M. Kitamura, "Detection of Sensor Failures in Nuclear Plant Using Analytic Redundancy", Trans. Am. Nucl. Soc., 34, pp581-583, 1980.
- [25] D. Cho, P. Paoletta, "Model-Based Failure Detection and Isolation of Automobile Powertrain Systems", Proc. of ACC, pp2898-2905, 1990.
- [26] P. S. Min, "Diagnosis of On-Board Sensors in Internal Combustion (IC) Engines", Proc. of ACC, pp1065-1070, 1989.
- [27] C. D. deBenito, S. J. Eckert, "Control of an Active Suspension System Subject to Random Component Failures", presented at the ASME Winter Annual Meeting, Chicago, ASME Paper No.88-WA/DSC-33, 1988.

- [28] T. H. B. Jewitt, B. Lawton, "The Use of Speed Sensing for Monitoring the Condition of Military Vehicle Engines", *Proc Inst of Mech Eng, Part D*, v200 n 1, pp45-51, 1986.
- [29] J. W. Freestone, E. G. Jenkins, "The Diagnosis of Cylinder Power Faults in Diesel Engines by Flywheel Speed Measurement", *Proc Inst of Mech Eng, Part D*, v200 n 1, pp37-43, 1986.
- [30] H. Peng, M. Tomizuka, "Lateral Control of Front Wheel Steering Rubber Tire Vehicles", Publication of PATH project, ITS, U C Berkeley, UCB-ITS-PRR-90-5, July 1990.
- [31] Wei-Bin Zhang, Rob E. Parson, Tom West, "An Intelligent Roadway Reference System for Vehicle Lateral Guidance/ Control", Proceedings of 'American Control Conference', p281, San Diego, CA., 1990.
- [32] C. Doniselli, G. Mastinu, "Theoretical Considerations About Active Pneumatic Tyres", *The Dyn of Vehicles on Roads and on Tracks, Proc. of 12th IAVSD-Symposium*, Lyon France Aug 26-30, pp114-129, 1991.
- [33] E. Bakker, L. Nyborg, H. B. Pacejka, "Tyre Modelling for Use in Vehicle Dynamic Studies", International Congress and Exposition, Detroit, MI, SAE paper 870421, 1987
- [34] E. Bakker, H. B. Pacejka, L. Lidner, "A New Tire Model with an Application in Vehicle Dynamic Studies", *SAE Trans., J of Passenger Cars*, Vol. 98, SAE Tech. Paper No. 890087, 1989.
- [35] H. Leiber and A. Czinczel, "Four years of Experience with 4-wheel anti skid brake (ABS)", SAE 830481, 1983
- [36] H. Leiber et al., "Anti-Skid system (ABS) for passenger cars", Bosch Technical and Scientific Report, 1982
- [37] S. Yoneda, Y. Naitoh, and H. Kigoshi, "Rear brake lock up control system of Mitsubishi Starion", SAE paper 830482, 1983



- [38] H. Tan, "Adaptive and robust controls with application to vehicle traction control", Ph.D. Dissertation, University of California, Berkeley, 1988
- [39] H. Tan, and M. Tomizuka, "A discrete time robust vehicle traction controller design", ACC Proceedings, pp.1053-1058, 1989
- [40] H. Tan, and M. Tomizuka, "An adaptive sliding mode vehicle traction controller design", ACC proceedings, Vol.2 of 3, pp.1856-1861, 1990
- [41] R. Fling and R Fenton, "A describing function approach to anti skid design", IEEE Trans. Vehicular Technology. Vol. VT-30, pp.134-144, Aug. 1981
- [42] T. Tabo, N. Ohka, H. Kuraoka, and M. Ohba, "Automotive anti-skid system using modern control theory", in proc. IECON, 1985, pp.390-395
- [43] R. Gunter and H. Ouwerkerk, "Adaptive brake control system", in proc. Instit. Mech. Engg., 1972, Vol.186, pp.885-880
- [44] J. Layne, K. Passino, and S. Yurkovich, "Fuzzy learning control for anti-skid braking systems", in proc., IEEE conf. Decision Contr., Tuscon, AZ, Dec. 1992, pp.2523-2528
- [45] S. Taheri, "A feasibility study of the use of a new non linear control law for automobile anti lock braking systems", Proc or the ACC, San Diego, CA 1990
- [46] S. Taheri, E. Law, "Investigation of integrated slip control braking and closed loop four wheel steering system for automobiles during combined hard braking and severe steering" Proc or the ACC, San Diego, CA 1990
- [47] Rudolf Limpert, "Motor Vehicle Accident Reconstruction And Cause Analysis", The Michie Co., Charlottesville Virginia 1989.
- [48] Teo, C.L., "Frequency Reshaped Linear Quadratic Regulator with Applications to the Control of Flexible Arm", Ph.D. dissertation, UC Berkeley, 1988.
- [49] Peng, Huei, "Vehicle Lateral Control for Highway Automation", Ph.D. dissertation, UC Berkeley, 1992.

- [50] Gupta, N, "Frequency Shaped Cost Functionals: Extension of Linear Quadratic Gaussian Methods", *J. of Guidance and Control*, Vol. 3, No. 6, Nov-Dee 1980, pp529-535.
- [51] Anderson, B.D.O., Mingori, D.L., "Use of Frequency Dependence in Linear Quadratic Control Problem to Frequency shape Robustness", *AIAA J. of Guidance*, Vol. 8, No. 3, May-June 1985, pp397-401.
- [52] S. Patwardhan, M.Tomizuka, W. Zhang, I? Devlin, "Theory and Experiments of Tire Blow-out Effects and Hazard Reduction Control for Automated Vehicle Lateral Control System", *Proc. American Control Conf.*, Baltimore 1994.
- [53] S. Patwardhan, M.Tomizuka, "Slip Angle Control for Improving Cornering Performance of Automobiles", Unpublished.
- [54] I? Kachroo, and M. Tomizuka, "Vehicle traction control and its applications", PATH report (in press)
- [55] D. Love, M. Tomizuka, "Longitudinal Maneuvering Control for Automated Highway Systems Based on a Magnetic Reference/Sensing System" (PATH report under preparation).
- [56] G. Tavazza, "The Prevention of Bead Dislodgement of Tires and the Importance of Limited Run Flat Capability on Safety", *Tenth Int. Technical Conf on Experimental Safety Vehicles*, Oxford, England, July 1-4, pp243-248, 1985
- [57] Yuji Uemura, et al, "Tire Pressure Warning System", *Tenth Int. Technical Conf on Experimental Safety Vehicles*, Oxford, England, July 1-4, pp288-294, 1985
- [58] D. M. Wilbers, J. L. Speyer, "Detection Filters for Aircraft Sensor and Actuator Faults", *Proc. ICCON'89 Int. Conf. on Control and Applications*, Jerusalem, April 1989.
- [59] W. D. Kappler, H. Godthelp, "Effects of Tyre Pressure on Vehicle Handling", *Int. J. of Vehicle Design*. vol. 9 nos 4/5, pp517-532, 1988.

- [60] D. Bahnholzer, "The Design of the Running Gear of Light Passenger Car For Comfort and Safety", *Int. J. of Vehicle Design. Special Issue on Vehicle Safety*, pp129-146, 1986.
- [61] E. Wong, "Introduction to Random Processes", Springer-Verlag, Berlin, 1983.
- [62] H. Peng, M. Tomizuka, "New tire model for thetoyota celica test vehicle", PATH internal report, Apr 1991.

## Appendix A

### Direction cosines of a rotating frame

Consider a rotating frame  $X_R Y_R Z_R$  and a fixed frame  $X_F Y_F Z_F$ . Let the rotating frame be called as  $R$  and the fixed one as  $F$ . Let the components of angular velocity of rotation of  $R$  in  $X_R$ ,  $Y_R$ , and  $Z_R$  directions be  $[\omega_{x_r} \ \omega_{y_r} \ \omega_{z_r}]^T$ . Let the direction cosines  $D_r(t)$  of  $R$  at some instance  $t$  in time be:

$$D_r(t) = \begin{bmatrix} l_1 & l_2 & l_3 \\ m_1 & m_2 & m_3 \\ n_1 & n_2 & n_3 \end{bmatrix}$$

This means that the direction cosines of  $X_R$ ,  $Y_R$ , and  $Z_R$  axis are  $[l_1 \ m_1 \ n_1]^T$ ,  $[l_2 \ m_2 \ n_2]^T$ , and  $[l_3 \ m_3 \ n_3]^T$  respectively.

Consider a small time interval  $dt$ . During this time interval,  $R$  rotates by amount  $\omega_{x_r} \cdot dt$  about  $X_R$  axis, by  $\omega_{y_r} \cdot dt$  about  $Y_R$  axis, and by  $\omega_{z_r} \cdot dt$  about  $Z_R$  axis. Since these are small differential rotations, the results will be independent of the sequence in which these rotations occur. In this derivation,  $\omega_{x_r} \cdot dt$  will be applied first, followed by  $\omega_{y_r} \cdot dt$  and  $\omega_{z_r} \cdot dt$ . After successively applying these rotations, the direction cosines of the  $R$  frame at time  $t + dt$  will be:

$$D_r(t + dt) = D_r(t) \begin{bmatrix} 1 & 0 & 0 \\ 0 & \cos(\omega_{x_r} \cdot dt) & -\sin(\omega_{x_r} \cdot dt) \\ 0 & \sin(\omega_{x_r} \cdot dt) & \cos(\omega_{x_r} \cdot dt) \end{bmatrix}$$

$$\begin{bmatrix} \cos(\omega_{yr} \cdot dt) & 0 & \sin(\omega_{yr} \cdot dt) \\ 0 & 1 & 0 \\ -\sin(\omega_{yr} \cdot dt) & 0 & \cos(\omega_{yr} \cdot dt) \end{bmatrix} \begin{bmatrix} \cos(\omega_{zr} \cdot dt) & -\sin(\omega_{zr} \cdot dt) & 0 \\ \sin(\omega_{zr} \cdot dt) & \cos(\omega_{zr} \cdot dt) & 0 \\ 0 & 0 & 1 \end{bmatrix}$$

Since the rotation angles are small, one can make the approximations of  $\cos(\omega_{zr} \cdot dt) \approx 1$ ,  $\cos(\omega_{yr} \cdot dt) \approx 1$ ,  $\cos(\omega_{zr} \cdot dt) \approx 1$ , and  $\sin(\omega_{zr} \cdot dt) \approx \omega_{zr} \cdot dt$ ,  $\sin(\omega_{yr} \cdot dt) \approx \omega_{yr} \cdot dt$ ,  $\sin(\omega_{zr} \cdot dt) \approx \omega_{zr} \cdot dt$ . This gives:

$$D_r(t + dt) = D_r(t) \begin{bmatrix} 1 & -\omega_{zr} \cdot dt & \omega_{yr} \cdot dt \\ \omega_{zr} \cdot dt & 1 & -\omega_{zr} \cdot dt \\ -\omega_{yr} \cdot dt & \omega_{zr} \cdot dt & 1 \end{bmatrix}$$

Subtracting  $D_r(t)$  from both sides and dividing by  $dt$  gives:

$$\dot{D}_r = D_r \begin{bmatrix} 0 & -\omega_{zr} & \omega_{yr} \\ \omega_{zr} & 0 & -\omega_{zr} \\ -\omega_{yr} & \omega_{zr} & 0 \end{bmatrix} \quad (\text{A.1})$$

Equation A.1 gives the matrix differential equation required to find out the direction cosines of a rotating frame when the angular velocity of rotation is specified in the rotating frame.

This equation can also be applied when the frame  $R$  rotates by small angles  $\delta_x$ ,  $\delta_y$ , and  $\delta_z$  about the three axis  $X_R$ ,  $Y_R$ , and  $Z_R$  respectively. If  $AD$ , represents the change in the direction cosines of  $R$ , then Eq A.1 becomes:

$$AD = D_r \begin{bmatrix} -\delta_x & \delta_y & \delta_z \\ \delta_x & -\delta_y & \delta_z \\ -\delta_y & \delta_x & 0 \end{bmatrix} \mathbf{q} \quad (\text{A.2})$$

## Appendix B

### Tire Force Generation

The empirical relations for calculating the tire forces as suggested by Bakker [33] [34] are:

$$F_{ta}(\alpha, \lambda, F_P, r_c) = D_x \sin(C_x \tan^{-1}(B_x \phi_x)) + S_{vx} \quad (\text{B.1})$$

$$F_{tb}(\alpha, \lambda, F_P, r_c) = D_y \sin(C_y \tan^{-1}(B_y \phi_y)) + S_{vy} \quad (\text{B.2})$$

where,

$$\phi_x = (1 - E_x)(\lambda + S_{hx}) + \frac{E_x}{B_x} \tan^{-1}(B_x(\lambda + S_{hx}))$$

$$\phi_y = (1 - E_y)(\alpha + S_{hy}) + \frac{E_y}{B_y} \tan^{-1}(B_y(\alpha + S_{hy}))$$

and,  $B_i, C_i, D_i, E_i, S_{hi}$  and  $S_{vi}$  are the coefficients to be tuned to fit the test data. Their values are [62]:

$$B_y = 0.22 + \frac{5200 - F_P}{40000}$$

$$C_y = 1.26 + \frac{F_P - 5200}{32750}$$

$$D_y = -0.00003F_P^2 + 1.0096F_P - 22.73$$

$$E_y = -1.6$$

$$S_{hy} = 0$$

$$S_{vy} = 0$$

$$(\lambda > 0)$$

$$B_x = 22 + \frac{F_P - 1940}{645}$$

$$C_x = 1.35 - \frac{F_P - 1940}{16125}$$

$$D_x = 2000 + \frac{F_P - 1940}{0.956}$$

$$E_x = -3.6$$

$$S_{hx} = 0$$

$$S_{vx} = 0$$

$$(\lambda \leq 0)$$

$$B_x = 22 + \frac{F_P - 1940}{430}$$

$$C_x = 1.35 - \frac{F_P - 1940}{16125}$$

$$D_x = 1750 + \frac{F_P - 1940}{0.956}$$

$$E_x = 0.1$$

$$S_{hx} = 0$$

$$S_{vx} = 0$$

Figure B.1 and B.2 show the typical plots of the longitudinal and lateral tire force characteristics respectively.

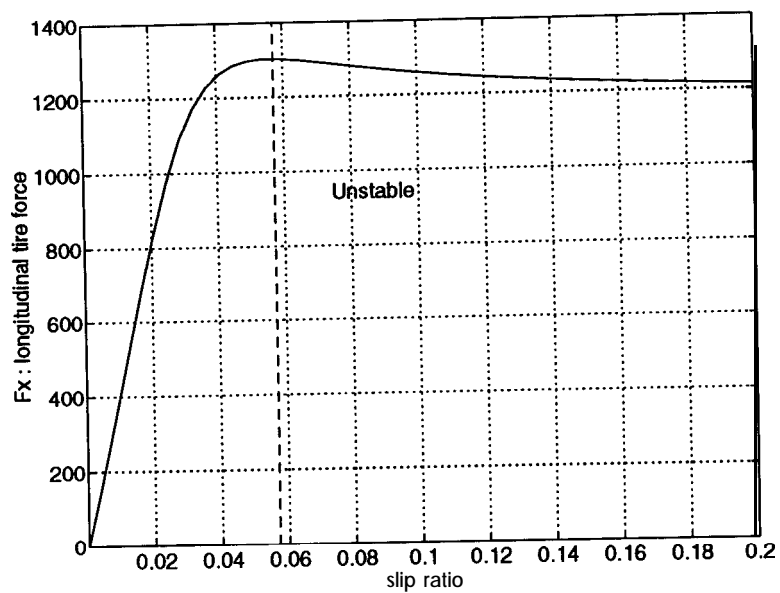


Figure B.1: Longitudinal tire force characteristics

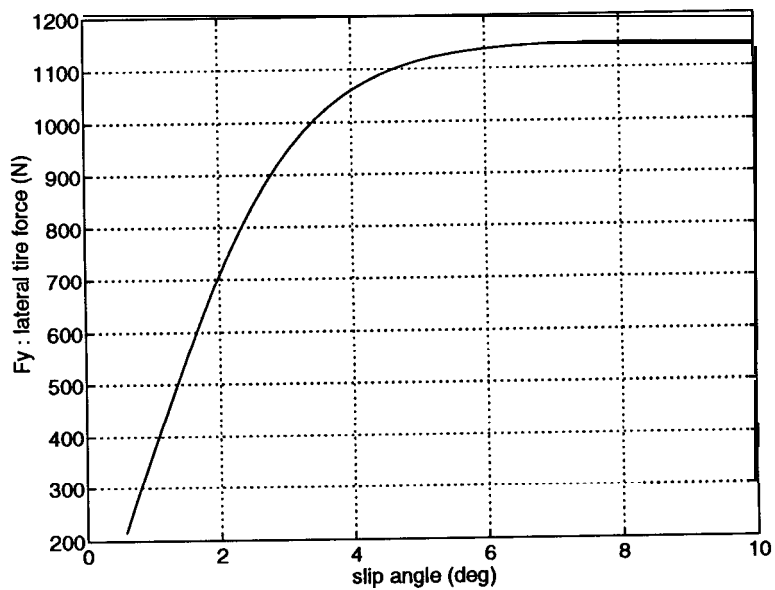


Figure B.2: Lateral tire force characteristics



## Appendix C

### Simplified Model

In simplified model, vertical, roll, and pitch motions are neglected. If longitudinal velocity is constant or slowly changing, then the nonlinear complex model can be simplified. This is justified in IVHS because longitudinal control algorithms will be maintaining the vehicle longitudinal velocity constant. The number of state variables is only four, two for each of the lateral and yaw motions. Referring to Fig. C.1, nomenclature of the simplified model is:

- $y_r$  : lateral distance between the mass center and the center line of road
- $\epsilon$  : yaw angel of vehicle body
- $\epsilon_d$  : desired yaw angel set by the road
- $d_s$  : distance from vehicle mass center to magnetic sensor
- $v$  : Longitudinal velocity
- $\rho$  : radius of curvature of road
- $\delta$  : front wheel steering angle
- $m$  : mass of the vehicle
- $I_z$  : mass moment of inertia of the vehicle about vertical axis (thru. CG)

The symbols in 3.1 are defined as follows:

$$A_1 = \frac{-1}{m}[C_{s1} + C_{s2} + C_{s3} + C_{s3}]$$

$$A_2 = \frac{1}{m}[-l_1(C_{s1} + C_{s2}) + l_2(C_{s3} + C_{s3})]$$

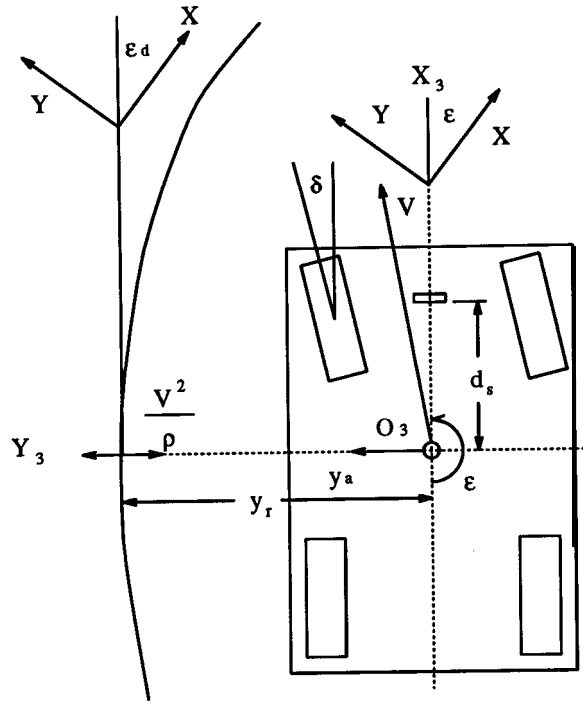


Figure C.1: Schematic of simplified vehicle

$$A_3 = \frac{1}{I_z} [-l_1(C_{s1} + C_{s2}) + l_2(C_{s3} + C_{s3})]$$

$$A_4 = \frac{-1}{I_z} [l_1^2(C_{s1} + C_{s2}) + l_2^2(C_{s3} + C_{s3})]$$

$$B_1 = \frac{1}{m} [F_{x1} + F_{x2} + C_{s1} + C_{s2}]$$

$$B_2 = \frac{-l_1}{I_z} [F_{x1} + F_{x2} + C_{s1} + C_{s2}]$$

$$d_1 = \bar{d}_1 - V\dot{\epsilon}_d + \frac{A_2}{V}\dot{\epsilon}_d$$

$$d_2 = \bar{d}_2 - \ddot{\epsilon}_d + \frac{A_4}{V}\dot{\epsilon}_d$$

$\bar{d}_1$  and  $\bar{d}_2$  represent wind and other disturbances.